216715 NEWCOM++

DR9.2

Definition and evaluation of JRRM and ASM algorithms

Contractual Date of Delivery to the CEC: *T0+24*

Actual Date of Delivery to the CEC: *T0+24*

Editor(s): *Pawel Sroka (PUT)*

Participating institutions: *CNIT; CNRS; IST-TUL; PUT; UPC.*

Contributors: (names) Virginia Corvino (CNIT-Bo), Andrea Carniani (CNIT-Bo), Marco Moretti (CNIT-Pi), Giulio Dainelli (CNIT-Pi), Samir M. Perlaza (CNRS), Mérouane Debbah (CNRS), Samson Lasaulce (CNRS), Wassim Jouini (CNRS), Jacques Palicot (CNRS), Christophe Moy (CNRS), Antonio Serrador (IST-TUL), Nuno Cota (IST-TUL), Luís M. Correia (IST-TUL), Hanna Bogucka(PUT), Pawel Sroka (PUT), Emanuel Bezerra Rodrigues (UPC), Miguel López-Benítez (UPC), Anna Umbert (UPC), Ferran Casadevall (UPC), Jordi Pérez-Romero (UPC)

Internal Reviewer(s) (names and affiliations): Sergio Benedetto (ISMB)

Workpackage number: *WPR.9*

Nature: *R*

Total Effort Spent: *12PM*

Dissemination Level: *Public*

Version (1,2,…): *2*

Abstract:

This deliverable (DR9.2) describes the radio resource management, joint radio resource management and advanced spectrum management strategies developed in each of the tasks of WPR.9 during the second year of study. The proposed algorithms together with the results of evaluation in scenarios identified in the deliverable DR9.1 are presented. A special attention is given to JRRM in heterogeneous networks, OFDMA spectrum management and measurements, and game-theoretical optimization of cognitive networks.

Keyword list: RRM, JRRM, ASM, Game Theory, OFDMA Spectrum Management, Cognitive Networks

TABLE OF CONTENTS

LIST OF FIGURES

LIST OF TABLES

LIST OF ACRONYMS

ADC	Analogical to Digital Converter
ADF	Adaptive Delay-Based Fairness
AP	Access Point
ASM	Advanced Spectrum Management
ATF	Adaptive Throughput-Based Fairness
AWGN	Additive White Gaussian Noise
BER	Bit Error Rate
BL	Bandwidth Limiting
BS	Base Station
BWA	Broadband Wireless Access
CDF	Cumulative Distribution Function
CDMA	Code Division Multiple Access
CINR	Carrier-gain-to-Interference-and-Noise Power Ratio
CQI	Channel Quality Indicator
CR	Cognitive Radio
CSI	Channel State Information
CT	Cordless Telephone
D-FIFO	Delay-Based First In First Out
DAB	Digital Audio Broadcasting
DAC	Digital to Analogical Converter
DCS	Digital Cellular System
DMMF	Distributed Max-Min Fit
DPC	Dirty Paper Coding
DRA	Dynamic Resource Allocation
DRF	Distributed Reverse Fit
DSA	Dynamic Sub-carrier Allocation/Dynamic Spectrum Assignment
DSL	Digital Subscriber Line
DVB-T	Digital Video Broadcasting - Terrestrial
E-GSM	Enhanced Global System for Mobile communications
ERMES	European Radio MEssage System
FDD	Frequency-Division Duplex
FDMA	Frequency Division Multiple Access
FLC	Fuzzy Logic Controllers
FM	Frequency Modulation

GMDSS	Global Maritime Distress and Safety System
GNR	Gain-to-Noise Ratio
GSM	Global System for Mobile communications
HHO	Horizontal HandOver
HNB	Home NodeBs
HOL	Head-of-Line
HSDPA	High-Speed Downlink Packet Access
IP	Internet Protocol
ISM	Industrial, Scientific and Medical
JRRM	Joint Radio Resource Management
KPI	Key Performance Indicator
LTE	Long Term Evolution
LWT	Largest-Weighted-Throughput
MAI	Multiple Access Interference
MCS	Modulation and Coding Scheme
MILP	Mixed-Integer Linear Programming
MIMO	Multiple Input Multiple Output
M-LWDF	Modified Largest Weighted Delay First
MMF	Max Min Fairness
MMOM	Multicellular Multi-carrier Optimisation Model
MR	Max Rate
MT	Mobile Terminal
MU	Multi-User
NRT	Non-Real Time
NSE	Network Spectral Efficiency
OFDM	Orthogonal Frequency Division Multiplexing
OFDMA	Orthogonal Frequency Division Multiple Access
PAMR	Public Access Mobile Radio
PC	Personal Computer
PDF	Probability Density Function
PF	Proportional Fairness
PFA	Probability of False Alarm
PMI	Precoding Matrix Indicator
PMR	Professional/Private Mobile Radio
PS	Power Shaping
PSC	Packet Scheduling
PSD	Power Spectral Density

PSNR	Peak-Signal-to-Noise-Ratio
QAM	Quadrature Amplitude Modulation
QoS	Quality of Service
QPSK	Quadrature Phase-Shift Keying
R-GSM	Railway Global System for Mobile communications
RAT	Radio Access Technique
RBW	Resolution BandWidth
RF	Radio Frequency
RFID	Radio Frequency IDentification
RMS	Root-Mean Square
RN	Relay Node
RRA	Radio Resource Allocation
RRM	Radio Resource Management
RRU	Remote Radio Unit
RT	Real Time
S-PCS	Satellite Personal Communication Systems
SDM	Space Division Multiplexing
SDMA	Space Division Multiple Access
SDR	Software Designed Radio
SES	Simple Exponential Smoothing
SFDR	Spurious-Free Dynamic Range
SINR	Signal-to-Interference-plus-Noise-Ratio
SPDT	Single Pole Double Throw
SRA	Static Resource Allocation
TDD	Time Division Duplex
TDMA	Time Division Multiple Access
TTI	Time Transmission Interval
TU	Typical Urban
TV	Television
UE	User Equipment
UEPS	Urgency and Efficiency based Packet Scheduler
UMTS	Universal Mobile Telecommunication System
USB2	Universal Serial Bus 2
USRP	Universal Software Radio Peripheral
UT	User Terminal
VBW	Video BandWidth
VHO	Vertical HandOver

VoIP	Voice over IP
WCDMA	Wideband Code Division Multiple Access
WG	Working Group
WiMAX	Worldwide Interoperability for Microwave Access
WWW	World Wide Web
ZF	Zero-Forcing

1 INTRODUCTION

1.1 Objectives

The study in WPR.9 is focused on the development and evaluation of advanced Radio Resource Management (RRM) and spectrum management techniques for wireless communications systems in heterogeneous scenarios. In such scenarios different access techniques co-exist, so by a joint use of the available resources significant gains and a more efficient use of the spectrum can be achieved. Moreover, the developed strategies may be improved by introduction of cognitive network functionalities to provide the ability to adapt to changing conditions

The main idea of this deliverable, entitled "Definition and evaluation of JRRM and ASM algorithms" is to address the different aspects of RRM, JRRM and ASM by describing selected algorithms and their evaluation. Although the analysis can be performed without considering applications and end use situations, the RRM and ASM algorithms and strategies in heterogeneous networks depend on particular systems. Therefore, this deliverable offers the perspective of considering specific systems or technologies, by presenting various models and algorithms in different use cases.

The following chapters present the main areas of investigation and outline the results achieved in year two of study within the framework of WPR.9.

1.2 Document structure

This document is organised as follows: following this introductory chapter, two main chapters present the results of work within WPR.9 during the second year of study:

- Chapter 2 deals with RRM and JRRM algorithms at different levels, comprising the work of working groups WG1, WG2 and WG3 in three subsections respectively:
    - The JRRM algorithms and their evaluation in heterogeneous networks is of scope in Section 2.2, with the main focus on the multicell multicarrier power optimisation, and vertical hand-over (VHO)
    - Section 2.3 deals with the resource allocation problem in a cellular OFDMA system, with the analysis both on single-cell and multi-cell level.
    - In Section 2.4 game theory is applied for optimization of the RRM in cognitive radio. Two different techniques have been considered: the taxation of resources and the resource bandwidth limiting with successive interference cancellation.
- Chapter 3 presents the outcomes of investigation within working groups WG4 and WG5 in the advanced spectrum management field. The results and proposed algorithms are given in two subsections:
    - Section 3.2 describes the results of the measurement campaign to detect spectrum availability, with the aim to establish spatial and temporal usage patterns from primary users in different licensed bands.
    - In Section 3.3 a machine learning based strategy has been proposed for dynamic spectrum assignment (DSA).

Finally, in chapter 4 the main conclusions and the summary of integration activities within WPR.9 are outlined.

2 RRM AND JRRM ALGORITHMS AND THEIR EVALUATION

2.1 Introduction

Radio resource management (RRM) is the system level control of co-channel interference and other radio transmission characteristics in wireless communication systems, for example cellular networks, wireless networks and broadcasting systems. As the number of wireless systems and standards constantly increases, the need for efficient usage of the limited existing radio resources calls for the deployment of new strategies and revolutionary visions. Centralized or distributed strategies that control the level of multiple access interference (MAI) are expected to deliver enormous gains in terms of spectral and power efficiency. In the remainder of this section we will mainly focus on two possible RRM scenarios: a) the *cellular scenario*, where there is one or more base stations that control the access to the radio channels and b) the *decentralized scenario*. The former case will be studied assuming that there is one or more controllers knowing the transmission parameters of all the terminals they manages and RRM will be addressed mainly by employing mathematical optimization tools. The latter case will be analyzed assuming the lack of centralized information and the impossibility of exchanging signaling messages between the transmitters and will be the studied following a game theory approach.

Moreover, the constant development of new radio access technologies drives the research towards strategies that are able to integrate the functionalities of the different systems, which are often complementary in terms of data rate and coverage. This is the goal of efficient Joint Radio Resource Management (JRRM), which executes high level decisions and implements management policies, and can support advanced auto-tuning solutions. Beyond-3G system will integrate a network of heterogeneous systems to offer an increasing range of services. While the task of RRM is solving the problem of how allocating radio resources among users, dealing with the dissimilarities and complementarities of the multiple RATs from a joint perspective is the task of JRRM. In the next Section, we will present a JRRM simulator expressly designed to test different JRRM strategies and execute offline optimisation.

2.2 JRRM Strategies and Algorithms

2.2.1 Multicellular Multi-Carrier Power Optimisation Model

In this section it is provided a multicellular multi-carrier optimisation model (MMOM) overview. Besides other features, this model is capable to produce the transmitted power distribution characterisations for 5 regions/zones across cell. This model can be used to optimise power distribution in OFDM based base stations (BSs), such WLANS or WiMAX.

It is assumed that a train station platform is composed of N_{cells} squarely cells that share the whole available spectrum, i.e., the frequency reuse is equal to one. In each cell there is a base station and K users. The BS assigns them a subset of the radio channels.

Assuming also that the modulation technique is multi-carrier and the multiple access scheme is OFDMA, then the system bandwidth is partitioned into orthogonal subcarriers and each user is assigned a different subset of subcarriers. To perform resource allocation, the BS needs to know channel gains and interference levels on all subcarriers for all users in the cell. To reduce allocation complexity, sets of adjacent subcarriers are grouped into *subchannels*. As long as the bandwidth spanned by a subchannel is smaller than the channel coherence bandwidth, the channel spectrum can be approximated as flat in the subchannel. Thus, one can assume that the choice of performing resource allocation on subchannels rather than on single subcarriers causes almost no loss in diversity: power remains constant and coding is done across the tones in each subchannel. Channel assignment is orthogonal within a cell: each subchannel can be assigned to one (and only one) user within a cell.

Let k be a generic user belonging to the cell i. The received signal-to-interference-plus-noise ratio (SINR) for user k on subchannel n is given by

$$\gamma_{k,n}^{(i)} = \frac{P_n^{(i)} \left| G_{k,n}^{(i)} \right|^2 b_{k,n}^{(i)}}{I_{k,n}^{(i)} + N_0 B} \tag{2.1}$$

where $P_n^{(i)}$ represents the power transmitted by BS i on subchannel n, $G_{k,n}^{(i)}$ is the channel gain between user k and BS i on the n-th link, $b_{k,n}^{(i)}$ is an allocation variable that is set to one when the channel n is allocated to user k in the cell i and zero otherwise. N_0 is the power spectral density of the zero-mean thermal noise and B is the bandwidth of each subchannel. The interference term $I_{k,n}^{(i)}$ affecting user k in cell i on the n-th channel is given by:

$$I_{k,n}^{(i)} = \sum_{\substack{j=1 \\ j \neq i}}^{N_{cells}} P_n^{(j)} \left| G_{k,n}^{(j)} \right|^2 \tag{2.2}$$

Model main settings (based on the train station scenario) are as follows:

- $N_{cells} = 5$
- Number of users $K = 4$
- Total available bandwidth $B = 20$ MHz @ $f_0 = 5$ GHz
- Number of subcarriers $N = 16$
- Radius of each cell $R = 50$ m
- Path loss model: $L = d^{\wedge}(P_L)*(\lambda/(4\pi))^{\wedge}-2$, where d is the distance between the user and the center of the cell, $P_L = 4$ is the path loss exponent, $\lambda = c/f_0$.
- Rms delay spread of the multipath channel $\sigma_t = 1$ μs
- Target rate per subcarrier $R_{target} = 1.25$ Mbit/s

Further details about this model can be found in [1].

2.2.2 Reference Scenario

The reference scenario used in this work is the Train Station Scenario described in NEWCOM++ WPR9 - DR.9.1 [2]. This scenario is challenging since it enables studies on a hot spot area where users start by being static, and then are allowed to move crossing different cellular RAN layers/coverage areas. Thus, this scenario is capable to trigger several Joint Radio Resource Management (JRRM) mechanisms.

The train station scenario is characterised by the following parameters:

- Users mobility: static;
- Users' distribution: randomly uniform distributed;
- Train Station size platform: 200x20m;
- The number of users waiting in the station platform depends on the sub-scenario variation;

Table 2.1 – Number of BSs in the train station scenario

RANs	#BSs	Radius [m]
R99	1	400
R5	1	300
WLAN	5	50
WiMAX	1	20x200

In Table 2.1 the number of BSs located in the train station is defined. UMTS R99 and R5 BSs are located at the station platform centre. However, WLAN APs are distributed in a line along the station platform, like the example presented in Figure 2.1.

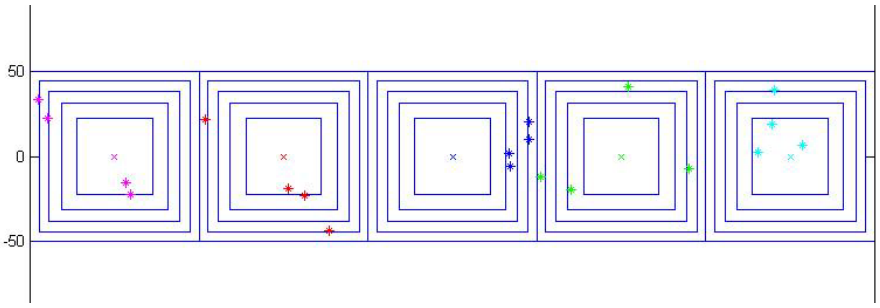

Figure 2.1 – Train Station APs' (WLANs) distribution with random users attached

For system level simulations a set of services is defined and described briefly in Table 2.2.

Table 2.2 – Set of services

Service	Penetration [%]	Service Duration or Volume
Voice	56	60 s
Video	4	60 s
Streaming (WiMax)	8	90 s
FTP (WiMAX)	6	Statistics according to [3].
WSN (WiMAX)	7 coords+200 nodes	250 kibt/s (average)
e-mail	10	300kB
WWW	12	180kB

The expected outputs are as follows:

- BSs downlink Transmitted power characterisation – is a set of PDFs that characterise several regions across BS area, these PDFs results are based on a multicellular multi-carrier power optimisation described in section 3 of this report;
- JRRM Delay – is the expected average delay, for each packet at MAC layer, that users will experience due to radio resource availability;
- JRRM Throughput – is the instantaneous bit rate produced by active users/services;
- JRRM Blocking Probability – is the expected probability that a user can experience when JRRM is present;
- Number of VHOs – is the number of VHOs that was processed by the JRRM entity in the simulation, in a given time frame (e.g., one hour). This is very dependent on mobility and traffic overload conditions;
- PSNR for video users – is the Peak-Signal-to-Noise Ratio, which is a metric usually utilized to evaluate performance of video traffic;
- The number, on average, of active users per service.

2.2.3 Simulation Results

2.2.3.1 Train Station

In this section main results are presented, mainly the ones associated to transmitted power distributions, being them useful to system level simulation tools.

Figure 2.2 represents an example (Zone 1) on how BS individual cell area can be characterised, this figure show a cell area histogram and associated PDF. Note that these Zones have the same area in the cell. Therefore, each zone have different radius as showed by Table 2.3.

The PDFs summary is presented in Table 2.3, where each cell zone is fully characterised. The BS distance interval was selected to ensure that the bounded areas have the same geographical area, thus ensures that on average the number of users inside are equal (since users are uniformly distributed). Observing these results it is possible to conclude that the average power will increase from zone 1 to zone 5, not only due to distance, but also due to interference, caused mainly by the frequency reuse pattern, which this model aims to minimise.

At system level and in the simulation tool, the previous functions were implemented in order to provide new and more realistic values for the WLANs (when single frequency scenario for all APs is used), on the radio channel power characterisation. Originally the JRRM tool uses a propagation path loss model and an Interference Model (IM), now with the use of the set of functions reported in Table 2.3, it is possible to generate power for each cell zone (5 distance intervals) considering single frequency planning (frequency reuse pattern equal to 1) and consequent interference and packet scheduler optimisation that minimises interference by minimising power at each sub-carrier transmitted to MTs.

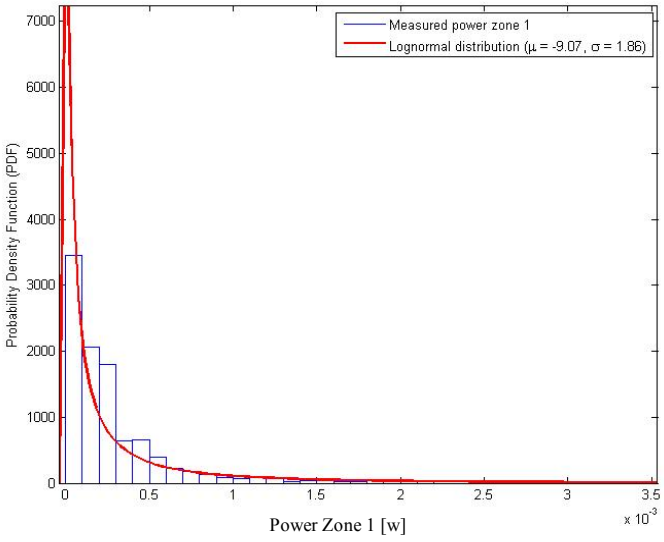

Figure 2.2 – Example of OFDMA power distribution histogram (Zone 1 d<22)

For assessing the impact of this model on JRRM performance, the "original" WLAN interference model was used on the train scenario. This model is based on measurements made on buildings, like shopping centres, including all sources of interference at 2.4GHz. The IM model is characterised by a Normal PDF, having mean μ=-100 and variance σ^2=10. Thus, using these arguments in a Normal variable random generator function it is possible to obtain a random interference ranging around -100dBm. Note that for this model case a multi frequency planning is assumed. In the MMOM case, it is assumed the existence of single frequency planning (for WLANs) and, intrinsically includes inter cell interference, thus power distributions for each cell zone do not requires extra interference computation.

Table 2.3 – PDFs summary for the train scenario

Zone	BS distance d, interval [m]	Function	Parameters
1	$d \leq 22$	Lognormal (μ; σ)	(-9.07; 1.86)
2	$22 \leq d < 31$		(-7.07; 0.6)
3	$31 \leq d < 38$		(-6.21; 0.45)
4	$38 \leq d < 44$		(-5.68; 0.39)
5	$44 \leq d < 50$		(-5.25; 0.35)

Three different traffic loads were generated, named LT, MT, HT, meaning Low, Medium and High Traffic respectively. In Table 2.4, it is possible to observe that the number of active users per service using both models do not differ significantly, however, JRRM (horizontal and vertical) handovers, JRRM Delay and JRRM Throughput have some relevant differences. One can highlight the JRRM delay that presents differences by two orders of magnitude. This JRRM Delay, which mainly comes from WLANs' group, confirms the intrinsic differences of both WLAN radio channel models and associated considerations.

Table 2.4 – Results of WLAN channels' models impact on JRRM performance

Model	Traffic Load	Block	Delay [ms]	#VHO	#HHO	#Active Users	#SPEECH	#WWW	#VIDEO	#EMAIL
IM	LT	0.0	0.15	0	5	39.5	29.9	3.8	2.3	3.6
	MT	2.3	0.20	0	0	50.6	37.9	4.0	4.4	4.2
	HT	9.4	0.28	0	0	55.4	40.8	6.7	3.1	4.8
MMOM	LT	0.0	24.47	16	53	39.7	30.7	3.7	2.1	3.2
	MT	5.8	54.71	37	86	51.9	38.6	5.7	3.1	4.4
	HT	6.0	62.34	31	81	57.4	42.7	6.6	3.0	5.1

The JRRM throughput in the train station scenario using the IM model was on average 249 Mbps and using the MMOM was about 223 Mbps. This difference is again associated to both models, which means that WLANs' access was less efficient using MMOM, having also a negative impact on the JRRM delay. Nevertheless, JRRM delay is acceptable since it is under tens of milliseconds delay, assuming the presence of WLAN-OFDM based on single frequency reuse planning.

2.2.3.2 Traffic Transmission over WiMAX

In this Section some results related to the traffic transmission occurring over the WiMAX system imagined to operate in the train scenario are reported.

In fact it is assumed that a WiMAX system is covering the train station area in overlap with the other systems cited above. According to the JRRM strategy implemented, all the video streams, together with the FTP traffic, is directly transmitted through the WiMAX system. Nevertheless, it is assumed that in the area a certain number of IEEE 802.15.4 devices and relevant coordinators are deployed for sensing purpose. Since 802.15.4 devices are energy-constrained, in order to reduce the transmitted power to be used, it is assumed that these sensing nodes do not transmit their data directly to the WiMAX base station, which could be not accessible due to distance, but rather they transmit to some special nodes deployed on purpose, namely 802.15.4 coordinators. In particular, each sensor node is

connected to the closest coordinator, and the set of 802.15.4 nodes connected to a certain coordinator compete to send their data according to the Carrier Sensing Multiple Access with Collision Avoidance (CSMA/CA) protocol. Then, the data gathered by coordinators are stored in buffers, until they are selected for transmission by the base station. In fact, the base station performs a centralized scheduling of video streams, FTP data and sensing traffic coming from 802.15.4 coordinators, by considering the application supported and the relevant characteristics (e.g., delay sensitiveness, channel state). In the following results related to the case of 8 video streams, 6 FTP users, and 7 802.15.4 coordinators gathering data from 200 802.15.4 sensors are reported.

In Figure 2.3 it is reported the Cumulative Distribution Function (CDF) of the outage rate perceived by video users. In particular outage rate is defined as the number of frames over which the PSNR measured by each video user is under a certain threshold considered as satisfactory, divided by the total number of transmitted video frames. It can be noticed that 70% video users perceive outage rate smaller than 10%, which can be considered as satisfactory usually.

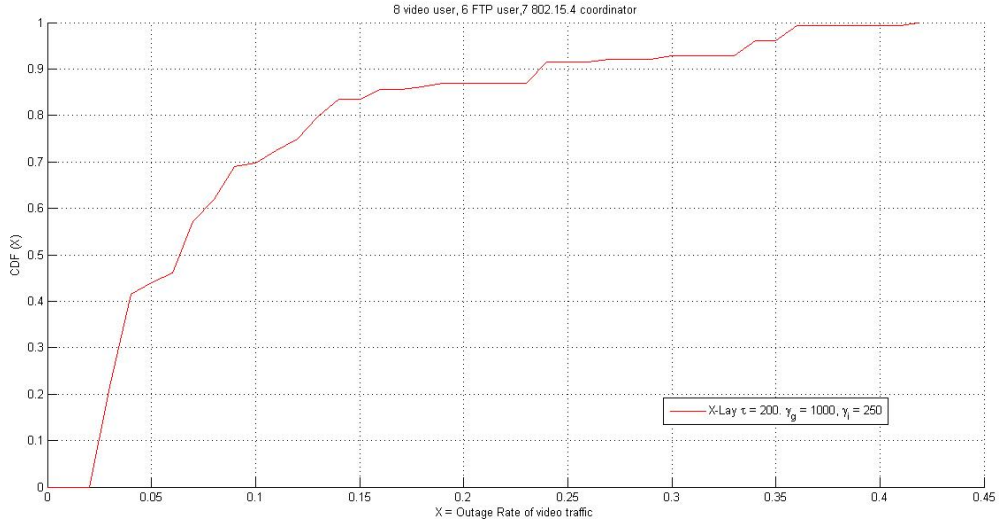

Figure 2.3 – CDF of Video Users' Outage Rate

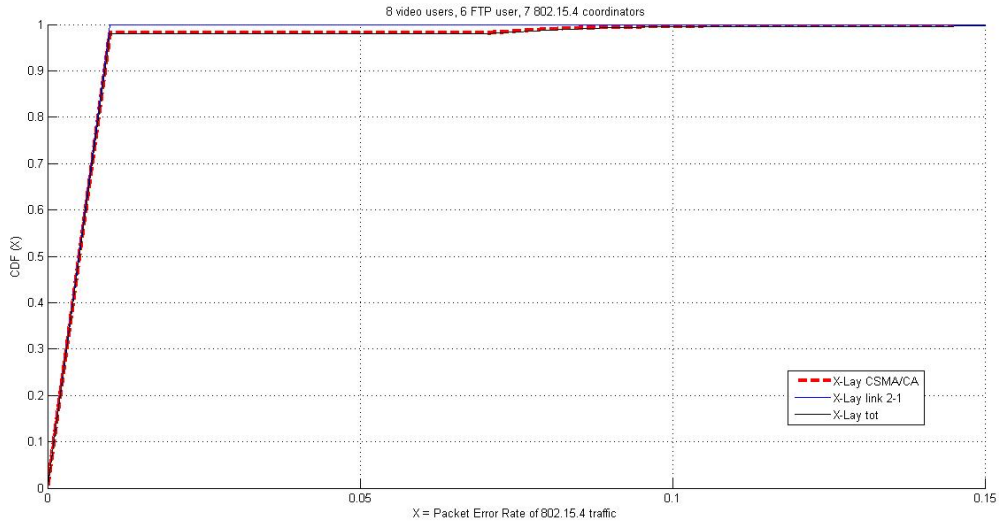

Figure 2.4 – CDF of Packet Error Rate for 802.15.4 Traffic

In Figure 2.4 the CDF of Packet Error Rate (PER) for FTP traffic is reported, where PER is defined as the ratio of the number of erroneous transmitted packets over the total number of transmitted FTP

packets. In this case performance is excellent. In particular, in this case it is reported also the amount of losses due to the link between 802.15.4 nodes and coordinators, which are assumed to happen only due to CSMA/CA (so, errorless channel), and the link between the coordinators (which can be considered as nodes of level 2 in a hierarchical network) and the WiMAX base station. In this case losses are assumed to occur due to channel fluctuations. Then, it is clear that total loss derives by both CSMA/CA and the link between coordinators and BS. It could be noticed that here packets are the amount of bits generated by each sensor node, which is 200 bit at a bit rate equal to 250 kbit/s.

Finally, in Table 2.5 it is reported the Block Error Rate (BLER) computed for each 802.15.4 coordinator, which is defined as the number of erroneous transmitted transport blocks divided by the total number of transmitted transport blocks. In this case, blocks are defined as the amount of bits coming from a certain source transmitted in a certain time frame. Hence, blocks are usually larger than packets for sensor nodes. Also in this case it can be noticed that performance are excellent.

Table 2.5 – 802.15.4 coordinators' BLER

Coordinator index	BLER
1	0.000882
2	0.001951
3	0.000232
4	0.000312
5	0.000000
6	0.001326
7	0.000000

2.2.4 Heterogeneous Networks VHO Model

When scanning literature concerning VHOs, it is not frequent to find simple analytical models capable of extracting the main characteristics of a VHO process. For example in [4], [5], [6] and [7] relatively complex models are used to optimise and trigger VHOs, based on radio signal levels among others. However, a simple model that depends on geographical considerations is very useful to assess JRRM performance; based on simple considerations, the impact of several parameters (at user and network levels), on the JRRM QoS performance can be evaluated. The model proposed in this section is capable of extracting cellular Horizontal Handover (HHO) parameters; however, it is mainly devoted to VHOs.

Using a HHO analytical model as starting point, where user's cell crossing probabilities, crossing rates, drops, blocking can be evaluated, [7], this proposed model assumes that a given RAN cluster type, Figure 2.6, can be modelled as a single cell (using cellular HHO characteristics). This approach enables the use of the previous model mechanism to extract some VHOs assumptions and theoretical results. This means that users' previous transitions between cells borders of a given RAN are now translated to transitions between RANs borders (cluster based). This model is based on the traffic generation and on the heterogeneous network overall capacity. Thus, it is required to start defining the number of active users, including the use of multiple services. In the model the following conditions are assumed: network stability, infinite population, uniform users' distribution in the area, Poisson and exponential distributions for service session arrival and duration processes, respectively.

The proposed theoretical model is defined by the following mechanism.

The number of active users N_{AU}, is the sum of voice and video users $N_{AU\text{-}s}$ and data users $N_{AU\text{-}Da}$ as follows:

$$N_{AU} = N_{AU-s} + N_{AU-Da} \tag{2.3}$$

where $N_{AU\text{-}s}$ is defined by,

$$N_{AU-s} = \lambda_{s[\text{session/s}]} \cdot \tau_{s[\text{s/session}]} \cdot N_{CovU} \cdot P_{Sps} \cdot (1 - P_{Be}) \tag{2.4}$$

and,

- λ_s is the service/session s, arrival rate;
- τ_s is the service/session duration for the service s;
- N_{CovU} is the number of coverage users;
- P_{Sps} is the service s, penetration probability;
- P_{Be} is the expected JRRM blocking probability.

and $N_{AU\text{-}Da}$ is defined by:

$$N_{AU-Da} = \sum_{s=1}^{N_{ds}} \lambda_{s[\text{session/hour}]} \cdot \left(\frac{DV_{s[\text{bytes/session}]} \cdot 8}{Rb_{s[\text{bps}]}} + \tau_{Ce[\text{s}]} \right) \cdot N_{CovU} \cdot P_{Sps} \tag{2.5}$$

where DV_s is the data volume for a given service s, τ_{Ce} is expected JRRM overall delay and Rb_s is the average bit rate per service. Assuming one service per user, then the user bit rate is Rb_U=Rb_s.

The total JRRM average bit rate, Rb_t, is defined according to,

$$Rb_{t[\text{bps}]} = \frac{1}{N_{AU}} \sum_{U=1}^{N_{AU}} Rb_{U[\text{bps}]} \tag{2.6}$$

Taking the service area, S_a, then the active users density ρ_{AU} is as follows:

$$\rho_{AU[\text{km}^{-2}]} = \frac{N_{AU}}{S_a} \tag{2.7}$$

Knowing the number of active users and the JRRM average bit rate per user, then for a given time interval, Δt, it is possible to compute the total generated traffic T_{AN}, for one hour period:

$$T_{AN[\text{Bytes/hour}]} = N_{AU} \cdot \frac{Rb_t}{8} \cdot \Delta t \tag{2.8}$$

Finally the total traffic density $T_{\rho N}$, also for a given period, Δt, is given by:

$$T_{\rho N[\text{Bytes/hour/km}^2]} = \rho_{AU} \cdot \frac{Rb_t}{8} \cdot \Delta t \tag{2.9}$$

The amount of traffic allocated to each type of RAN r, $T_{\rho N,r}$, is a percentage of total traffic density that will be initially transported/attributed to each RAN, this percentage is being defined by $P_{Init,r}$.

$$T_{\rho N,r[\text{Bytes/hour}]} = P_{Init,r[\%]} \cdot T_{\rho N} \cdot S_{r[\text{km}^2]} + V_{t[\text{Bytes/hour}]} \tag{2. 10}$$

where S_r represents the area occupied by a given RAN type r, and V_t represents the traffic that comes/goes from/to other RANs by the VHO mechanism. V_t is defined based on the percentage applied to a given RAN traffic that by the VHO process will move traffic among RANs. V_t is described as follows:

$$V_{t[\text{Bytes/hour}]} = P_{VHO} \cdot T_{\rho N,r} \tag{2.11}$$

Naturally, when P_{VHO} is different from 0, then the destination RAN should add traffic in the same amount than other traffic source RAN should decrease. P_{VHO} can be negative or positive depending on the VHO traffic flux management policy.

Note that $P_{Init,r}$ is conservative, thus is constrained by the following condition:

$$100\% = \sum_{r=1}^{N_{RAN}} P_{Init,r} \tag{2.12}$$

$T_{\rho N}$, is very useful since heterogeneous network capacity can be computed also based on network resources per area, then the overall network capacity density T_{CN}, is computed according to,

$$T_{CN[\text{Bytes/hour/km}^2]} = \sum_{r=1}^{N_{RAN}} T_{CN,r}\,, \tag{2.13}$$

where $T_{CN,r}$ is the network capacity of each RAN type r defined as follows:

$$T_{CN,r[\text{Bytes/hour/km}^2]} = \sum_{bs=1}^{N_{BS,r}} \frac{C_{bs,r[\text{Bytes/hour}]}}{Cov_{bs,r[\text{km}^2]}}, \tag{2.14}$$

where $C_{bs,r}$ is the RAN r BS capacity and $Cov_{bs,r}$ is the BS coverage area.

After capturing the traffic generated by users and the network capacity, it is important to establish a link to JRRM QoS parameters. However, an analytical model to capture the overall heterogeneous network performance at JRRM level is not straightforward, since the intermediate steps are complex and usually obtainable only by simulation approaches. Nevertheless, a simplistic approach to this problem needs to capture the relation between traffic generation and network capacity, similar to an Erlang-B model relation. Using this model/ratio, it is possible to roughly predict the network blocking probability. To compute this relation, a shape correction parameter B_α was defined to obtain the JRRM blocking probability (matching or following Erlang's traffic tables), P_B, taking as input the users' multi-service traffic generation density $T_{\rho N}$, over the heterogeneous traffic capacity density, T_{CN}.

$$P_{B[\%]} = \left(\frac{T\rho_N}{T_{CN}}\right)^2 B_\alpha \tag{2.15}$$

For computing P_B, based on $T_{\rho N}/T_{CN}$., it was required a non linear correction parameter B_α. This parameter is needed to introduce the traffic channels efficiency effect. Thus, P_B follows the Erlang–B model trend, Figure 2.5 a).

For computing the JRRM delay τ_{Cd}, Figure 2.5 b), based on $T_{\rho N}/T_{CN}$, a similar approach was taken, thus, a non linear correction parameter D_α, was also defined.

$$\tau_{Cd[\text{s/packet}]} = \left(\frac{T\rho_N}{T_{CN}}\right)^2 D_\alpha \tag{2.16}$$

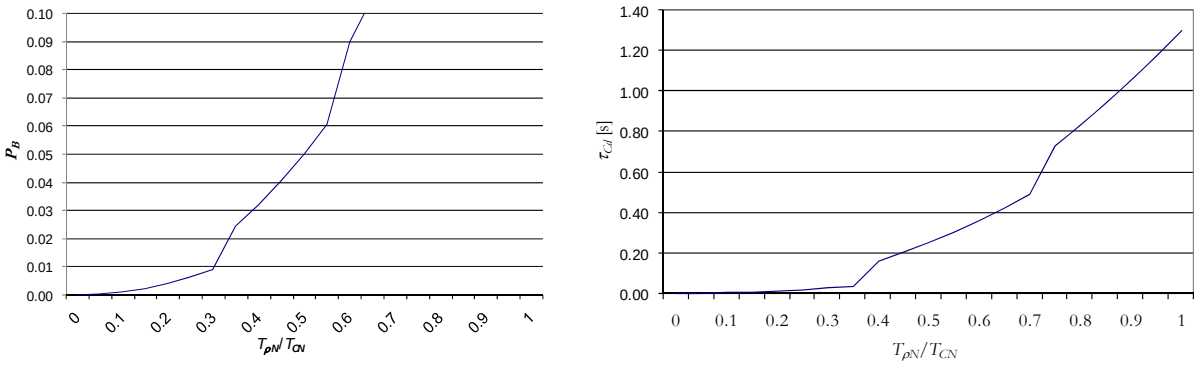

a) b)

Figure 2.5 – Blocking probability and delay as function of traffic generation density and network capacity density ratio

In Table 2.6, both B_α and D_α values are defined. These were obtained by curve fitting by minimizing the error with Erlang-B curves.

Table 2.6 – Shape values for Bα and Dα

$T_{\rho N}/T_{CN}$	≤0.3	0.3< ≤0.55	0.55< ≤0.85	0.85<
B_α	0.1	0.2	0.25	0.3
$T_{\rho N}/T_{CN}$	≤0.4	0.4< ≤0.7	0.7<	NA
D_α	0.3	1	1.3	

Generally for each individual RAN *r,* it is also possible to compute blocking probability and delay, which are based on each RAN traffic. The multi-service generated traffic density $T_{\rho N,r}$ and RAN capacity density $T_{CN,r}$, are used to compute $P_{B,r}$ and $\tau_{d,r}$, according to the following:

$$P_{B,r}[\%] = \left(\frac{T\rho_{N,r}}{T_{CN,r}} \right)^2 B_\alpha \tag{2.17}$$

$$\tau_{d,r}[\text{s/packet}] = \left(\frac{T\rho_{N,r}}{T_{CN,r}} \right)^2 D_\alpha \tag{2.18}$$

Based on the previous assumptions and parameters, it is possible to produce several other output parameters by computing and/or combining with other interesting parameters/models available in literature, like for example, the horizontal cell crossing rate η_{HHOr}, presented in [8] and defined by (4.16). Hexagonal cells, and uniformly distributed directions of movement in 2π are assumed.

$$\eta_{HHO_r[/s]} = \frac{4\overline{v_r}}{\sqrt{3}\pi R_r} \tag{2.19}$$

being $\overline{v_r}$ the average speed and R_r the cell radius of a given RAN type *r*.

Using the cell crossing rate it is possible to compute the number of HHOs, N_{HHOr}, in a given RAN *r* and time interval Δt,

$$N_{HHO_r} = \eta_{HHO_r[/s]} \cdot N_{AU_r} \cdot \Delta t_{[s]} \cdot P_{CHr} \tag{2.20}$$

where P_{CHr} is the JRRM influence in the number of HHOs and N_{AUr} is the number of active users attached to a given RAN *r*.

The drop probability P_D, (handover calls) is computed according to (2.19) where network equilibrium is assumed (cell handover incoming rate equal to outgoing rate).

$$P_D = \frac{P_H P_{HF}}{1 - P_H \left(1 - P_{HF}\right)} \tag{2.21}$$

P_{HF} is the handover failure probability (HHO calls) assuming that new calls and handover ones are processed in a same way, then P_{HF}=P_B is also assumed. P_H, is the handover probability computed as follows:

$$P_H = \frac{\eta_{HHO_r}}{\frac{1}{\tau_s} + \eta_{HHO_r}} \tag{2.22}$$

Another interesting parameter is the HHO calls average arrival rate, λ_h, computed as follows:

$$\lambda_h = \frac{P_H(1 - P_B)}{1 - P_H(1 - P_{HF})} \lambda_s \tag{2.23}$$

Scanning the literature concerning VHOs, it is not easy to find simple models capable of extracting the main characteristics of a VHO process assuming the presence of multiple RANs. However, it is very useful to setup a simple approach/model to extract theoretical VHO related parameters. One proposal is to assume that a given RAN type cluster, Figure 2.6, can be modelled as a single cell. This assumption, enables the use of the previous model mechanism (established for dealing with HHOs) to extract some VHOs assumptions and theoretical results. This means that users' previous cell transitions are now translated to transitions between RANs (clusters based). In order to group RANs into coverage and Bit rate families, it was defined the Low-, Medium- and High-, Bit rate Networks (LBN, MBN, HBN), where one can map for example with UMTS R99, R5 and WLANs respectively.

Based on the previous assumptions one can define several parameters for VHO studies. For example, the *r* RAN crossing rate or VHO crossing rate η_{VHOr}, assumes RAN clusters' distributions similar to the case presented by Figure 2.6, where different RANs have different levels of coverage and cluster radius, thus in some RANs service continuity can be only provided by other RANs. To compute η_{VHOr}, the previous assumptions are also assumed, like user uniformly distributed directions of movement in 2π, where η_{VHOr} is defined by,

$$\eta_{VHO_r[/s]} = \frac{4\overline{v_r}}{\sqrt{3}\pi R_{rc}} \tag{2.24}$$

where R_{rc} is the RAN cluster approximated radius.

The number of VHOs in a given JRRM scenario, and time interval Δt, is given by,

$$N_{VHO_r} = \eta_{VHO_r[/s]} \cdot N_{AU_r} \cdot \Delta t_{[s]} \cdot P_{CVr} \tag{2.25}$$

where P_{CVr} is the JRRM influence in the number of VHOs.

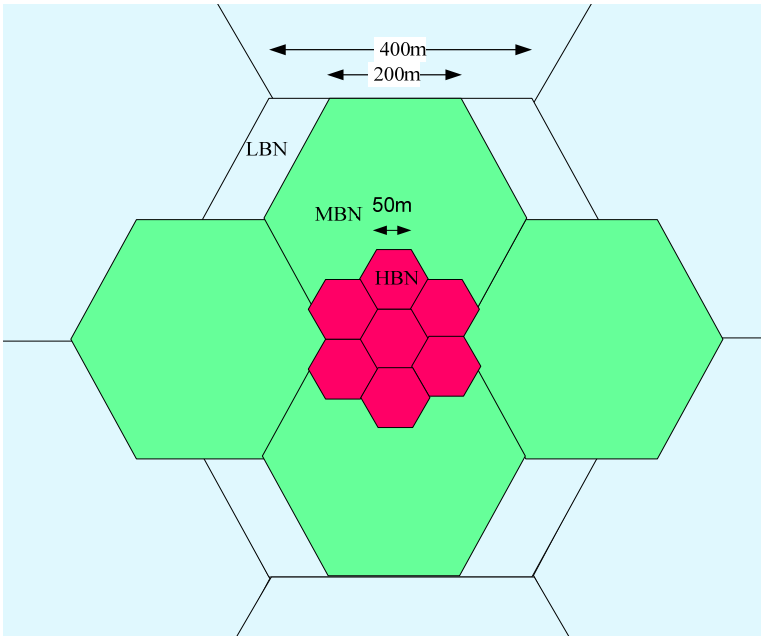

Figure 2.6 – Different RAN clusters (example)

Similar to HHOs, the VHO drop probability P_{VD}, (VHO calls) is computed, where users mobility equilibrium is again assumed. For the VHO failure probability P_{VHF}, P_B was again assumed.

$$P_{VD} = \frac{P_{VH} P_{VHF}}{1 - P_{VH}\left(1 - P_{VHF}\right)} \tag{2.26}$$

The VHO probability $P_{VH,r}$ for a given RAN r, can be now estimated as follows:

$$P_{VH,r} = \frac{\eta_{VHO_r}}{\frac{1}{\tau_s} + \eta_{VHO_r}} \tag{2.27}$$

For the VHO calls average arrival rate, λ_{vh} is computed as follows:

$$\lambda_{vh} = \frac{P_{VH}(1 - P_B)}{1 - P_{VH}(1 - P_{VHF})} \lambda_s \tag{2.28}$$

2.2.5 Theoretical Scenarios

In order to present some possible results produced by the previous model, one has to decide which are the most relevant and interesting ones, as output and input parameters. Since the focus of this activity is JRRM performance, then, the overall JRRM QoS and VHOs related parameters in the model should be the most explored ones. Therefore, as outputs one has: JRRM bit rate Rb_t, average user bit Rb_u, blocking P_B, delay τ_{Cd}, users capacity density ρ_{AU}, RANs VHO related probabilities and PSNR in case of video streaming transmission. For scenario inputs' variation one considers the following parameters: users' speed profile penetration, services centric (packet switch-PS or circuit switch-CS), relatively RANs clusters coverage size, the number of BSs, service penetration ratio (CS/PS), Initial JRRM traffic distribution and VHO traffic percentage flow among RANs. The IST-AROMA project reference scenario [9], is used as starting point for some parameters, namely service traffic generation.

In the following lines, a set of scenarios is taken into account to evaluate the influence of each input parameter on the overall QoS:

2.2.5.1 Users' Mobility Profile

To evaluate the impact of users' mobility profiles onto VHOs, high and low mobility trends were defined, as shown by Table 2.7. Note that fast, slow and static users correspond to vehicular, pedestrian and indoor users.

Table 2.7 – Users' Mobility Profile Scenarios

		Mobility		
		Fast	Slow	Static
Speed [km/h]		50	3	0
Users' speed profile penetration [%]	High Mobility (HM)	35	30	35
	Medium Mobility (MM)	15	25	60
	Low Mobility (LM)	5	10	85

2.2.5.2 Services' Switching Type Variation

To better understand the impact that services' penetration has on the network, one defines a few trends where CS and PS centric service trends can be compared with the reference one. Session arrival rates for CS and PS oriented services are defined according to Table 2.8. Note that the network session arrival rate is not fully in equilibrium due to individual service penetration rates. This naturally, leads to more or less users using a giving service group. Thus, the effective session generated by each switching group is not balanced, leading to a non linear number of users for each service group. Nevertheless, Table 2.8 presents service trends (CS or PS centric) providing the capability to compare the impact on the different JRRM QoS parameters. The values presented are applied in all services of each switching group.

Table 2.8 – Service Switching group trends

	Services group (arrival rate [session/hour])	
	Circuit Switch (CS)	Packet Switch (PS)
CS – Centric	1.5	0.5
Ref.	1.0	1.0
PS – Centric	0.5	1.5

2.2.5.3 RANs Clusters Coverage

Concerning the RAN cluster radius variation and their impact on VHOs, one can use a relative size as reference point, and then increase or decrease the overall cluster radius on each RAN. Therefore, besides the reference one, two other different coverage sizes were defined: HCov, MCov and LCov scenarios, standing for high, medium and low coverage, respectively. The HCov corresponds to the cluster radius size duplication, and LCov for half size when compared with the reference one.

2.2.5.4 Cellular Coverage Trend

To access the impact that a cellular structure trend has on the VHO probability, three scenarios were defined: the Macro-, Ref. and Micro-centric, Table 2.9, presenting the number of BSs for each RAN/cluster in each scenario.

Table 2.9 – Scenario Set for Cellular Coverage Trend

	Number of BSs		
RAN	Micro - Centric	Ref.	Macro – Centric
LBNs	1	2	4
MBNs	8	4	2
HBNs	14	7	4

2.2.5.5 Cellular Coverage Trend Service Penetration Variation

To evaluate the impact that service penetration has on the JRRM overall parameters, three different service penetration profiles were defined, as in Table 2.10. CS and PS services can have different penetration rates. However, the sum is 100%, and their combination can be defined in order to produce a CS/PS ratio (2, 1 and 1/2), which can be used to understand their influence on JRRM QoS parameters.

Table 2.10 – Service Penetration Ratio Scenarios Set

CS/PS		2	1	½
Voice	CS	0.58	0.45	0.30
Video-telephony		0.09	0.05	0.03
Streaming	PS	0.09	0.14	0.20
FTP		0.06	0.10	0.15
E-mail		0.09	0.13	0.17
WWW		0.09	0.13	0.15

2.2.5.6 JRRM Theoretical Parameters' Variation

The model includes two JRRM parameters, $P_{Init,r}$ and P_{VHO}, which aim to simulate the traffic distribution and JRRM influence policy, and the service priority policy influence on the BS selection procedure respectively. Taking into account the first one, it is possible to setup some distribution percentages over the generated traffic and delivered to the correspondent RAN, enabling the QoS evaluation in each RAN. Table 2.11 presents two scenario variations over the reference one (LBN – Centric and HBN – Centric). These variations are useful to understand the impact of traffic distribution in each RAN QoS. The LBN (one single BS in cluster), will be the RAN type that will have more difficulties to observe high levels of traffic since compared with other RANs it provides low capacity and high coverage. Therefore, LBN related traffic percentage distributed by the JRRM entity should be low, to keep LBN QoS indicators under control.

The second parameter P_{VHO} proposed by the model, is related to VHO traffic transfer among RANs. Similar to previous cases, in Table 2.12 it is presented some traffic transfer variations among LBN, MBN and HBN. Again, these traffic scenario variations take the same name as in the previous case. Basically the idea is to transfer traffic from one RAN to another; however, these transfer percentages

have a physical limit, which is related to geographical superposition among RAN clusters. The VHO transfer rule, if negative, means that traffic flow will be the opposite with respect to the one symbolised by the arrow.

Table 2.11 – JRRM traffic distribution variation scenarios

	JRRM traffic distribution [%]		
RAN	LBN - Centric	Ref.	HBN – Centric
LBN	10	7	4
MBN	60	45	35
HBN	30	48	61

Table 2.12 – JRRM VHOs strategies scenarios

	JRRM VHOs [%]		
VHO Rule	LBN - Centric	Ref.	HBN – Centric
LBN→MBN	-10	0	10
MBN→HBN	-5	0	5

2.2.6 Theoretical Results

Based on the previous scenarios' set, the model is capable of producing a considerable number of different results, however, for space and readability reasons a selection of the most relevant ones are presented in the next sub-sections.

2.2.6.1 Users' Mobility Profile Impact

For the High Mobility (HM) profile, the VHO probability reaches 66% for HBNs and 39% for MBNs, as shown in Figure 2.7. This means that users in a HM profile and those attached to HBNs will most probably experience a VHO to another RAN. For MBN, this probability is relatively smaller, since the MBNs' coverage is higher and users will spend more time crossing a MBN cluster.

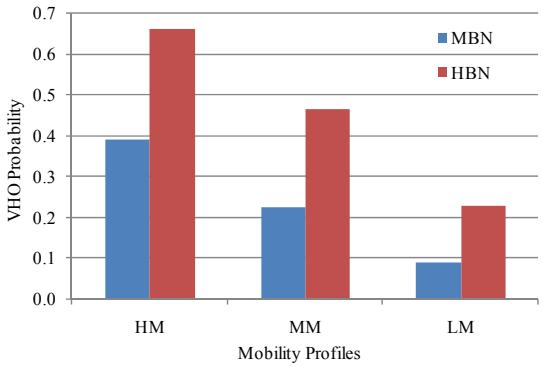

Figure 2.7 – Mobility profiles impact on VHOs probability for MBN and HBNs

These results are very useful for JRRM designers, since they give an estimate of VHO overhead knowing the scenario mobility profile. For example a train station or business city centre will have different mobility profiles, giving different impacts on the JRRM signalling overhead on VHO

processes. The crossing rate results follows the VHO probability, being both useful to estimate the VHO load, which is interesting to estimate signalling load at JRRM level.

2.2.6.2 Services Penetration Trend Impact

The users' capacity density, which is the network equivalent number of active users per km^2, represents the heterogeneous network capacity for processing users' sessions for a given network QoS level. Figure 2.8 presents the model results for the different switching group ratio (CS/PS). One can see that, for PS-Centric, the number of users is smaller compared to the CS-centric case. This is due to the fact that usually CS-Centric based services (voice and video telephony) have effective longer sessions. Thus, the number of active users in the network will be higher, compared to the PS-Centric case.

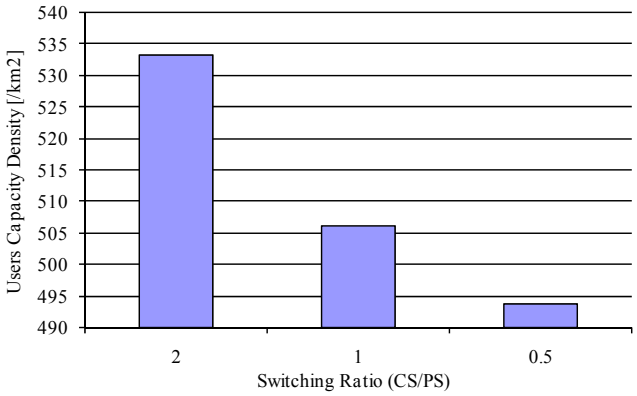

Figure 2.8 – Users capacity density as function switching type ratio

2.2.6.3 RANs Clusters Coverage Impact

Concerning RANs' Cluster radius impact on VHOs, it is expected that HBNs are more susceptible of having more VHOs, as shown in Figure 2.9. In the HCov scenario, the VHO probability is lower, because the clusters sizes are higher, therefore users' cluster cross events are less frequent, because they spend a longer time inside a given cluster's (RAN type) borders.

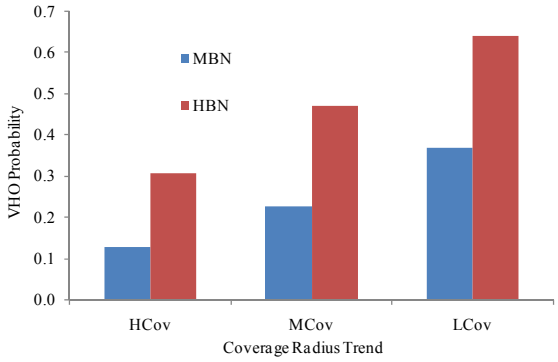

Figure 2.9 – VHO Probability as a function of coverage size

Note that in the case of LBNs, they have adjacent and continuous coverage, therefore it does not make sense presenting VHO probability, but rather HHO probability.

2.2.6.4 Cellular Coverage Trend Impact

In Figure 2.10, MBNs and HBNs have an increasing VHO probability when coverage moves to the Macro-centric case, since they decrease their relative area in the cluster, having less users staying

inside their coverage. Thus, MBNs and HBNs will have more crossing users to other RANs. The Macro-Centric scenario is dominated by LBN coverage.

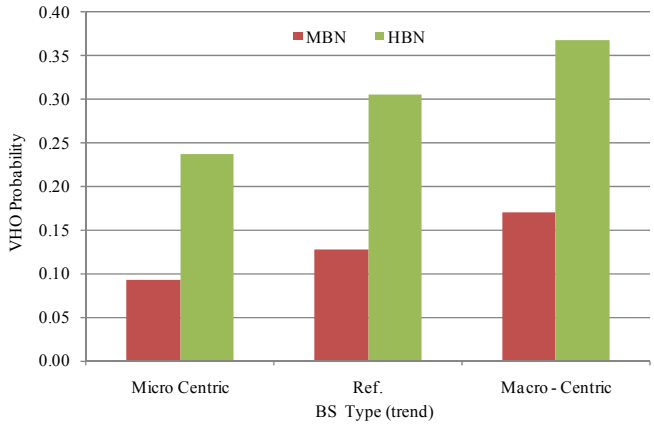

Figure 2.10 – VHO Probability as a function RANs clusters sizes

2.2.6.5 Service Penetration Variation

According to Figure 2.11, the JRRM delay results for CS/PS=2 ratio produce much less JRRM delay compared to the CS/PS=½ ratio case. Note that delay starts on 30ms and goes up to 200ms (which in most cases is an unacceptable value). Thus, one concludes that PS based services' dominance in the network produces very high delays, leading to a very poor network quality. This is observed because PS services take/use more radio resources from the available RANs (e.g. radio channels or bandwidth).

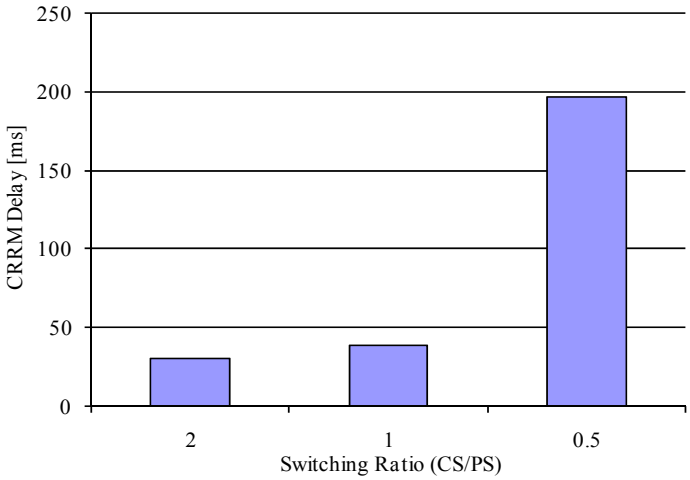

Figure 2.11 – Services penetration ratio impact on JRRM Delay

2.2.6.6 JRRM Theoretical Parameters' Impact

This sub-section presents the JRRM theoretical parameters' variation results. These are presented observing simultaneously two dimensions, one dimension is the initial traffic and the second is the VHO policy percentage distribution variation/trend. These variations are performed according to Table 2.11 and Table 2.12 parameters, expecting to have significant and different impacts on RANs' QoS indicators. These results are presented and discussed bellow.

In Figure 2.12, it is possible to observe the LBN blocking probability variation. The worst case, from the LBN view perspective, is when initial traffic distribution and VHO policy push traffic to LBNs

(LBN-Centric) in both axels, leading LBN blocking probability to about 13%. It is also possible to observe that initial traffic distribution have more influence when compared with the VHO variation policy. This is because the VHO percentage has less freedom on amplitude range. The best case is when initial distribution tends to HBN-Centric, in this situation LBN initial traffic percentage will move from 10 to 4% of the total generated traffic. Though this seams a small variation, with 4% LBN will handle less than 50% previous case (LBN-Centric), leading the LBN blocking probability to be less than 1%.

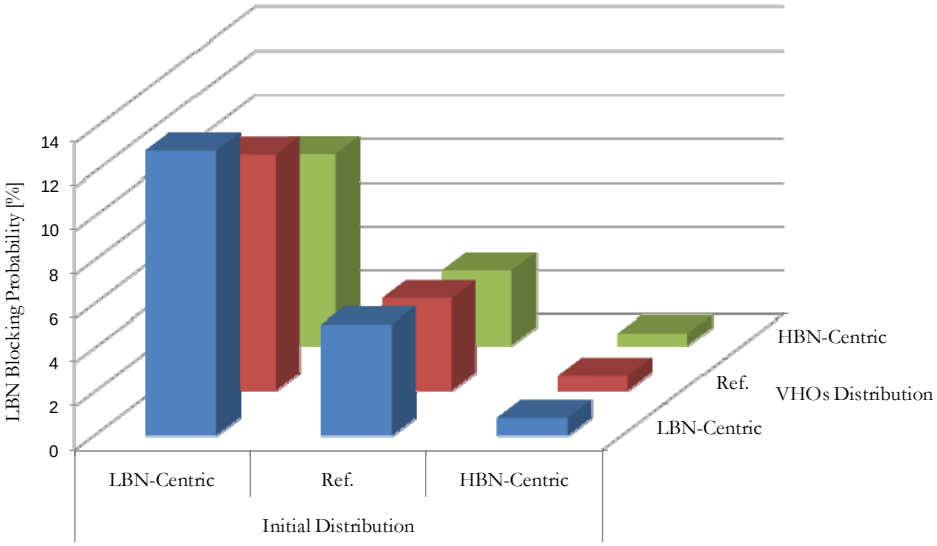

Figure 2.12 – JRRM policies impact on LBN Blocking

Other QoS indicator is delay, Figure 2.13 presents results for LBNs and here, similar to P_B, delay presents parallel trend. However, note that delay values for LBN are only "acceptable" when HBN-Centric case is plotted, this means that offered traffic to LBN should be less in order to reach the delay values set by services' constrains.

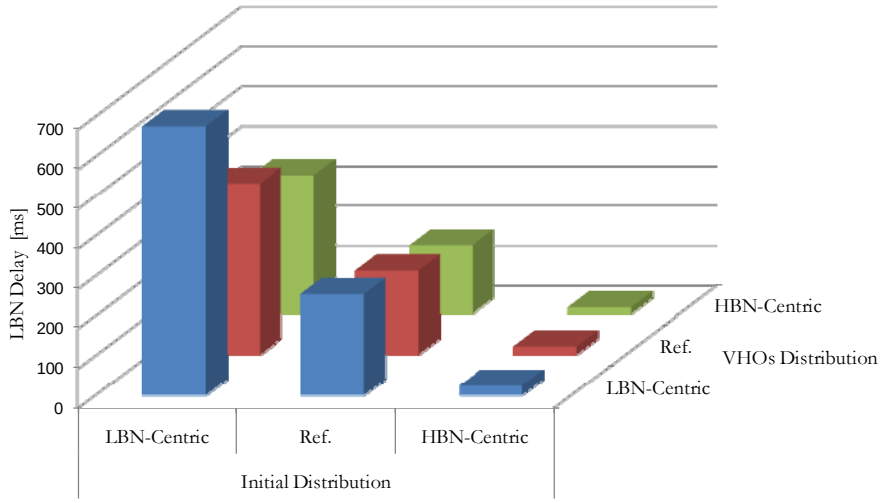

Figure 2.13 – JRRM policies impact on LBN Delay

2.3 Spectrum Allocation for OFDMA Networks

2.3.1 Single-Cell Studies

The wireless shared channel in cellular networks is a medium over which many Mobile Terminals (MTs) compete for resources. In such a scenario, spectral efficiency and fairness are crucial aspects for resource allocation. From a cellular operator perspective, it is very important to use the channel efficiently because the available frequency spectrum is scarce and the revenue must be maximized. From the users' point of view, it is more important to have a fair resource allocation so that they can meet their Quality of Service (QoS) requirements and maximize their satisfaction. The time-varying nature of the wireless environment, coupled with different channel conditions for different MTs, poses significant challenges to accomplishing these goals. In general, these objectives cannot be achieved simultaneously and an efficient trade-off must be achieved. In recent years Radio Resource Management (RRM) has been envisaged as one of the most efficient techniques to achieve a desirable trade-off among these two conflicting objectives in cellular multi-carrier systems.

Many next generation wireless systems are based on Orthogonal Frequency Division Multiple Access (OFDMA), which provides a high degree of flexibility that can be exploited by RRM algorithms. There are different sources of diversity in an OFDMA-based system, such as time, frequency and multiuser diversities. Following the path opened by the seminal article by Wong et al. [10], many Radio Resource Allocation (RRA) algorithms have been proposed to take advantage of these kinds of diversity, such as the dynamic allocation of subsets of sub-carriers for different MTs (Dynamic Sub-carrier Assignment (DSA)), and the adaptation of the Modulation and Coding Scheme (MCS) and power for each sub-carrier according to the instantaneous channel conditions (bit and power loading). Furthermore, Packet Scheduling (PSC) algorithms are responsible for deciding when the MTs will access the shared channel and with which transport format depending on the Channel State Information (CSI).

Many separate or joint RRA solutions including DSA, bit loading and power loading were based on combinatorial optimization. Most of the works in literature follow either the margin adaptive approach, formulating dynamic resource allocation with the goal of minimizing the transmitted power with a rate constraint for each user [11], or the rate adaptive approach aiming at maximizing the overall rate with a power constraint [12], [13]. In this latter case, the optimal solution for resource allocation in the downlink is often found as an application of the well-known waterfilling algorithm.

On the other hand, many works have been using Utility Theory to propose solutions for all the aforementioned RRA algorithms, including also multi-carrier PSC. The issues of efficiency, fairness and satisfaction of resource allocation have been well studied in economics, where utility functions are used to quantify the level of customers' satisfaction when the system allocates certain resources to them. Utility theory performs the optimization of a utility-pricing system, which is established based on the mapping of some performance criteria (e.g. rate, delay) or resource usage (e.g. sub-carriers, power) into the corresponding pricing values [14].

In this work, we will focus on the provision of Non-Real Time (NRT) services, such as World Wide Web (WWW) browsing, and Real-Time (RT) services, such as Voice over IP (VoIP). For the NRT services, the data rate is the most important QoS metric. The optimization problem can be formulated based on instantaneous or average data rates. The former case is stricter because QoS and fairness has to be guaranteed in each Transmission Time Interval (TTI), while the time window considered in the optimization problem based on average data rates adds a time diversity that relax the requirements on QoS and fairness. On the other hand, the delay metric is the most relevant aspect for the QoS of RT services.

The present work will be divided in two parts. In the first part, we will study rate adaptive sub-carrier and power allocation using optimization based on instantaneous data rates for Non-Real Time (NRT) services. In the second part, we will study multi-carrier packet scheduling using utility functions based on average data rates or delay for NRT or Real-Time (RT) services, respectively. The objective of the

paper is to study the trade-off between system spectral efficiency and fairness among the users when the RRM algorithms mentioned above are used.

2.3.1.1 System Model

The considered scenario is a single cell with hexagonal shape. We consider a network with one transmitter (base station) and J receivers (users). The transmitted Orthogonal Frequency Division Multiplexing (OFDM) signal is time slotted, where in every time slot at most one user can be served over each sub-carrier. The considered environment is Typical Urban (TU) [15] where each user experiences independent transmit conditions. The channel is a frequency-selective Rayleigh fading channel, with the coherence time such that each sub-carrier experiences only flat fading. It is assumed that the channel fading rate is slow enough so that the frequency response does not change during a TTI interval. Each user also experiences shadowing with log-normal distribution. A perfect knowledge of the CSI at the transmitter side is assumed, with no signalling overhead transmitted. The signal strength at the receiver side depends on the path-loss calculated by:

$$L = 128.1 + 37.6 \log_{10} d \tag{2.29}$$

where d is the distance to the base station in km.

The bit allocation on each sub-carrier is determined using the Shannon's capacity model shown in (2.30) below [14]:

$$c_{j,k} = \log_2\left(1 + \Gamma p_k \rho_{j,k}\right) \tag{2.30}$$

where $c_{j,k}$ is the achievable transmission rate in bits/s/Hz of user j over subcarrier k, p_k is the transmit power allocated at sub-carrier k, $\rho_{j,k}$ is the Gain-to-Noise Ratio (GNR) of user j at subcarrier k, and Γ is the SNR gap given by $\frac{1.5}{-\ln 5BER}$ [14] (the considered target Bit Error Rate (BER) was 10^{-6}).

Assuming discrete modulation levels {0, 2, 4, 6, ...}, the achievable transmission rate in bits/s/Hz of the k-th sub-carrier assigned to the j-th MT is given by:

$$c_{j,k} = 2\left\lfloor \frac{1}{2}\log_2\left(1 + \Gamma p_k \rho_{j,k}\right) \right\rfloor \tag{2.31}$$

where $\lfloor x \rfloor$ is an operator that returns the largest integer less than x.

Once we have the achievable transmission rate per Hertz of each sub-carrier, the data transmission rate of each MT can be calculated. In the sub-carrier allocation process, we assume that each sub-carrier can only be assigned to one single MT. Assuming that a sub-carrier set Ψ_j is assigned to the j-th MT, its transmission rate is calculated as:

$$r_j = \sum_{k \in \Psi_k} r_{j,k} = \sum_{k \in \Psi_k} c_{j,k} \cdot \Delta f \tag{2.32}$$

where $c_{j,k}$ is the channel capacity per Hertz of the k-th subcarrier assigned to the j-th MT and Δf is the sub-carrier bandwidth.

It was assumed that the MTs remained stationary, hence there is no need to implement any handover scheme. All users are assumed to have an infinite amount of data to transmit during the whole simulation run (full-buffer model). For the case of RT service, which is a delay-sensitive service, we consider an infinite number of discrete packets of the same size with a given inter-arrival time.

Finally, the resource allocation information (sub-carrier assignment, modulation and coding schemes, etc.) is sent to each MT in a separate control channel, so that the MTs can decode the data in their own sub-carriers.

2.3.1.2 Sub-carrier and Power Allocation Based on Combinatorial Optimization

1) Algorithms Formulation

In this section, we present a study on Radio Resource Allocation (RRA) combinatorial optimization based on the rate adaptive approach aiming at maximizing the overall rate with a power constraint [12], [13].

Rate adaptive RRA often leads to algorithms whose implementation is very complex. In fact the allocation problem is in general not convex since the allocation variable is integer and can assume only two values: 1 when the channel is allocated to a specific user and 0 otherwise. In most cases the optimal solution can be found only evaluating all possible allocations and the complexity grows exponentially in the number of users and sub-carriers. Therefore, most of the literature has been focused on the development of sub-optimal heuristics that have a lower computational complexity but that still yield good results. Many algorithms make the problem convex by relaxing the integer constraint on the allocation variable. Unfortunately, non-integer solutions are hardly applicable in many scenarios where a sub-carrier should be actually allocated or not to a user. In the following we will focus on the RRA problem outlining its most common formulations and solutions.

Sum Rate Maximization

The most common mathematical formulation of the RRA problem is:

$$\begin{aligned} &\max_{p,x} \sum_j \sum_k c_{j,k} \cdot x_{j,k} \\ &s.t. \\ &\sum_j x_{j,k} \le 1, \quad \forall k \\ &\sum_j \sum_k p_{j,k} \le P_{\max} \\ &x_{j.k} \in \{0,1\}, \quad \forall j,k \end{aligned} \tag{2.33}$$

where $P_{\max}$ is the maximum allowed transmit power of the Base Station (BS). The optimization variables are $\boldsymbol{x}$, the vector of the allocations, and $\boldsymbol{p}$, the vector containing the power levels of all sub-carriers.

In its original formulation the problem (2.33) has been solved in [12] by assigning each sub-carrier to the user that maximizes its gain on it and then performing waterfilling over all the sub-carriers. On one hand, such a solution maximizes the cell throughput but on the other hand is extremely unfair tending to privilege the users that are closest to the BS and neglecting all the others.

Max-Min Rate Adaptive

The RRA allocation (2.33) tends to starve the users with the worse channel gains, i.e. the users that are more distant from the BS. Thus, in [13] the RRA problem has been formulated with the goal of maximizing the minimum capacity offered to each user, thus introducing fairness among the users. In general, fairness among the MTs comes at the cost of a decreased overall throughput of the cell. The max-min RRA problem is formulated as follows:

$$\begin{aligned} &\max_{p,x} \min_{j} c_{j,k} \cdot x_{j,k} \\ &s.t. \\ &\sum_{j} x_{j,k} \le 1, \quad \forall k \\ &\sum_{j} \sum_{k} p_{j,k} \le P_{\max} \\ &x_{j.k} \in \{0,1\}, \quad \forall j,k \end{aligned} \tag{2.34}$$

Unfortunately, the problem in the formulation (2.34) is not convex and the authors in [13] study an heuristic that is based on:

a) Transmitting the same amount of power ($P_{\max} / K$) on each channel;

b) Implementing an assignment strategy that iteratively assigns each sub-carrier to the user with the smallest rate.

Sum Rate Maximization with Proportional Rate Constraints

The max-min RRA (2.34) guarantees that all users achieve a similar data rate. However, different users may require different data rates. In this case the max-min solution is not able to comply with the different user requirements. The RRA algorithm presented in [16] is designed to allocate radio resources proportionally to different rate constraints that reflect different levels of service. The RRA problem is formulated as follows:

$$\begin{aligned} &\max_{p,x} \sum_{j} \sum_{k} c_{j,k} \cdot x_{j,k} \\ &s.t. \\ &\sum_{j} x_{j,k} \le 1, \quad \forall k \\ &\sum_{j} \sum_{k} p_{j,k} \le P_{\max} \\ &x_{j.k} \in \{0,1\}, \quad \forall j,k \\ &r_1 : r_2 : \ldots : r_J = \gamma_1 : \gamma_2 : \ldots : \gamma_J \end{aligned} \tag{2.35}$$

where r_j indicates the rate for user j, defined as $r_j = \sum_{k} c_{j,k} \cdot x_{j,k}$ and γ_j (j = 1, ..., J) is a set of predetermined values that are used to ensure proportional fairness among users. The optimization in (2.35) is a mixed binary integer programming problem and as such is in general very hard to solve. Thus, also in this case the problem is solved using a suboptimal heuristic and the optimization (2.35) is performed in two steps. In the first step, following the approach taken in [13], the sub-carriers are allocated trying to comply as much as possible with the proportional rate constraints and assuming a uniform power distribution. In the second step, having fixed the sub-carrier allocation, the power is distributed to the users so that the proportional rate constraints are met exactly.

2) Simulation Results

In this section the simulation-specific parameters as well as the simulation results are presented. The main simulation parameters are presented in Table 2.13.

The metrics used for evaluation and comparison of the investigated resource allocation algorithms were:

- Total cell throughput (resource allocation efficiency factor);
- Fairness index, according to (2.38).

Table 2.13 – Simulation parameters.

Parameter	**Value**
Number of cells	1
Maximum BS transmission power	1 W
Cell radius	500 m
MT speed	static
Carrier frequency	2 GHz
Number of sub-carriers	192
Sub-carrier bandwidth	15 kHz
Path loss	using (2.29)
Log-normal shadowing standard dev.	8 dB
Small-scale fading	Typical Urban (TU)
AWGN power per sub-carrier	-123.24 dBm
BER requirement	10−6
Link adaptation	continuous using (2.30)
Transmission Time Interval (TTI)	0.5 ms
Traffic model	Full buffer
Throughput filtering time constant (f_{thru})	50
Number of realizations for each point	500

In order to evaluate the fairness among the users in a scenario with NRT services, we define a fairness index ϕ_j^{NRT} , which is based on throughput and calculated for each MT in the cell. The user fairness index changes with time and is defined as:

$$\phi_j^{NRT}[n] = \frac{T_j[n-1]}{T_j^{req}} \tag{2.36}$$

Where T_j^{req} is the throughput requirement of the *j*-th MT. The throughput $T_j[n]$ is calculated using a low-pass Simple Exponential Smoothing (SES) filtering as indicated in (2.37) [14].

$$T_j[n] = \left(1 - \frac{1}{f_{thru}}\right) \cdot T_j[n-1] + \left(\frac{1}{f_{thru}}\right) \cdot r_j \tag{2.37}$$

where r_j is the instantaneous transmission rate of the *j*-th MT given by (2.32) and f_{thru} is a filtering time constant. Next, we define a fairness index for the whole system, which is given by (2.38) [17].

$$\Phi^{NRT}[n] = \frac{\left(\sum_{j=1}^{J} \phi_j^{NRT}[n]\right)^2}{J \cdot \sum_{j=1}^{J} \left(\phi_j^{NRT}[n]\right)^2} \tag{2.38}$$

where J is the number of MTs in the cell and ϕ_j^{NRT} is the fairness index of the j-th MT given by (2.36). Notice that $\frac{1}{J} \le \Phi^{NRT} \le 1$. A perfect fair allocation is achieved when $\Phi^{NRT} = 1$, which means that the throughput allocated to all MTs are equally proportional to their throughput requirements (all user fairness indexes are equal). The worst allocation occurs when $\Phi^{NRT} = 1/J$, which means that all sub-carriers were allocated to only one MT.

For the sum rate maximization with proportional rate constraints two different sets of rate constraints have been studied: the case where the rate constraints are set equal for all users (Prop rate 1), i.e. $\gamma_j = 1$ (j = 1, ..., J), and the case where the rate constraints are set proportional to the user path loss (Prop rate 2).

Figure 2.14 shows the total cell throughput for the different algorithms: the sum rate maximization algorithm achieves the highest throughput and the max-min the lowest. The results show also the flexibility of the algorithm with proportional rate constraints. As expected, when the set of rate constraints are all equal its behaviour is almost identical to the max-min algorithm. On the other hand, when the system tends to favour the users nearer to the BS, the throughput approaches the sum rate results.

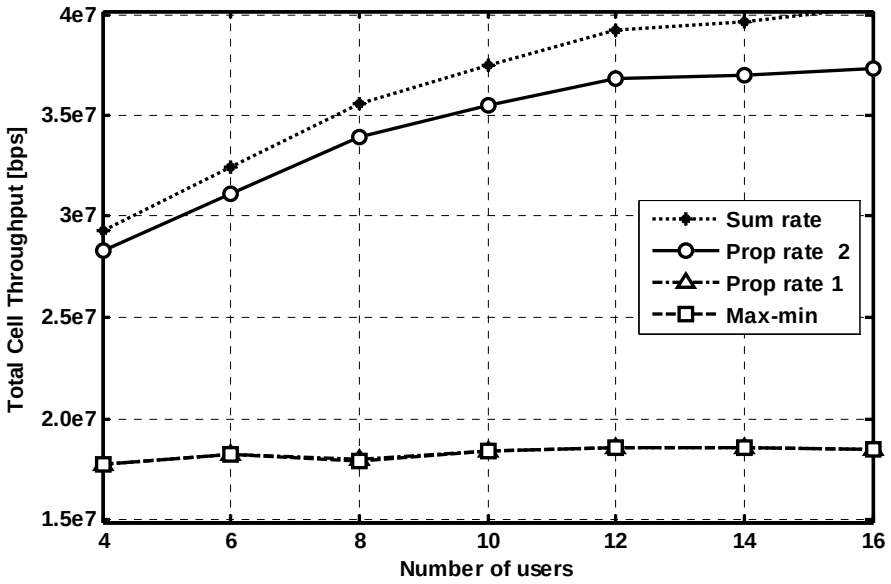

Figure 2.14 – Achievable throughput as function of the number of users.

Figure 2.15 shows the mean fairness index (according to the definition in (2.38)) for the various RRA algorithms. In this case the max-min and the algorithm with equal rate constraints outperform all the others. The algorithm with rate constraints proportional to the path loss, even if it guarantees access to all users, is not very fair. This is due to the fact that in our simulation setting, the difference in path loss can be several orders of magnitude large. Thus, users close to cell boundaries will have a much smaller throughput than users near the BS.

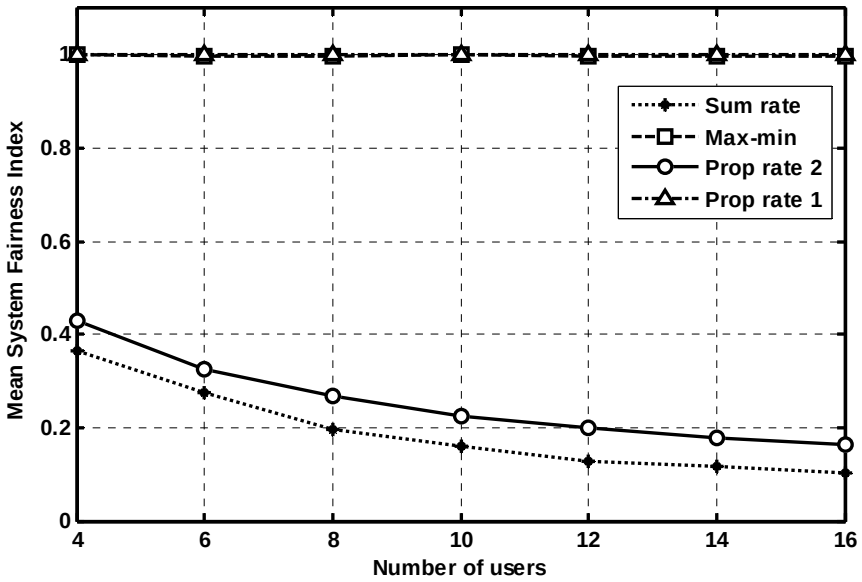

Figure 2.15 – Measured fairness as function of the number of users.

2.3.1.3 Packet Scheduling Based on Utility Theory

1) Algorithms Formulation for NRT Services

In this section we formulate PSC algorithms that use Utility Theory in order to find an efficient trade-off between system spectral efficiency and throughput-based fairness among MTs that use NRT services. The considered optimization problem is the maximization of the total utility with respect to the throughput (average data rate), which is calculated using a low-pass Simple Exponential Smoothing (SES) filtering as indicated in (2.39) [14].

$$T_j[n] = \left(1 - \frac{1}{f_{thru}}\right) \cdot T_j[n-1] + \left(\frac{1}{f_{thru}}\right) \cdot r_j \tag{2.39}$$

where r_j is the instantaneous transmission rate of the *j*-th MT given by (2.32) and f_{thru} is a filtering time constant.

Assuming that the time constant of the exponential filter is sufficiently large, it is proven in [14] that the DSA problem has a closed form solution. The MT j^* is chosen to transmit on the *k*-th sub-carrier in TTI *n* if it satisfies the condition given by (2.40):

$$j^* = \arg\max_j \left\{U_j'\left(T_j[n-1]\right) \cdot c_{j,k}[n]\right\}, \quad \forall j \tag{2.40}$$

where $U_j'(\cdot)$ is the marginal utility of the *j*-th MT, $T_j[n-1]$ is the throughput of the *j*-th MT up to TTI $n-1$, and $c_{j,k}[n]$ denotes the instantaneous achievable transmission efficiency of the *j*-th MT on the *k*-th sub-carrier.

We will consider a family of utility functions of the form presented in (2.41) below [18].

$$U_j\left(T_j[n]\right) = \frac{T_j[n]^{1-\alpha}}{1-\alpha} \tag{2.41}$$

where α is a non-negative parameter that determines the degree of throughput-based fairness. The fairness of the utility function becomes stricter as α increases.

According to (2.40), this is equivalent to consider a priority function of the PSC algorithm given by:

$$P_{j,k}^{PSC} = \frac{c_{j,k}[n]}{T_j[n-1]^{\alpha}}, \quad \forall j,k; \quad \alpha \in [0,\infty) \tag{2.42}$$

For each of the *K* sub-carriers in the system, a multi-carrier PSC algorithm calculates the priority functions for all *J* MTs according to (2.42) and assigns it to the MT that has the highest priority value.

We will show in the following that, depending on the value of the parameter α, the general utility framework presented above can be designed to work as any of three well-known classical PSC algorithms: Max-Rate (MR), Max-Min Fairness (MMF) and Proportional Fairness (PF). Furthermore, we present the Adaptive Throughput-Based Fairness (ATF) PSC algorithm, which can achieve an adaptive trade-off between spectral efficiency and throughput-based fairness according to the cellular operator's objectives.

Max-Rate

The MR PSC algorithm is able to maximize the system spectral efficiency because it considers a linear utility function $U_j(T_j[n]) = T_j[n]$, which yields a constant marginal utility $U_j'(T_j[n]) = 1$ [14]. One can notice that this can be achieved setting $\alpha = 0$ in (2.41). According to (2.42), this is equivalent to consider a priority function related to the MR algorithm given by (2.43) below.

$$P_{j,k}^{MR} = c_{j,k}[n], \quad \forall j,k \tag{2.43}$$

As the final result, each sub-carrier will be assigned to the MT that has the highest channel gain on it. The MR criterion maximizes the system capacity at the cost of unfairness among the MTs, because those with poor radio link quality will probably not have chance to transmit.

Max-Min Fairness

The utility function of the MMF algorithm is the limit of the function in (2.41), when $\alpha \to \infty$ [18]. According to (2.41) and (2.42), the priority function is dependent on the marginal utility $U_j'(T_j[n])$ and the achievable instantaneous transmission efficiency $c_{j,k}[n]$. However, in the case of the MMF criteria and when considering MTs with lower data rates, the influence of the marginal utility when $\alpha \to \infty$ is so high that the influence of the channel quality becomes negligible. Taking this fact into account, we can assume a more simplified priority function for the MMF algorithm given in (2.44), which is also known in the literature as the "Fair Throughput" criterion [19].

$$P_{j,k}^{MMF} = \frac{1}{T_j[n-1]}, \quad \forall j,k \tag{2.44}$$

which gives priority to the MT that has experienced the worst throughput so far. In this way, in terms of throughput, it is the fairest criterion possible, since all MTs will have approximately the same throughput in the long-term. However, since this criterion maximizes the throughput of the worst MTs, it will provide low aggregate system throughput.

Proportional Fairness

A trade-off between spectral efficiency and fairness can be achieved by means of a PF PSC algorithm [20]. In utility theory, the logarithmic utility function is associated with the proportional fairness [14]. In the general family of utility functions presented in (2.41), the logarithmic function can be achieved when $\alpha \to 1$ (see proof on [18]). Therefore, according to (2.42), the priority function of the PF algorithm is given by (2.45).

$$P_{j,k}^{PF} = \frac{c_{j,k}[n]}{T_j[n-1]}, \quad \forall j,k \tag{2.45}$$

Adaptive Throughput-Based Fairness

The ATF PSC algorithm, which was proposed in [21], joins in a unified framework the three aforementioned classical PSC algorithms (MR, MMF and PF). In the light of utility theory, it was shown that a general PSC algorithm based on (2.41) is able to provide several degrees of fairness. The ATF algorithm adaptively explores this flexibility in order to achieve an efficient trade-off between spectral efficiency and throughput-based fairness planned by the network operator. However, it is difficult to design an adaptive control of the parameter α because it is defined over a large range of values. Instead of that, the ATF algorithm transforms the priority function of (2.42) into another priority function that is based on a parameter β, which is defined over a controlled range and provides the possibility of a stable and simple adaptive control. The priority function of the ATF algorithm is presented in (2.46) below.

$$P_{j,k}^{ATF} = \frac{c_{j,k}[n]^{1-\beta}}{T_j[n-1]^{\beta}}, \quad \forall j,k; \quad \beta \in [0,1] \tag{2.46}$$

Notice that in a conceptual point of view, the priority functions on (2.42) and (2.46) perform in the same way. The ATF algorithm is able to work as the classical PSC algorithms by means of the adaptation of the parameter β. The values of β = {0, 0.5, 1} corresponds to the MR, PF and MMF, respectively.

The ATF algorithm is based on the definition of a fairness index ϕ_j^{NRT}, which is based on throughput and calculated for each MT in the cell. The user fairness index changes with time and is defined as:

$$\phi_j^{NRT}[n] = \frac{T_j[n-1]}{T_j^{req}} \tag{2.47}$$

Where T_j^{req} is the throughput requirement of the *j*-th MT. Next, we define a fairness index for the whole system, which is given by (2.48) [17].

$$\Phi^{NRT}[n] = \frac{\left(\sum_{j=1}^{J} \phi_j^{NRT}[n]\right)^2}{J \cdot \sum_{j=1}^{J} \left(\phi_j^{NRT}[n]\right)^2} \tag{2.48}$$

where *J* is the number of MTs in the cell and ϕ_j^{NRT} is the fairness index of the *j*-th MT given by (2.47). Notice that $\frac{1}{J} \le \Phi^{NRT} \le 1$. A perfect fair allocation is achieved when Φ^{NRT} = 1, which means

that the throughput allocated to all MTs are equally proportional to their throughput requirements (all user fairness indexes are equal). The worst allocation occurs when $\Phi^{NRT} = 1/J$, which means that all sub-carriers were allocated to only one MT.

The objective of the ATF algorithm is to assure a strict fairness distribution among the MTs, i.e. the system fairness index $\Phi^{NRT}[n]$ must be kept around a planned value $\Phi^{NRT}_{t\arg et}$. Therefore, the ATF algorithm adapts the parameter β in the scheduling policy presented in (2.46) in order to achieve the desired operation point. In order to do that, the new value of the parameter β is calculated using a feedback control loop of the form:

$$\beta[n] = \beta[n-1] - \eta \cdot \left(\Phi^{NRT}_{filt}[n] - \Phi^{NRT}_{t\arg et}\right) \tag{2.49}$$

where $\Phi^{NRT}_{filt}[n]$ is a filtered version of the system fairness index using a SES filtering, $\Phi^{NRT}_{t\arg et}$ is the desired value for the index, and the parameter η is a step size that controls the adaptation speed of the parameter β. A SES filter, which is suitable for time series with slowly varying trends, was used to suppress short-run fluctuations and smooth the time series $\Phi^{NRT}[n]$.

2) Algorithms Formulation for RT Services

In this section we formulate PSC algorithms that use Utility Theory in order to find an efficient trade-off between system spectral efficiency and delay-based fairness among MTs that use RT services. The considered optimization problem is the maximization of the total utility with respect to the delay of the Head-of-Line (HOL) packet. The HOL delay can be calculated approximately by (2.50):

$$d_j^{HOL}[n] = d_j^{HOL}[n-1] + \frac{d_{TTI}\left(T_j[n-1] - r_j[n]\right)}{T_j[n-1]} \tag{2.50}$$

where $d_j^{HOL}[n]$ is the delay of the HOL packet of the *j*-th user, d_{TTI} is the duration of the Transmission Time Interval (TTI), $T_j[n-1]$ is the average data rate (throughput) up to the previous scheduling period given by (2.37) and $r_j[n]$ is the instantaneous achievable transmission rate given by (2.32). If the *j*-th user has not been served by any sub-carrier in the nth TTI, $r_j[n]$ is equal to zero.

Taking (2.50) into account, we can see that the derivative of $U_j\left(d_j^{HOL}\right)$ with respect to r_j can be expressed as:

$$\frac{\partial U_j}{\partial r_j} = \frac{\partial U_j}{\partial d_j^{HOL}} \cdot \frac{\partial d_j^{HOL}}{\partial r_j} = \frac{\partial U_j}{\partial d_j^{HOL}} \cdot \left(-\frac{d_{TTI}}{T_j}\right) \tag{2.51}$$

Since the TTI duration is sufficiently small, we can use the Lagrange theorem of the mean, which says that [22]:

$$\begin{aligned}
&\sum_{j=1}^{J} U_j\left(d_j^{HOL}[n]\right) - \sum_{j=1}^{J} U_j\left(d_j^{HOL}[n-1]\right) \\
&\approx \sum_{j=1}^{J} \frac{\partial U_j}{\partial r_j}|_{r_j=r_j[n-1]} \cdot \left(r_j[n] - r_j[n-1]\right) \\
&= -\sum_{j=1}^{J} \frac{\partial U_j}{\partial d_j^{HOL}} \cdot \frac{d_{TTI}}{T_j[n-1]} \cdot \left(r_j[n] - r_j[n-1]\right) \\
&= \sum_{j=1}^{J} \left| \frac{\partial U_j}{\partial d_j^{HOL}} \right|_{d_j^{HOL}=d_j^{HOL}[n]} \cdot \frac{d_{TTI}}{T_j[n-1]} \cdot \left(r_j[n] - r_j[n-1]\right)
\end{aligned} \tag{2.52}$$

Considering that $r_j[n-1]$ is known and fixed in the nth TTI, the optimization objective function can be further simplified and expressed as

$$\max \sum_{j=1}^{J} \left| \frac{\partial U_j}{\partial d_j^{HOL}} \right| \cdot \frac{r_j[n]}{T_j[n-1]} \tag{2.53}$$

Therefore, the DSA problem employs the following reasoning: the MT j^* is chosen to transmit on the *k*-th sub-carrier in TTI *n* if it satisfies the condition given by (2.54):

$$j^* = \arg\max_j \left\{ \left| U_j'\left(d_j^{HOL}[n-1]\right) \right| \cdot \frac{c_{j,k}[n]}{T_j[n-1]} \right\}, \ \forall j \tag{2.54}$$

where $U_j'(\cdot)$ is the marginal utility of the jth MT, $T_j[n-1]$ is the throughput of the *j*-th MT up to TTI n − 1, and $c_{j,k}[n]$ denotes the instantaneous achievable transmission efficiency of the *j*-th MT on the *k*-th sub-carrier.

We denote $U_j\left(d_j^{HOL}\right)$ as the utility function of the *j*-th MT when experiencing a HOL delay of d_j^{HOL}. It is clear that the longer the HOL delay a user experiences, the lower level of satisfaction the user has. Thus, we can assume that $U_j\left(d_j^{HOL}\right)$ is a decreasing and strictly concave function, which implies the derivative of $U_j\left(d_j^{HOL}\right)$, $\partial U_j\left(d_j^{HOL}\right)/\partial d_j^{HOL}$, is a negative and decreasing function. Hence, the higher priority value is obtained by the user experiencing the longer HOL delay.

We consider a family of utility functions of the form presented in (2.55) below:

$$U_j\left(d_j^{HOL}\right) = -\frac{\left(d_j^{HOL}\right)^{1+\delta}}{1+\delta} \tag{2.55}$$

where δ is a non-negative parameter that determines the degree of delay-based fairness. The fairness of the utility function becomes stricter as δ increases.

According to (2.54), this is equivalent to consider a priority function of the PSC algorithm given by:

$$P_{j,k}^{PSC} = \frac{c_{j,k}[n]}{T_j[n-1]} \cdot \left(d_j^{HOL}[n-1]\right)^{\delta}, \ \forall j,k; \ \delta \in [0,\infty) \tag{2.56}$$

For each of the *K* sub-carriers in the system, a multi-carrier PSC algorithm calculates the priority functions for all *J* MTs according to (2.56) and assigns it to the MT that has the highest priority value.

Reference DR9.2

We will show in the following that, depending on the value of the parameter δ, the general utility framework presented above can be designed to work as any of three well-known classical PSC algorithms: Proportional Fairness (PF), Delay-Based First In First Out (D-FIFO) and Modified Largest Weighted Delay First (M-LWDF). Furthermore, we present the Adaptive Delay-Based Fairness (ADF) PSC algorithm, which can achieve an adaptive trade-off between spectral efficiency and delay-based fairness according to the cellular operator's objectives.

Proportional Fairness

In the framework presented in (2.56), we can achieve a PF policy using a linear utility function $U_j\left(d_j^{HOL}\right) = -d_j^{HOL}$. One can notice that in this case the parameter δ was set to zero. Hence, we do not take into consideration the HOL delay d_j^{HOL} in the general priority function given by (2.56). For this reason, we expect that PF will not provide high delay-based fairness. On the other hand, PF is able to provide a good efficiency in the resource usage in a scenario with RT services, since the channel quality plays an important role on the PF priority function, which is shown again by (2.57) below.

$$P_{j,k}^{PF} = \frac{c_{j,k}[n]}{T_j[n-1]}, \quad \forall j,k \tag{2.57}$$

Delay-Based First In First Out

D-FIFO is the fairest algorithm in terms of delay because it gives priority to the MT with the highest HOL packet delay. This is achieved by considering a very large value for the parameter δ. When $\delta \to \infty$, one can see in (2.56) that the delay component $d_j^{HOL}[n-1]$ becomes much more prominent than the transmission efficiency or throughput components ($c_{j,k}[n]$ and $T_j[n-1]$, respectively). Taking this into account, we can simplify the priority function for the D-FIFO algorithm, which is commonly known as [23]:

$$P_j^{D-FIFO} = d_j^{HOL}[n-1], \quad \forall j \tag{2.58}$$

Notice that D-FIFO does not use CSI of the sub-carriers, ignoring the frequency diversity offered by the OFDMA system. Therefore, D-FIFO assumes a TDMA behaviour, giving to the user chosen for transmission at TTI *n* the right to transmit over all the sub-carriers. This strategy is not efficient in the resource usage, so it is expected to provide lower system throughput.

Modified Largest Weighted Delay First

If we consider a utility function of the form $U_j\left(d_j^{HOL}\right) = -\left(d_j^{HOL}\right)^2 / 2$, in other words setting $\delta = 1$, we have a priority function of the M-LWDF algorithm [24] given by (2.59) below.

$$P_{j,k}^{M-LWDF} = \frac{c_{j,k}[n]}{T_j[n-1]} \cdot d_j^{HOL}[n-1], \quad \forall j,k \tag{2.59}$$

Comparing (2.57), (2.58), and (2.59), one can notice that M-LWDF is a trade-off between PF and D-FIFO. In this way it should provide intermediate delay-based fairness and intermediate resource usage efficiency.

Adaptive Delay-Based Fairness

It was shown in the previous sections that the variation of the parameter δ provides the possibility to control the delay-based fairness for RT services. However, it is difficult to control this parameter because its range $[0,\infty)$ is very large. Instead of that, we propose the use of a new parameter τ defined over the range $[0,1]$, which is much easier to control. We proposed to change the general priority function given by (2.56) in order to use the new parameter τ, as can be seen in (2.60).

$$P_{j,k}^{PSC} = \left(\frac{c_{j,k}[n]}{T_j[n-1]} \right)^{1-\tau} \cdot \left(d_j^{HOL}[n-1] \right)^{\tau}, \ \forall j,k; \ \tau \in [0,1] \tag{2.60}$$

It is straightforward to notice that varying the values of the parameters δ and τ over their respective ranges in (2.56) and (2.60), provides the same trade-off balancing between system capacity and delay-based fairness.

The framework presented in (2.60) is general in the sense that depending on the value of τ, ADF works as any of the classical algorithms mentioned previously. The values of τ = {0, 0.5, 1} corresponds to the PF, M-LWDF and D-FIFO, respectively. Besides that, intermediate values correspond to hybrid versions of those PSC algorithms. However, our main objective is to adaptively control the parameter τ in order to find an efficient trade-off between efficiency in the resource usage and fairness in the distribution of delays.

In order to do that, we need first to calculate the delay-based fairness in the system. The ADF algorithm is based on the definition of a fairness index ϕ_j^{RT}, which is based on delay and calculated for each MT in the cell. The user fairness index changes with time and is defined as:

$$\phi_j^{RT}[n] = \frac{d_j^{buffer}[n]}{d_j^{req}} \tag{2.61}$$

Normally, the delay requirement of the *j*-th MT d_j^{req} is the same for all users of the same type and is equal to the delay budget of the RT service (maximum time that a packet can spend in the buffer before being discarded). $d_j^{buffer}[n]$ is the average delay of the packets in the buffer of the *j*-th MT and is calculated through a SES filtering in the following way.

$$d_j^{buffer}[n] = \left(1 - \frac{1}{f_{delay}} \right) \cdot d_j^{buffer}[n-1] + \frac{1}{f_{delay}} \cdot \overline{d_{j,inst}^{buffer}}[n] \tag{2.62}$$

where $\overline{d_{j,inst}^{buffer}}[n]$ is the instantaneous mean delay of all the packets present in the buffer of the *j*-th user at TTI *n*, and f_{delay} is a filtering time constant .

Next, we define a fairness index for the whole system, which is given by (2.63) [17].

$$\Phi^{RT}[n] = \frac{\left(\sum_{j=1}^{J} \frac{1}{\phi_j^{RT}[n]} \right)^2}{J \cdot \sum_{j=1}^{J} \left(\frac{1}{\phi_j^{RT}[n]} \right)^2} \tag{2.63}$$

where J is the number of MTs in the cell and ϕ_j^{RT} is the fairness index of the j-th MT given by (2.61). Notice that $\frac{1}{J} \le \Phi^{RT} \le 1$. A perfect fair allocation is achieved when $\Phi^{RT} = 1$, which means that the average packet delays of all MTs are equally proportional to their delay requirements (all user fairness indexes are equal). The worst allocation occurs when $\Phi^{NRT} = 1/J$, which means that all sub-carriers were allocated to only one MT, i.e. the average packet delay of one user is very low while the others are very high..

The objective of the ADF algorithm is to assure a strict delay-based fairness distribution among the MTs, i.e. the system fairness index $\Phi^{RT}[n]$ must be kept around a planned value Φ_{target}^{RT}. Therefore, the ADF algorithm adapts the parameter τ in the scheduling policy presented in (2.60) in order to achieve the desired operation point. In order to do that, the new value of the parameter τ is calculated using a feedback control loop of the form:

$$\tau[n] = \tau[n-1] - \lambda \cdot \left(\Phi_{filt}^{RT}[n] - \Phi_{target}^{RT}\right) \tag{2.64}$$

where $\Phi_{filt}^{RT}[n]$ is a filtered version of the system fairness index using a SES filtering, Φ_{target}^{RT} is the desired value for the index, and the parameter λ is a step size that controls the adaptation speed of the parameter τ. A SES filter, which is suitable for time series with slowly varying trends, was used to suppress short-run fluctuations and smooth the time series $\Phi^{RT}[n]$.

Urgency and Efficiency based Packet Scheduling

The Urgency and Efficiency based Packet Scheduling (UEPS) [25] can be considered as a modification of the M-LWDF approach. Substituting a utility function of the form $U_j\left(d_j^{HOL}\right) = e^{-a\left(d_j^{HOL} - d_j^{DL}\right)} \Big/ \left(1 + e^{-a\left(d_j^{HOL} - d_j^{DL}\right)}\right)$, which is called a relaxed z-shaped function (shown in Figure 2.16), into (2.54), we obtain the priority function of the UEPS algorithm given below.

$$P_{j,k}^{UEPS} = \frac{c_{j,k}[n]}{T_j[n-1]} \cdot \left| -a \cdot e^{-a\left(d_j^{HOL}[n-1] - d_j^{DL}\right)} \Big/ \left(1 + e^{-a\left(d_j^{HOL}[n-1] - d_j^{DL}\right)}\right)^2 \right|, \quad \forall j,k \tag{2.65}$$

where d_j^{DL} is the delay constraint (deadline) of the packet, and a is a constant.

The UEPS algorithm, designed for the purpose of mixed-traffic scenario, provides intermediate resource usage efficiency, similarly to the M-LWDF scheduler. However, due to the specific features of the employed utility function, the obtained delay-based fairness values will be higher than for M-LWDF.

Largest-Weighted-Throughput

The scheduling scheme endeavours to solve the following problem: given the per-link throughput, the waiting time of the HOL packets, and the delay constraints of the applications, which user should be served so that the system spectral efficiency is maximized and the delay constraints of the packets are satisfied. The rule described in (2.66) is an adaptation of the Largest-Weighted-Throughput (LWT) algorithm [26], where the priority of each HOL packet is given by its throughput weighted by a function of the waiting time and the delay constraints.

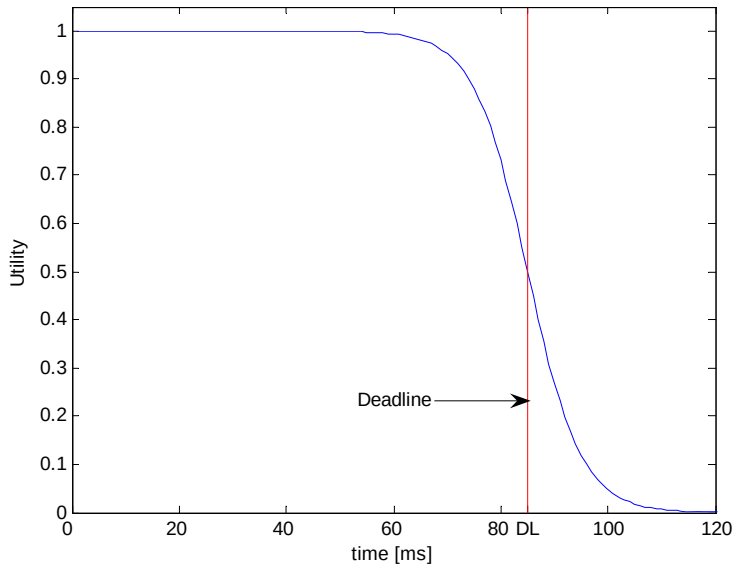

Figure 2.16 – Relaxed z-shaped utility function for $a = 0.2$

$$P_{j,k}^{LWT} = \frac{\zeta\left(d_j - \frac{L}{T_j[n-1]}\right)}{d_j^{\frac{1}{\alpha}}} \cdot c_{j,k}[n-1], \quad \forall j,k,$$

$$\zeta(x) = \begin{cases} 1 & x \geq 0 \\ 0 & x < 0 \end{cases}, \qquad (2.66)$$

$$d_j = d_j^{DL} - d_h^{HOL}[n-1]$$

where L is the packet length in bits, d_j^{DL} is the delay constraint (deadline) of the packet. Since the original LWT algorithm has been design for TDMA systems, a modification has been made, where the throughput of the whole OFDM symbol has been replaced with the transmission capability $c_{j,k}[n\text{-}1]$ of user j on subcarrier k.

The LWT algorithm offers a possibility of adaptive trade-off between efficiency maximizing and delay-based fairness depending on the α factor. Thus, a careful selection of α value can enable an elastic approach with capacity maximization in low load scenario and fairness maximization in case of high load.

3) Simulation Results for NRT Services

The simulation parameters used for the evaluation of the utility-based PSC algorithms in the scenario with NRT services are given in Table 2.13 and Table 2.14.

The metrics used for evaluation and comparison of the investigated packet scheduling algorithms were:

- Total cell throughput (indication of the system spectrum efficiency);
- Fairness index, according to (2.48).

Table 2.14 – Simulation parameters.

Parameter	Value
Power allocation	Equal power among sub-carriers
Throughput requirement (T_j^{req})	1.4 Mbps
Throughput filtering time constant (f_{thru})	50
Minimum β value	0
Maximum β value	1
ATF PSC control time window	0.5 ms
ATF PSC target fairness index (Φ_{target}^{NRT})	0.5 or 0.9
ATF PSC step size (η)	0.1
ATF PSC filtering time constant	10
Simulation time span	30 s
Number of realizations for each point	10

Figure 2.17 shows the system fairness index calculated using (2.48) for different cell loads. We run simulations with two different ATF target fairness indexes: 0.5 and 0.9. It can be observed that ATF is successful to achieve its main objective, which is to guarantee a strict fairness distribution among the MTs. This is achieved due to the feedback control loop that dynamically adapts the parameter β of the ATF priority function (see (2.46)). As expected, MMF provided the highest fairness, very close to the maximum value of 1, while MR proved to be the most unfair strategy. PF presented a trade-off between MMF and MR. The advantage of the ATF algorithm in comparison with the others is that it can be designed to provide any required fairness distribution, while the classical PSC strategies are static and do not have the freedom to adapt themselves and guarantee a specific performance result.

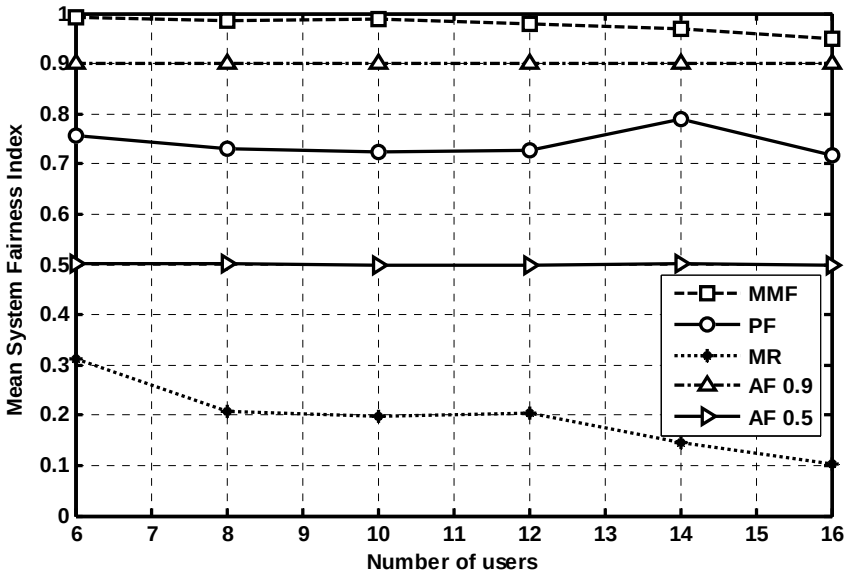

Figure 2.17 – Comparison of utility-based packet scheduling algorithms regarding the system fairness index.

The total cell throughput for different cell loads is shown in Figure 2.18. As expected, MR was able to maximize the spectral efficiency, while MMF presented the lowest cell throughput. Since PF is a trade-off between MR and MMF, its performance lied between them. Looking at Figure 2.17, one can expect that depending on the value of the AF target fairness index, the AF resource efficiency would be somewhere in the middle between the performances of MMF, PF and MR. This can be observed in Figure 2.18. On one hand, when the AF target fairness index is set to 0.5, AF works as a hybrid scheduling policy between PF and MR. On the other hand, the AF performance in terms of total cell throughput lies between MMF and PF when the target fairness index is set to 0.9

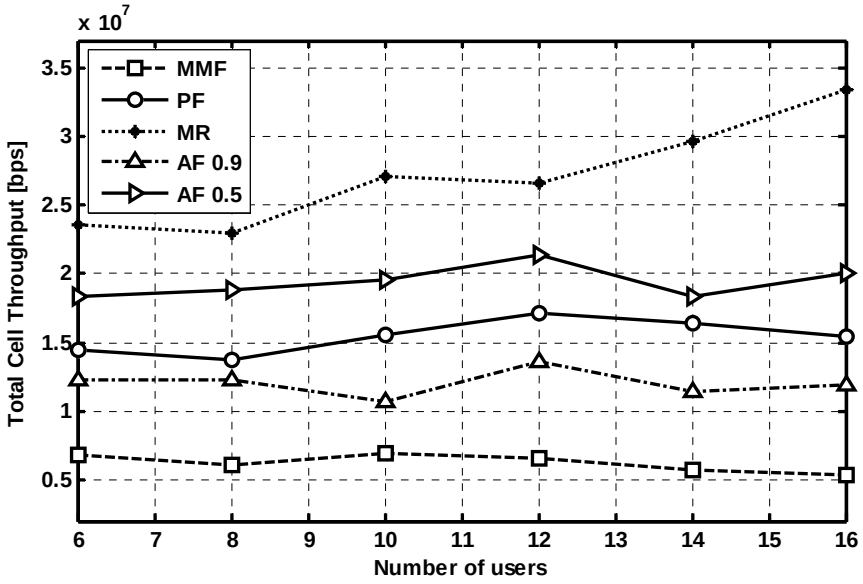

Figure 2.18 – Comparison of utility-based packet scheduling algorithms regarding the total cell throughput.

4) Simulation Results for RT Services

The simulation parameters used for the evaluation of the utility-based PSC algorithms in the scenario with RT services are presented in Table 2.13 and Table 2.15.

The metrics used for evaluation and comparison of the investigated packet scheduling algorithms were:

- Total cell throughput (indication of the system spectrum efficiency);
- Fairness index, according to (2.63).

In Figure 2.19 the results for fairness are shown. We can see that the two extremes are clear: D-FIFO provides the best fairness while PF is the worst. In particular, PF shows a monotonically behaviour, decreasing with the increase of the load and D-FIFO keeps a fairness value of 1 starting from 750 users. This high fairness comes at the expense of high delays and low satisfaction because D-FIFO is not efficient in the resource allocation. M-LWDF, UEPS (a = 0.2), LWT (α = 0.5) and ADF (dynamic τ) have an intermediate behaviour between D-FIFO and PF, in accordance with our expectations. One can notice that there is a point in system capacity where LWT and M-LWDF increase their fairness very fast to values close to one. This is due to the fact that when the system approaches an overload situation, the delay term in their priority functions (see (2.59) and (2.66)) becomes more and more important in the scheduling decision in comparison with the channel state. Notice that this influence of the delay term is stronger in LWT than M-LWDF, since the fairness of the former starts to increase sooner than the latter. The UEPS algorithm shows higher delay-based fairness than LWT for low system loads and is able to provide stable fairness in high system loads without saturating the buffers of the users, due to the specific properties of employed utility function. However, ADF presents even more stable delay-based fairness because it is able to keep the target of 0.9 that we set for these simulations.

Table 2.15 – Simulation parameters.

Parameter	Value
Link adaptation	Discrete (QPSK, 16-QAM)
Power allocation	Equal power among sub-carriers
Traffic model	Delay-sensitive full buffer with discrete packets
Packet size	32 bytes
Inter-arrival time	2 ms
Delay requirement (d_j^{req})	100 ms
Delay filtering time constant (f_{delay})	10
Minimum τ value	0
Maximum τ value	1
ADF PSC control time window	0.5 ms
ADF PSC target fairness index (Φ_{target}^{RT})	0.9
ADF PSC step size (λ)	0.1
ADF PSC filtering time constant	10
Simulation time span	15 s
Number of realizations for each point	50

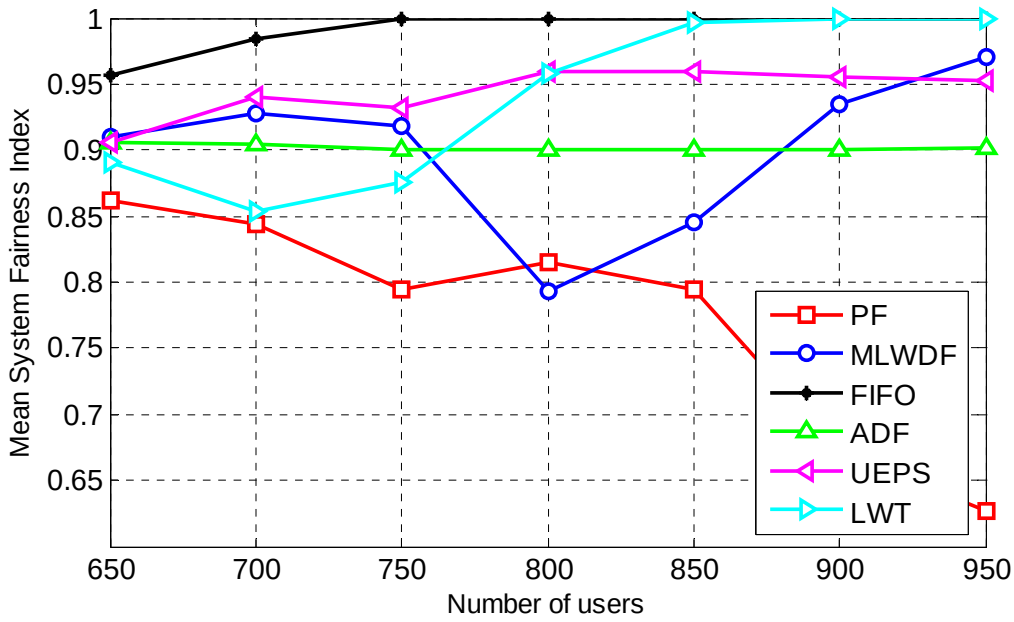

Figure 2.19 – Comparison of utility-based packet scheduling algorithms regarding the system fairness index.

In Figure 2.20 the cell throughput is given. As expected, the worst performance was presented by D-FIFO, because it only takes the delay information into account, which may lead to an inefficient resource allocation. The other algorithms, which give more importance to the channel quality and use

the resources more efficiently, show similar behaviour with higher spectral efficiency. UEPS and LWT present slightly lower cell throughput than M-LWDF and ADF for the majority of the load range considered in the simulations. Looking at Figure 2.19 and Figure 2.20, one can conclude that M-LWDF, UEPS (a = 0.2), LWT (α = 0.5) and ADF (dynamic τ) can achieve a good trade-off between resource efficiency and user fairness in a scenario with RT users. The difference is that LWT and ADF have scheduling frameworks that allow the adaptive control of a parameter that controls the degree of delay-based fairness experienced in the network. Figure 2.19 showed an explicit example how ADF is able to perform this strict control of the fairness.

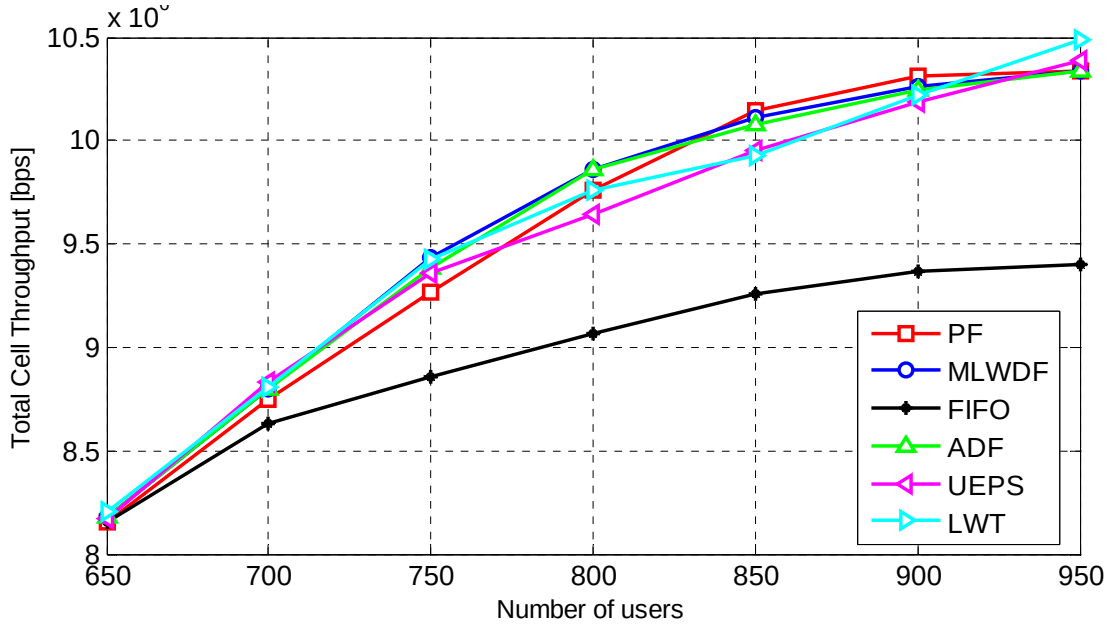

Figure 2.20 – Comparison of utility-based packet scheduling algorithms regarding the total cell throughput.

2.3.1.4 General Conclusions

In this work, we can draw two sets of conclusions regarding the trade-off between spectral efficiency and user fairness in OFDMA-based networks:

- Comparison between combinatorial optimization-based RRA and utility-based PSC in a scenario with NRT services;

The first comparison can be done by looking at sections 2.3.1.2-2) and 2.3.1.3-3). Two RRM approaches were evaluated: rate adaptive resource allocation (sub-carriers and power) based on instantaneous data rate and utility-based packet scheduling based on average data rate (throughput). Comparing the two approaches, one can see clearly the direct relationship between sum rate maximization RRA and MR PSC, and also max-min RRA and MMF PSC. Furthermore, possible trade-offs were presented, such as sum rate maximization with proportional rate constraints in the case of RRA, and PF and ATF in the case of PSC.

It was concluded from simulation results in a single-cell scenario that is possible to achieve an efficient trade-off between system spectral efficiency and fairness using any of the two RRM approaches. The total cell throughput and fairness index presented by the rate adaptive RRA were higher than the utility-based PSC because the former used power adaptation.

- Comparison between utility-based PSC algorithms suitable for NRT or RT services.

The conclusion of the second comparison can be done by comparing the simulation results presented in sections 2.3.1.3-3) and 2.3.1.3-4). Analyzing the simulation results we can draw a didactic map of the relations between the two objectives mentioned above, which can be seen in Table 2.16.

Reference DR9.2

Table 2.16 – Relations between utility-based PSC algorithms, spectral efficiency and fairness.

	NRT services	RT services
MR	High spectral efficiency and low throughput-based fairness	-
MMF	Low spectral efficiency and high throughput-based fairness	-
PF	Static trade-off between efficiency and fairness for NRT services	-
ATF	Controllable trade-off between efficiency and fairness for NRT services	-
PF	-	High spectral efficiency and low delay-based fairness
D-FIFO	-	Low spectral efficiency and high delay-based fairness
M-LWDF	-	Static trade-off between efficiency and fairness for RT services
ADF	-	Controllable trade-off between efficiency and fairness for RT services
UEPS	-	Static trade-off between efficiency and fairness for RT services, higher fairness than M-LWDF
LWT	-	Controllable trade-off between efficiency and fairness for RT services

We can conclude that there are PSC algorithms that are able to find the trade-off between efficiency and fairness, such as PF (for NRT services) and M-LWDF or UEPS (for RT services). However, these algorithms are only able to provide a static trade-off. The main advantage of the ATF, ADF and LWT algorithms is the fact that they provide a dynamic and controllable trade-off according to the cellular operator's objectives. We presented simulation results in Figure 2.19 and Figure 2.20 that exemplified the dynamic control of the trade-off by using the ATF and ADF algorithms.

2.3.2 Radio resource allocation in a multi-cellular setting

Orthogonal frequency division multiplexing (OFDM) [27] is a widely deployed technology. Provided that the cyclic prefix is suitably sized, it is robust against the multipath fading and allows a flexible usage of the existing radio resources [28]. Therefore, it has been used successfully for digital video broadcasting (DVB-T) and wireless local area networks (e.g., 802.11a). Several emerging standards for cellular broadband networks, such as 802.16e (WiMAX) or the future 3GPP Long Term Evolution (LTE) [29] are based on orthogonal frequency division multiple access (OFDMA) [30]. In an OFDMA system, users are multiplexed in frequency, based on an underlying OFDM system, i.e. each user is assigned a different sub-channel. In multi-cellular environments inter-cell interference, caused by

neighbouring cells using the same frequency band, is the main factor affecting the system performance.

Inter-cell interference can be mitigated in several ways.

- Code division multiple access (CDMA)-based systems, use different scrambling codes in different cells to decorrelate the users and reduce the interference.
- Conventional FDMA/TDMA systems (like GSM) reduce the interference power by using different sets of frequencies in neighbouring cells by employing a frequency reuse pattern.
- A third possibility is to apply space-division multiplexing (SDM). Base stations and/or mobile terminals are equipped with multiple antennas: the extra degree of freedom given by the antenna arrays is employed to spatially filter the co-channel interference.

Recently, dynamic resource allocation has been studied in multi-cell scenarios as efficient means to reduce interference among neighbouring cells. The aim is to assign radio resources to the users using some optimization criterion so that the co-channel interference is reduced and a full reuse of the existing radio resources is possible. There are several algorithms proposed in literature. In the case resource allocation is performed just on the base of the position of the users within the cell we refer to *static* resource allocation (SRA) algorithms [32]-[34] otherwise to *dynamic* resource allocation (DRA) algorithms. DRA algorithms can be classified on the base of the amount of coordination between the cells [35]: the different schemes range from completely centralized approaches [39]-[44], where one single entity controls everything, to fully distributed algorithms [45]-[50], where the cells do not exchange explicitly any information. Because DRA algorithms are usually very complex, most of the research has been focused on the downlink scenario. Nonetheless, some authors have investigated the impact of DRA algorithms defined also for the uplink [51]-[53].

Since DRA algorithms are mainly designed to exploit channel and multi-user diversity, they can be easily extended to exploit spatial diversity as well. The literature on resource allocation for systems equipped with multiple antennae is rather developed [54]-[61].

Extra interest in the problem of efficient DRA has very recently been arisen by the definition and the implementation of the *femtocell network* concept [62]-[67]. In future systems it is envisaged the use of radio hubs with very limited coverage whose deployment does not require any radio planning. For the viability of such networks the existence of good DRA algorithms is a necessary condition.

2.3.2.1 DRA algorithms

Problem formulation

In the following we will focus our interest mainly on DRA in the downlink. The multi-cell scenario is characterized by N_{cells} neighbouring cells that transmit over the same bandwidth, divided in N orthogonal subcarriers. Within each cell there is a BS and several multiple UEs. Because of the presence of inter-cell MAI, interference needs to be taken into account and the measure of the channel quality is the Signal-to-Interference-plus-Noise Ratio (SINR). The SINR for user k situated in cell j, calculated on subcarrier n is

$$SINR_k(n) = \frac{p^{(j)}(n)G_k^{(j)}(n)}{\sum_{\ell \neq j} p^{(\ell)}(n)G_k^{(\ell)}(n) + BN_0} \tag{2.67}$$

where $G_k^{(l)}(n)$ is the squared value of the channel gain between the BS in cell l and the user k calculated on subcarrier n, $p_n^{(l)}$ is the power transmitted in cell l on subcarrier n. The problem is complex and is usually solved by sub-optimal algorithms. Centralized algorithms offer better solution but are nonetheless extremely complex, distributed algorithms require less information and are usually easier to implement.

Centralized schemes

Base station coordination has emerged as a means to mitigate downlink co-channel interference. Ideally, if both data and channels of all users could be shared in real time, adjacent base stations could act as a large distributed antenna array and could employ joint beamforming, scheduling, and data encoding to simultaneously serve multiple co-channel users. However, a much lower level of coordination may be assumed in practice, depending on the bandwidth of the backbone network connecting the access points.

Centralized RRM schemes are characterized by the presence of a central entity, which is connected to all BSs and has full knowledge of the channel state information (CSI) for all users in all sub-carriers in all cells. This central controller is responsible for the allocation of all system resources, such as groups of sub-carriers, transmission power and modulation formats. The main limit of centralized schemes is their complexity and overhead: in most networks the amount of resources needed to feedback the CSI of all UEs, the computational effort necessary to generate the resource allocation and the signalling overhead to send the assignment information to the users make the centralized approach unfeasible. Nevertheless, centralized schemes are expected to provide the optimal allocation solution and thus represent an ideal benchmark for comparison with more realistic distributed schemes.

In [39] allocation is performed following a margin adaptive approach so as to minimize the overall transmission power while providing a given transmission rate to each user. To simplify the solution of the allocation problem the authors adopt just one transmission format per user and formulate it as a mixed integer linear programming problem. The performance loss due to the use of a single transmission format implies that the required SINR is the same for all subcarriers, i.e. $SINR_k(n) = SINR_k$ and is partially compensated by the exploitation of the multi-user diversity. In fact, as a consequence of resource allocation, the mean value of the gains of the assigned channels is larger than in the case of channel-independent allocation. The larger the number of users, the larger is the set of channels over which to perform the allocation and the larger is the multi-user diversity gain. Thus, link adaptation becomes progressively a less effective measure. Introducing the binary allocation variable $x_{k,n}$, which is set to 1 if channel n is assigned to user k and 0 otherwise, and assuming that in the system there are K users in N_{cells}, the centralized resource allocation is formalized as the following constrained minimization problem

$$
\begin{aligned}
&\min \sum_{j\in N_{cells}, n\in N} p^{(j)}(n) \\
&s.t. \\
&p^{(j)}(n) \le Q \sum_{k\in U(j)} x_{k,n} \quad \forall j,n \\
&G_k^{b(k)}(n)p^{b(k)}(n) - SIR_k \sum_{h,h\neq b(k)} G_k^{(h)}(n)p^{(h)}(n) \ge SIR_k BN_0(1-Q(1-x_{k,n})) \quad \forall k,n \\
&\sum_n x_{k,n} = r_k \quad \forall k \\
&\sum_{k\in U(j)} x_{k,n} \le 1 \quad \forall j,n \\
&x_{k,n} \in \{0,1\} \quad \forall k,n \\
&p^{(j)}(n) \ge 0 \quad \forall j,n
\end{aligned}
\tag{2.68}
$$

where $U(j)$ indicates the set of users in cell j and Q is a suitable large positive number. Constraints (1) are logic constraints, forcing power $p^{(j)}(n)$ to be 0 if sub-carrier n is not assigned in cell j. Constraints (2) state that, if user k is assigned sub-carrier n (i.e., if $x_{k,n} = 1$), the assigned power must be such that SINR requirements are satisfied. Constraints (3) state that at most one user per cell can be

assigned to a given subcarrier. Constraints (4) require that r_k sub-carriers must be assigned to each user *k* to satisfy the users' rate requirements. Problem (2.68) is a mixed integer linear programming (MILP) and has a complexity that grows exponentially with the number of users. A heuristic solution, based on a network flow approach, consists in iteratively solving a relaxation of the MILP formulation (2.68). The MILP formulation obtained by relaxing the interference constraints (2) can be solved in polynomial time by decomposing problem (2.68) into N_{cells} minimum cost flow problems. Channel allocation is then performed by iteratively solving the allocation problem in each cell and updating the resources costs in a centralized controller.

In [44] the authors cast the joint user scheduling and power allocation problem as a constrained non-convex optimization: the objective function (utility) to be maximized is the weighted system sum rate subject to per-base-station power constraints. The scheduling weights account for possibly different priorities of the users. The problem is NP-hard and the paper presents three iterative suboptimal algorithms that attain near-optimum results.

Distributed schemes

Centralized RRM produces near-optimum channel allocation at the expense of high signalling overhead, so distributed schemes are a realistic alternative to the centralized ones. Distributed DRA algorithms are usually iterative since there is no central entity responsible for receiving measurement reports or distributing resources to UEs or BSs.

In [48] the DRA problem is formulated as a margin adaptive problem with rate constraints defined per each user. Due to the interactions and dependencies between multi-user resource allocation per cell and multi-cell interference per sub-channel, the complexity of the original formulation is too complex to be practically tractable. Therefore, the authors propose a distributed criterion to ensure that distributed power control will necessarily converge for each subcarrier. The proposed criterion is based upon an upper bound on the spectral radius of the interference matrix on each subcarrier. Accordingly, resource allocation is split into three steps: subcarrier allocation, which selects the best subcarriers for each user, SINR target setting, which determines a SINR target set per user that enables to reach the target data rate, while enforcing the convergence of distributed power control, and finally distributed power control.

The work in [51] presents a DRA algorithm for the uplink that could be easily adapted to the downlink. Similar to [40], the allocation problem aims to minimize the transmitted power fulfilling rate constraints for each user in the cell. In this case, each cell allocates iteratively its resources aiming at maximizing its own objective function. Lacking centralized information, the proposed algorithm needs to be iterative since the allocation in a particular cell interferes with the allocation in all other cells. The convergence of the proposed scheme is guaranteed by progressively reducing the cell load until a stable traffic configuration is found.

MIMO scenario

In coordinated MIMO systems a set of cooperative transmitters are jointly exploited to outperform the performance of conventional systems. A coordinated system may comprise different types of transmitters that could be interconnected through fibre cable or by using the radio interface. In the former case these entities are referred to as Remote Radio Units (RRU), if transmitters are not base stations, or as coordinated cells, on the contrary. In case of wireless backhauling, these entities are called relay nodes (RN).

The usage of multisector and/or multisite cooperation has been proposed as a candidate technique for future wireless systems to increase spectral efficiency, especially in the cell edge. MIMO-aware scheduling can be performed in OFDMA systems, such as the LTE, where eNode-Bs decide on resource allocation based on indicators that the UE feeds back (CQI, and PMI). However, change of MIMO mode is not a fully dynamic process but a semi-static one. In LTE, a simple coordinated multipoint transmission can be performed based on information exchanged by the eNode-Bs through

the inter-eNode-B interfaces (X2). This information can be related to long term distribution of radiated power over the resource grid or can express the weakness of some resources to interfering power.

LTE-Advanced is studying more elaborated coordination schemes including techniques related to enhanced interference cancellation or cooperative MIMO. Techniques have been divided in two big groups: joint processing and scheduling/beamforming.

The main gain from coordinating multiple BSs is the interference mitigation possibility by reducing the impact of multi-sector interference. Moreover, joint signal processing techniques allow exploiting positively this interference resulting in some diversity gain.

The interference avoidance using dynamic coordination schemes gained a lot of interest in literature, and two main areas of study were formulated. One possibility is to apply the beamforming antennas to minimize the interference by focusing the transmission or reception in the direction of a particular terminal. On the other hand, the transmissions of neighbouring base stations can be coordinated further using the multipoint coordinated processing (transmission/reception), thus almost completely eliminating inter-cell interference [35].

Different aspects of multipoint MIMO coordination have been studied in [56], as a candidate solution to reduce inter-cell interference and consequently enhance the gains achieved by MIMO. A coordinated wireless network was investigated, where multiple base stations are connected to a central station where multi-user (MU)-MIMO precoding is jointly performed for all coordinated base stations.

a) Coordinated scheduling approach

One aspect of multipoint coordination can be the joint resource allocation including coordination for inter-cell interference avoidance. Several algorithms have been proposed in the literature, which focus on different methodology of coordination.

In [43] an optimal and a sub-optimal inter-cell scheduling strategy have been proposed, both of which coordinate the transmission of interfering cells. The proposed algorithms were derived using the Utility Theory, assuming the fully coordinated system (all cells are coordinated by one entity) and partial coordination in clusters of three cells. The efficiency optimization is performed assuming different levels of knowledge of interfering signals within and outside the coordination cluster. The optimization problem, given the power allocation profile, can be defined as:

$$\begin{aligned} &\max \sum_{i=1}^{K} U_i\left(T_i[t]\right) \\ &\sum_{i \in M} x_{il} \le 1, l \in F_n \ , \\ &x_{il} = \{0,1\} \end{aligned} \tag{2.69}$$

where K is the number of users in the entire network, M is the set of users served in cell n, $U_i(\cdot)$ is the utility function of user i, x_{il} denotes whether subcarrier l is allocated to user i (where $x_{il} = 1$ means that whether sub-carrier l is allocated to user i), and F_n is the set of sub-carriers available to the users in M. $T_i[t]$ is the average throughput of user i at slot t, and can be expressed by using an exponentially low-pass filter as (2.37). The instantaneous throughput $r_i[t]$ can be defined as:

$$r_i[t] = \Delta f \sum_{l \in F_n} C_{il}^{P}[S_l] x_{il} \ , \tag{2.70}$$

where Δf is the sub-carrier bandwidth, and $C_{il}^{P}[S_l]$ is the maximum reliable transmission capability on subcarrier l for user i under this sub-carrier's allocation strategy S_l in the entire network. Then the optimal scheduling strategy of subcarrier l at slot t for subcarrier l denoted by $S_l^*[t]$ satisfies:

$$S_l^*[t] = \arg\max \sum_{i \in M} \left\{ \left(U_i'(\bar{r}_i[t-1]) \cdot \Delta f \cdot C_{il}^{P}(S_l) + \sum_{\substack{j \in M_{\text{int}} \\ x}} U_j'(\bar{r}_j[t-1]) \cdot \Delta f \cdot \frac{\partial C_{jl}^{P}(S_l)}{\partial x_{il}} \cdot x_{jl} \right) \cdot x_{il} \right\}, \quad (2.71)$$

where $C_{il}^{P}[S_l]$ is calculated using the modified Shannon formula:

$$C_{il}^{P}[S_l] = \log_2\left(1 + \frac{-1.5}{\ln(5 \cdot BER)} \times SINR_{il}\right), \quad (2.72)$$

with $SINR_{il}$ calculated using (2.67), BER being the targeted bit error rate, and M_{int} denoting the set of users who are in the interfering cells and allocated subcarrier l. The first partial derivative of $C_{il}^{P}[S_l]$ with respect to x_{il} can be calculated as follows:

$$\frac{\partial C_{jl}^{P}(S_l)}{\partial x_{il}} = \frac{1}{\ln 2} \times \frac{(-1)\left(\frac{-1.5}{\ln(5 \cdot BER)} \cdot P_{jl} \cdot g_{jl} \cdot P_{(n,i)l} \cdot g_{(i,j)l}\right)}{\left(N_0 + \sum_{n \in C_{\text{int}\,er}} P_{nl} \cdot g_{nl}\right) + \frac{-1.5}{\ln(5 \cdot BER)} \cdot P_{jl} \cdot g_{jl} \times \left(N_0 + \sum_{n \in C_{\text{int}\,er}} P_{nl} \cdot g_{nl}\right)}, \quad (2.73)$$

where P_{jl} and g_{jl} are the transmit power of user j on subcarrier l and channel gain between user j and its serving cell antenna respectively. $P_{(n,i)l}$ is the transmit power on subcarrier l for user i served by cell n and $g_{(i,j)l}$ is the channel gain on subcarrier l between user i's serving cell antenna and user j. C_{inter} denotes the interfering cell antenna set [43].

Since the described optimal solution is not practical, a sub-optimal strategy has been proposed in [43] where the coordination is performed in clusters comprising three cells. Thus, the interference from cells outside the coordination cluster is calculated only using the estimates of pathloss and shadow fading.

The idea of coordinated scheduling, with MIMO SDMA technique employed, has been investigated in [61]. The issues of distributed dynamic resource allocation (DRA) in the downlink of a broadband wireless packet network with multiple access points and adaptive antennas have been analyzed. A several DRA strategies for efficient allocation in a distributed environment are proposed, such as Distributed Max-Min Fit (DMMF) and Distributed Reverse Fit (DRF), which are based on the Max-Min Fit criterion. Moreover, the novel concept of *Nulls Preallocation*, where each Access Point (AP) reserves some beamforming nulls for the most interfered users of neighbouring cells, and the Power Shaping technique (PS-DRA), which efficiently exploits static power preallocation on time slots have been deeply investigated.

A novel inter-cell interference avoidance scheme is presented in [41], in which the downlink OFDMA subchannels are allocated through inter-cell coordination in a multicell environment. The proposed scheme not only aims to achieve maximized network throughput but also focuses on providing improved throughput for cell or sector edge users that are most affected by inter-cell interference. The scheme is comprised of two different algorithms; one at the base station level, and the other at a central controller to which a group of neighbouring base stations are connected. Depending on the reported UT channel states, each BS performs an initial scheduling using iterative Hungarian algorithms and sends a potential "collision" list (list of resource blocks strongly affected by interference) to the central controller. Then the central entity solves any possible conflicts by restricting transmission in certain resource blocks by specified BSs.

b) Coordinated beamforming approach

A very promising concept, which is extensively studied in the literature, is the inter-cell interference avoidance by coordination of the MIMO beamforming process in neighbouring BSs. In [42] two types of coordination are considered: the capacity-achieving technique based on dirty paper coding (DPC), and a simpler technique based on zero-forcing (ZF) beamforming with per-antenna power constraints. Different scenarios of coordination are considered with both the distributed and co-located antennas, assuming that the scheduling process in performed jointly for sectors with co-located antennas.

In [60] authors consider the benefit of coordinating base-stations across multiple cells in a multi-antenna beamforming system, where multiple BSs may jointly optimize their respective beamformers to improve the overall system performance. This paper focuses on a downlink scenario where each remote user is equipped with a single antenna, but where multiple remote users may be active simultaneously in each cell. The beamformer design problem in this paper consists of minimizing total transmit power across all BSs subject to SINR constraints at the remote users The main presented idea is to exploit the uplink-downlink duality for multi-cell systems to derive the optimal downlink beamforming for each of the coordinated BSs. The resulting proposed algorithm is capable of finding the joint optimal beamformers for all base-stations globally and efficiently with its distributed implementation.

In [58] HSDPA cellular architectures where base stations coordinate to serve multiple users is considered. These base stations are assumed equipped with smart antenna systems which generate pilot beams according to a predefined algorithm, collect only an SINR report from the users, and provide opportunistic scheduling. A modification of the well known Joint Opportunistic Beamforming and Scheduling algorithm is proposed to include the inter-cell coordination. The main advantage of the proposed algorithm is the low feedback requirement when compared to other coordination schemes.

Femtocells

Over the last 100 years, the wireless capacity has increased due to some factors, such as: wider spectrum, division of the spectrum into smaller slices, better modulation schemes, and reduced cell sizes and transmit distance. There is no doubt that the last factor was the one that provided the largest gains, which come from the efficient spatial reuse of spectrum or, alternatively, higher area spectral efficiency

A recent development is femtocells, also called home base stations (BSs), which are short-range low-cost low-power BSs installed by the consumer for better indoor voice and data reception. The user-installed device communicates with the cellular network over a broadband connection such as digital subscriber line (DSL), cable modem, or a separate radio frequency (RF) backhaul channel. While conventional approaches require dual-mode handsets to deliver both in-home and mobile services, an in-home femtocell deployment promises fixed mobile convergence with existing handsets. Compared to other techniques for increasing system capacity, such as distributed antenna systems and microcells, the key advantage of femtocells is that there is very little upfront cost to the service provider [62].

The key arguments in favour of femtocells are the following [62]:

- **Better coverage and capacity**. Due to their short transmit-receive distance, femtocells can greatly lower transmit power, prolong handset battery life, and achieve a higher signal-to-interference- plus-noise ratio (SINR). These translate into improved reception and higher capacity.
- **Improved macrocell reliability**. If the traffic originating indoors can be absorbed into the femtocell networks over the IP backbone, the macrocell BS can redirect its resources toward providing better reception for mobile users.
- **Cost benefits**. Femtocell deployments will reduce the operating and capital expenditure costs for operators. The deployment of femtocells will reduce the need for adding macro-BS towers.
- **Reduced subscriber turnover**. Poor in-building coverage causes customer dissatisfaction, encouraging them to either switch operators or maintain a separate wired line whenever

indoors. The enhanced home coverage provided by femtocells will reduce motivation for home users to switch carriers.

The capacity benefits of femtocells are attributed to [62]:

- Reduced distance between the femtocell and the user, which leads to higher received signal strength.
- Lowered transmit power, and mitigation of interference from neighbouring macrocell and femtocell users due to outdoor propagation and penetration losses.
- As femtocells serve only around one to four users, they can devote a larger portion of their resources (transmit power and bandwidth) to each subscriber. A macrocell, on the other hand, has a larger coverage area (500 m – 1 km radius) and a larger number of users; providing quality of service (QoS) for data users is more difficult.

There are several technical challenges related with physical, MAC and network layers in femtocell networks [62]. Open research topics on RRM for both broadband (data) and voice femtocells are:

- **Spectrum Allocation**. The 3GPP LTE and WiMAX standards ensure intra-cell orthogonality among macrocellular users and mitigate inter-cell interference through fractional frequency reuse. Due to the absence of coordination between the macrocell and femtocells, and between femtocells, decentralized spectrum allocation between macrocell and femtocell users is an open research problem that can provide answers to the following questions:
  - Should macrocell and femtocell users be orthogonal through bandwidth splitting? Is there an "optimal" splitting policy? How does this vary with the femtocell density?
  - Alternatively, with shared bandwidth (i.e., universal frequency reuse), what fraction of the spectrum should the macrocell and femtocells assign their users?
  - Which of these two schemes is "better" in various configurations?
- **Interference Management**. An interference avoidance approach wherein users avoid rather than suppress mutual interference is more likely to work well in geography-dependent femtocell networks. The low cost requirement is likely to influence the design of low-complexity femtocell BS receivers (e.g., simple matched filter processing) and low-complexity transmission schemes for sensing nearby available frequency channels to avoid collisions. Interference avoidance can be achieved by means of frequency and time hopping [63], directional antennas [63], adaptive power control [64] and frequency planning [65].
- **MIMO Femtocells**. Femtocells can perform temporal link adaptation through adaptive modulation and coding; additionally, MIMO spatial link adaptation will enable a femtocell to switch between providing high data rates and robust transmission. High data rates are obtainable by transmitting multiple spatial streams (spatial multiplexing) over high SINR links. Over low SINR links, MIMO provides robustness through open and closed loop diversity schemes such as space-time codes and beamforming [54]. It would be interesting to analyze the effect of channel state information errors induced by co-channel interference on MIMO femtocell performance.
- **Self-Organization**. LTE and WiMAX networks require a higher level of self-organization at both macro/micro BSs and Home NodeBs (HNB) because of the flat network architecture. Cooperation is required among BSs and HNBs for successful handover and RRM information exchange [66]. To allow adaptation to changes in the network environment (i.e., configuration and properties of neighbouring macrocells/femtocells) an ongoing measurement and self-optimization process is performed to adapt parameters such as scrambling code, pilot- and maximum data transmit power, and the neighbour list. This ensures minimal impact on the macrocellular network and ensures that femtocell performance is maximized under the given constraints [67].
- **Auto-Configuration of Transmit Powers for Co-Channel Operation**. One aspect of the auto-configuration process is the configuration of the downlink and uplink transmit powers for pilot and data. This is a particularly critical issue when the femtocells reuse the same frequency band as an existing macrocellular network, since the powers define the femtocell

coverage area and have an impact on the interference, handover signalling, and dropped call rate [67].

2.4 Game Theory for Optimization of RRM, Distributed Algorithms for CR

Game theory [68], [69] a powerful tool for analyzing conflict situations, strategic interactions among agents (the players), their behaviour, and possible equilibrium solutions of these situations. As mentioned in the first WPR9 deliverable [70]: *Our general objective in Working Group 3 (WG3 - Game theory for optimisation of RRM, distributed algorithms for Cognitive Radio) is to consolidate partners' research in the direction of modelling the conflicting and competitive behaviour of the cognitive network users and nodes as a dynamic and flexible resource-sharing game, as well as of algorithms development for the desired demeanour towards efficient radio-resource usage*.

Here below, we consider a large set of transmitters to share a limited set of frequency bands (channels) to communicate with a unique receiver. When there exists a central controller (normally the receiver) a capacity achieving power allocation can be implemented by using an iterative water-filling algorithm [71][72]. In this case, the central controller knows the transmission parameters and instantaneous channel realizations of each transmitter over each channel. Thus, it is able to solve the global optimization problem and feed back the optimal power levels to each transmitter. However, in the absence of a central controller or the impossibility to interchange signaling messages between the transmitters to obtain a complete information of the network, achieving capacity becomes a non-trivial task [73]. Here, game theory has played a remarkable role, but solutions remain being highly suboptimal due to the lack of global information [74].

Below, we present our results in distributed mechanisms of dynamic allocation of resources for Cognitive Radio (CR) using game-theoretic approach, which in particular could be suitable for the up-link. These resources are considered as orthogonal channels, e.g. OFDM subcarriers. In our OFDMA-based network scenario, multiple CR nodes are secondary users of the network. Each node is able to detect available spectrum, and its goal is to acquire radio resources, and maximize the throughput at a minimum cost, expressed in energy consumption. In our considerations we do not care how the achieved data rates are mapped to data streams. For a proof of concept we also assume that a CR-node can acquire any subset of available subcarriers (SCs), and that there exists a collision-avoidance mechanism, used to prevent nodes from trying to access the spectrum at the same time instant. We study two scenarios, in which the players are deliberately limited in their accessible resources: 1) the taxation of resources, where the players are allowed to use different channels, and do not interfere; and 2) the resource bandwidth limiting with successive interference cancellation of the players.

2.4.1 Taxation of resources in OFDM-based CR

An intelligent Control Unit (CU) of a CR node makes decision concerning which SCs and how many of them it will use for the transmission. It can be considered as an element of the broader concept of the *cognitive engine* [71]. The CU acts as a player in our game for resources. In order to prevent a single player from occupying all resources, we limit the maximum number of SCs a node can acquire at a time, introduce the "social consciousness" mechanism such as network capacity factor in the utility function and employ resource taxation. Resulting throughput depends on the power levels allocated to acquired SCs, and we assume that this is done in an optimal way based on the so-called *water-pouring principle* [76]. After the application of water-pouring (calculation of the water-level), it may turn out that some SCs acquired cannot be used for the transmission with assumed reliability (due to their poor quality). In such a case, they are returned to the pool of available resources.

Let us define our game, which each CU plays against the other users. The elements of this definition are the players, the strategies, and the payoffs.

2.4.1.1 The players and their strategies

Following the spectrum-sensing algorithm, the CU of a CR-node can make decision on the number of acquired SCs. If there are N available SCs, K nodes, and each one can take any subset of these SCs (but no more than I SCs), the problem of finding the game solution becomes extremely complex. This is because the game is K-dimensional, and the number of possible outcomes of the game equals:

$$\Omega = \left[\sum_{i=0}^{I} \frac{N!}{i!(N-i)!}\right]^K \tag{2.74}$$

Thus, analyzing the existence of the Nash equilibriums becomes very complex particularly for high I, N and K values. As shown above, it is crucial to narrow the space of our analysis. For this purpose we let each CU take decisions independently while treating the rest of the players as one player (the CR-nodes community), and by eliminating its strategic choices which are disadvantageous. Naturally, a selfish player would occupy the maximum of available SCs, because such an action would maximize its throughput. However, from the fairness point of view, this behaviour would decrease the number of users served. The problem is related to the classical common resource utilization dilemma known as the *Tragedy of Commons* ([77]), which shows that selfish behaviour of the common-resource users leads to inefficient (even the poorest possible) utilization of these resources.

In order to eliminate disadvantageous strategic choices (eliminate dominated strategies [69]), we simply assume that, when a CU wants to use a number of i subcarriers, for sure these should be i strongest SCs (of the highest Carrier-gain-to-Interference-and-Noise Power Ratios (CINRs)), because making use of the strongest SCs results in highest spectral efficiency. A single player does not care, how efficient the other players are in utilizing their acquired resources, i.e. what are their CINRs at various SCs, but rather how many of these SCs the other players (all together) are going to use. The number of occupied SCs affects the network ability to serve the incoming users including the users who are already being served, but would like to acquire more resources in the future.

Thus, in our considered case, the game for each player becomes two dimensional only, and the number of possible game outcomes to be analyzed is significantly reduced: $\Omega_{\text{red}} = I \times N$.

To summarize, the strategies of a CU are all possible numbers of the strongest detected SCs (from 0 to I). The strategies of the rest of the CR-nodes community are the numbers of SCs this community may occupy all together. Moreover, the game is dynamic, i.e. the players take decisions subsequently thanks to the collision-avoidance procedure.

2.4.1.2 The payoffs

The payoff at each stage of the game is the value of the utility function and exhibits the game outcome, when the CU player chooses strategy i (i strongest SCs) while the rest of the community occupies j subcarriers. For our game, we suggest that the payoff reflected the normalized throughput (throughput divided by the subcarrier distance Δf) achieved by the CR-node and the network potential to serve other users (related to the notion of fairness). Thus, the proposed payoff function for player k (at the kth stage of the game), who acquires i SCs ($i \le I$), while the rest of the CR-nodes community is expected to occupy j SCs equals:

$$\tilde{\zeta}_{k\,i,j} = \left\{\frac{1}{N}\sum_{s\in\mathbf{S}_i}\log_2[1+\alpha\cdot P(f_s)\gamma(f_s)]\right\}\cdot\{N_k - i - j\} - \tau_{k\,i}, \tag{2.75}$$

where $\gamma(f_s) = |H(f_s)|^2 / (\mathsf{N}_0\Delta f + \mathsf{I}_0)$ is the CINR at the SC frequency f_s, whose index s belongs to the set $\mathbf{S}_i$ of indices of i strongest SCs (the cardinality of $\mathbf{S}_i$ is i), $H(f_s)$ and $P(f_s)$ are the channel characteristic and the power level allocated to this SC frequency f_s respectively, $\mathcal{N}_0$ is the noise power spectral density, $\mathcal{I}_0$ is the interference power, Δf is the SCs distance, α is the factor depending on the assumed Bit Error Probability (BEP) P_e, and N_k is the number of available SCs at the game stage k, i.e. for user k. (Note that for M-QAM, α can be approximated by $\alpha = -1{,}5 / \ln(0{,}5P_e)$ or more precisely

as in [76]) Let us note, that the optimal power level $P(f_s)$ allocated to SCs should be calculated according to the water-pouring principle, assuming that CINR values are perfectly known by the CU, i.e. the CSI is perfect, although in reality the player uses estimated CINR for each chosen subcarrier frequency f_s. The first factor in (2.75) represents the potential throughput of a single player at the kth stage of the game, while the second one represents the network potential to serve other players at subsequent game stages. This way, the players factor the *social aspect* of the network (to serve multiple users) in their decision-making. Finally, $\tau_{k\,i}$ is the tax value, that a player k has to "pay" at the kth stage of the game. This tax value should depend on the amount of resources used by a player. $\widetilde{\zeta}_{k\,i,j}$ represents the profit (revenue minus cost), and thus, if a single player faces poor channel-quality, and yet occupies a lot of SCs, its profit should be small or even negative due to poor spectral utilization and relatively high tax "to pay". Taxes should bring pressure to bear upon desirable players' behavior and the Pareto-optimal solution of the game. However, calculation of such an optimal tax is quite a difficult task, requires the knowledge of the CINRs at all SCs for all links, and results in many tax values specific for every player. These calculations can be done only centrally, e.g. at a base station, from where the tax values (and their updates every time the CINRs change) can be broadcasted. In our considered CR network, all decisions are expected from the intelligent CU. Therefore, we look at a simplified case of common (for all nodes) and invariant (with respect to CINRs changes) way of taxing the resources. Moreover, we concentrate on the linear taxation and arithmetically-progressive taxation. In both cases the tax can be defined as follows:

$$\forall k \in [1, K]: \quad \tau_{k\,i} = \tau_i = i \cdot (\tau_0 + i \cdot \Delta_\tau), \tag{2.76}$$

where $(\tau_0 + i \cdot \Delta_\tau)$ is the tax rate determined by the arithmetic progression, with the first element τ_0 and the common difference Δ_τ. Both τ_0 and Δ_τ should be carefully adopted to the number of SCs, the number of players and their anticipated behaviour. Let us note, that if $\Delta_\tau = 0$, the above formula defines the linear taxation, i.e. the tax value is a linear function of the number of acquired SCs. If $\Delta_\tau > 0$, the taxation is arithmetically-progressive. Both parameters τ_0 and Δ_τ should also depend on the average Signal-to-Interference-and-Noise ratio (SINR) (averaged over all SCs) experienced by CR-nodes in the system. Too high taxes encourage every player to not use any subcarrier, and results in poor usage of available resources, if the nodes SINRs are low.

Finally, the payoff of the other player, here referred to as "the rest of the CR-nodes community" is defined as the number of SCs that can be potentially occupied by this player:

$$\psi_{k_{i,j}} = j, \tag{2.77}$$

Although the values of payoffs decrease with increasing j:

$$\forall i \in [0, I] \;\; \forall j \in [0, N_k - I - 1]: \;\; \widetilde{\zeta}_{k\,i,j} \geq \widetilde{\zeta}_{k\,i,j+1} \tag{2.78}$$

(equality occurs for $i = 0$), it is not the case for increasing i:

$$\forall j \in [0, N_k - I] \, \exists i^*: \begin{cases} \widetilde{\zeta}_{k\,i-1,j} \leq \widetilde{\zeta}_{k\,i,j} & \text{for } 0 < i \leq i^* \\ \widetilde{\zeta}_{k\,i,j} \geq \widetilde{\zeta}_{k\,i+1,j} & \text{for } i^* \leq i < I \end{cases} \tag{2.79}$$

We may conclude the above considerations that there exist the Nash equilibrium for the above defined game, i.e. for strategies i^* defined by (2.79) and for $j = N_k - I$. It is well known however, that a Nash equilibrium may be far from optimality.

2.4.1.3 Simulation Results

For the purpose of our game-model verification and simulations, we have considered the following setup: the number of available SCs at the beginning of the game $N = 256$, the maximum number of

SCs each player can take I and the number of competing nodes K satisfy: $KI = N$ (potentially there is enough SCs to serve all nodes). Each node is allowed to transmit with the same power limit. For a given number of competing nodes K, the total power in the CR-nodes community (being the sum of the transmit powers of the CR nodes) has also been fixed, so that if some nodes do not use available SCs, the other nodes are allowed to increase their power. Thus, the interference level is constant. Moreover, two scenarios have been considered: equal average-SINR case (the 'E' case) when the average SINR $\bar{\gamma} = 30$ dB is the same for every node due to the Power-Control (PC) mechanism, and diverse average-SINR case ('D' case) when the PC mechanism has a tolerance of 1.5 dB, so that random deviation not exceeding 1 dB from the average SINR is possible for any node. For modern cellular systems the PC inaccuracy can be usually around 1.5 dB. This number has been chosen to observe differences in the obtained results for both scenarios.

The channel model considered is the two-paths Rayleigh-fading channel with the delay spread ranging from 0 to one fourth of the OFDM symbol, and the average power of the second path being –3 dB relative to the average power of the first path. The simulation time covered the channel coherence time, and 1000 channel realizations. The assumed BEP for uncoded QAM modulation is $P_e = 10^{-3}$.

In Figure 2.21simulation results are presented for the case of linear taxation of resources, i.e. for $\Delta_\tau = 0$ and various K and I values In Figure 2.21a, the spectral efficiency (sum-throughput averaged over the number of used SCs is presented, while in Fig. Figure 2.21b the throughput averaged over the number of all available SCs N is plotted vs. the tax-rate parameter value τ_0. Moreover, these results are compared with the Round-Robin (R-R) SCs allocation and with the *optimal* SCs allocation. The optimality here refers only to the spectral efficiency of all-resources distribution, which means that the subsequent SCs are allocated to nodes, which experience the highest CINRs at these SCs.

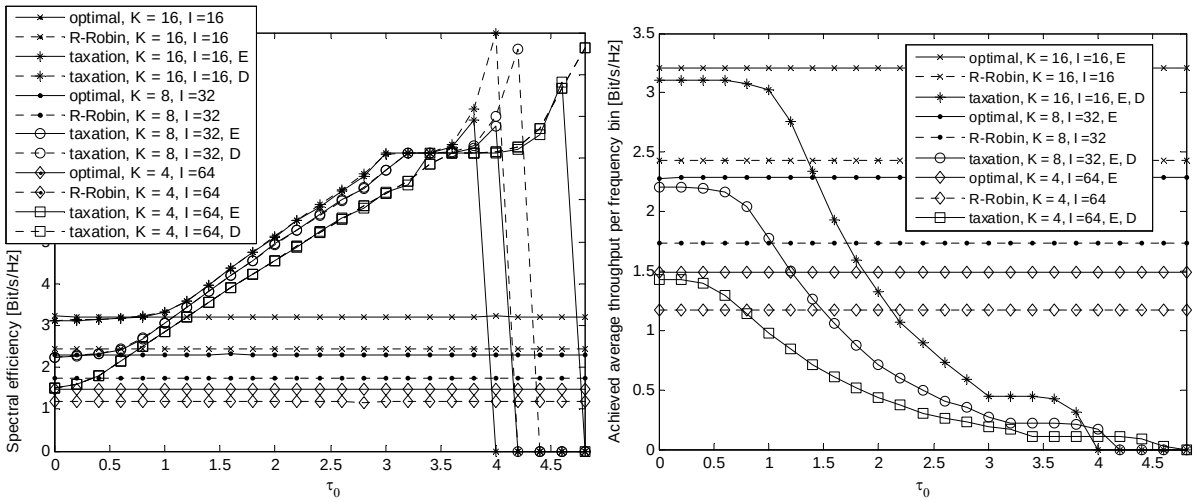

Figure 2.21 – Spectral efficiency (a) and the overall throughput averaged over N available SCs (b) vs. the linear tax-rate parameter value τ 0 (E – equal average SINR for all nodes, D –diverse SINR with 1 dB max deviation from $\bar{\gamma}$).

In Figure 2.22a and Figure 2.22b, analogous results for the arithmetically-progressive taxation of resources are presented vs. the tax-rate parameter value $\Delta_\tau (\tau_0 = 0)$. Let us note, that for the appropriately high tax values, the spectral efficiency is higher in our game model than even this optimal allocation of SCs, although the average throughput per SC decreases with an increase of the relevant tax-rate parameters: τ_0 and Δ_τ. Low average throughput for high tax-values occurs due to poor SCs utilization, which become too "costly" (in terms of low payoff). Moreover, the increase of the spectral efficiency, the decrease of the average throughput, and the decrease of the percentage of utilized SCs is more gradual for linear taxation than for the arithmetically-progressive taxation (where more rapid reaction of the system-model performance to the Δ_τ parameter change is observed). Thus the calibration of Δ_τ can be relatively more sensitive to the CSI imperfections than τ_0.

Reference DR9.2

To summarize, in our game-theoretic model, each player makes decisions independently based on the local CSI and the taxation parameters τ_0 and Δ_τ. For the sake of the algorithm efficiency, the payoff has been defined so as to reflect the throughput achieved by a CR-node and the network capacity of serving the CR-nodes community. For the sake of rationality, taxation of the SCs has been introduced. By treating the CR-nodes community as a single observed player, and by introducing the efficiency and rationality measures we can approach high overall and nodes' perceived spectral efficiency, high usage of the available SCs and 100% of served nodes with low complexity and in the distributed manner as opposed to solutions described in the literature. The base station role is only to beacon the tax-rate parameter value in its service area.

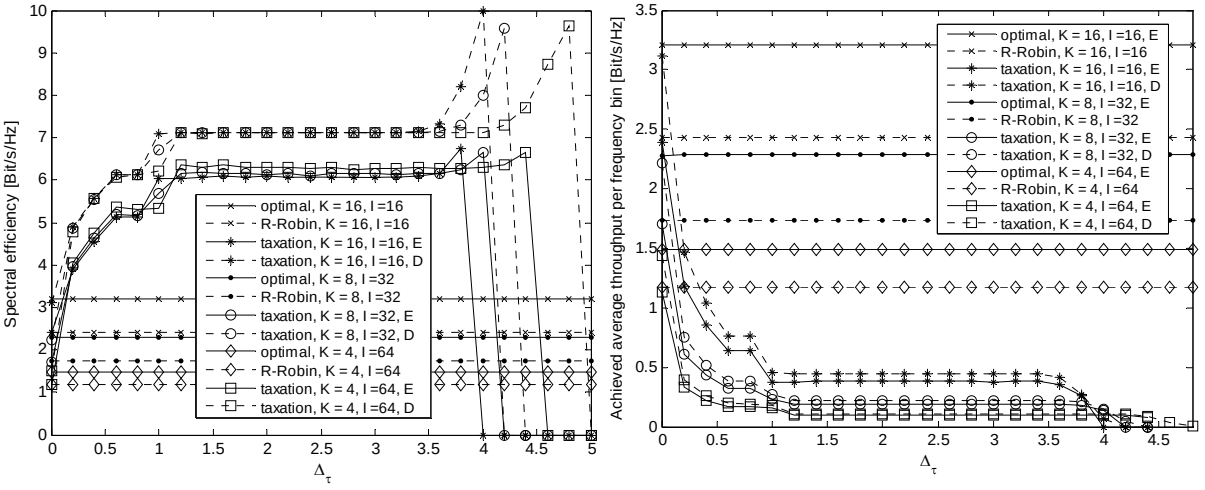

Figure 2.22 – Spectral efficiency (a) and the throughput averaged over N available SCs (b) vs the arithmetically-progressive tax-rate parameter Δτ. (E – equal average SINR for nodes, D –diverse SINR with 1 dB max deviation from $\overline{\gamma}$).

2.4.2 Bandwidth Limiting in Decentralized Vector Multiple Access Channels

As mentioned above, game theory in distributed RRM often provides solutions which remain suboptimal due to the lack of global information. To overcome this suboptimality, imposing orthogonal communications between transmitters using only a single channel has been a well-accepted solution, e.g., IEEE802.11 networks. Nonetheless, the choices of the total number of available channels as well as limiting the bandwidth to a single channel have been done in an ad hoc manner. Below, we provide an analysis of the benefits of bandwidth limiting (BL), i.e., reducing the number of channels each transmitter can use in vector MAC. More specifically, we provide an answer to the following question: is it worth to limit the number of channels each transmitter might use regarding the network spectral efficiency?

We consider two scenarios. In the first scenario, transmitters have to use non-intersecting sets of channels. In the second one, transmitters can freely exploit all the available channels. In the second case, the receiver implements multiuser decoding and successive interference cancelation (SIC). Here, each transmitter is aware of both the decoding order and its respective noise plus interference levels. Under these conditions, the optimal decentralized policy for each transmitter to maximize its own data rate is to use a water-filling power allocation scheme considering the multiple access interference as noise [71]. In both cases, the fact that transmitters maximize their own spectral efficiency independently of the others results in suboptimal usage of the spectrum, what is related again to the dilemma known as *the tragedy of the commons* [77].

2.4.2.1 System Model

Consider a set $\mathsf{K}=\{1,\ldots,K\}$ of transmitters communicating with a unique receiver using a set $\mathsf{N}=\{1,\ldots,N\}$ of equally spaced frequency bands (channels). In the information theory jargon, this network topology is known as vector MAC or parallel MAC [78]. Transmitters arrive sequentially to the network. Their index in the set K shows the order of arrival. All the radio devices are equipped with a unique antenna. Transmitter $k\in\mathsf{K}$ is able to simultaneously transmit over all the channels subject to a power-limitation,

$$\forall k\in\mathsf{K},\quad \frac{1}{N}\sum_{n=1}^{N}p_{k,n}\ \le p_{k,\max}, \tag{2.80}$$

where $p_{k,n}$ and $Np_{k,\max}$ denote the transmit power over channel n and the maximum transmittable power of transmitter k. We assume that all transmitters are limited by the same maximum transmittable power level, i.e., $\forall k\in\mathsf{K}$ and $\forall n\in\mathsf{N}$, $p_{k,\max}=p_{\max}$.

We denote the channel coefficients in the frequency domain between the receiver and transmitter k over channel n by $h_{k,n}$. For all $n\in\mathsf{N}$ and for all $k\in\mathsf{K}$, $h_{k,n}$ is a realization of a complex random variable h with independent and identically distributed (i.i.d) Gaussian real and imaginary parts with zero mean and variance ½. The channel gain is denoted by $g_{k,n}=\| h_{k,n}\|^2$. Then, the channel gains can be modeled by realizations of a random variable g with exponential distributions with parameter $\rho=1$, whose cumulative distribution function (c.d.f) and probability density function (p.d.f) are denoted by $F_g(\lambda)=1-e^{-\lambda}$ and $f_g(\lambda)=e^{-\lambda}$, respectively. The received signals sampled at symbol rate can be written as a vector $\mathbf{y}=(y_1,\ldots,y_N)$ where the entries y_n for all $n\in\mathsf{N}$ represent the received signal over channel n. Hence,

$$\mathbf{y}=\sum_{k=1}^{K}\mathbf{H}_k\mathbf{s}_k+\mathbf{w}, \tag{2.81}$$

where $\mathbf{H}_k$ is an N-dimensional diagonal matrix with main diagonal $(h_{k,1},\ldots,h_{k,N})$. The N-dimensional vector $\mathbf{s}_k=(s_{k,1},\ldots,s_{k,N})$ represents the symbols transmitted by transmitter k over each channel. The power allocation profile of transmitter k, the vector $(p_{k,1},\ldots,p_{k,N})$, is the diagonal of the diagonal matrix $\mathbf{P}_k=E\left[\mathbf{s}_k\mathbf{s}_k^H\right]$. The N-dimensional vector $\mathbf{w}$ represents the noise at the receiver. Its entries, w_n for all $n\in\mathsf{N}$, are modeled by a complex circularly symmetric additive white Gaussian noise (AWGN) process with zero mean and variance σ^2.

Regarding the channel state information (CSI) we assume that each transmitter perfectly knows its own channel coefficients and the noise plus interference level at each channel. This is the case when transmitters are able to sense its environment or the receiver feeds back this parameter as a signaling message to all the transmitters.

We denote the set of channels being used by transmitter k by L_k, i.e., $\forall k\in\mathsf{K}$ and $\forall n\in\mathsf{L}_k$, $p_{k,n}\neq 0$, and $\forall m\in\mathsf{N}\setminus\mathsf{L}_k$, $p_{k,m}=0$. Depending on the conditions over each set L_k, for all $k\in\mathsf{K}$, we consider two different scenarios.

2.4.2.2 Scenario 1: Spectral Resource partition

In this scenario, a given channel cannot be used by more than one transmitter. Thus, this is equivalent to define the sets L_k for all $k \in \mathsf{K}$ as a partition of the set N, i.e.,

- $\forall (j,k) \in \mathsf{K}^2$ and $j \neq k$, $\mathsf{L}_j \cap \mathsf{L}_k = \varnothing$,
- $\forall (j,k) \in \mathsf{K}^2$ and $j \neq k$, $\mathsf{L}_j \cup \mathsf{L}_k \subseteq \mathsf{N}$,
- $\forall k \in \mathsf{K}$, $|\mathsf{L}_k| > 0$.

Due to the asynchronous arrival of the users, we assume that there exists an order to access the set of channels N. We index the transmitters such that transmitter $k \in \mathsf{K}$ arrives in the k^{th} position.

2.4.2.3 Scenario 2: Spectral Resource Sharing

In this scenario we allow several transmitters to use the same channels. Thus, this is equivalent to define the sets L_k for all $k \in \mathsf{K}$ as a cover of the set N, i.e.,

- $\forall k \in \mathsf{K}, \quad \mathsf{L}_k \subseteq \mathsf{N}$,
- $\forall k \in \mathsf{K}$, $|\mathsf{L}_k| > 0$.

We assume that the receiver performs multiuser decoding and successive interference cancelation (SIC) at each channel. The decoding order is the same in all channels and it is related to the arrival order. Here, transmitter $k \in \mathsf{K}$, arriving in the k^{th} position, is decoded in the $K-k+1$ position.

To make a difference between scenario 1 and 2, we use the super index $^{(i)}$ with $i \in \{1,2\}$ for all the sets and variables associated with each of them. The noise plus multiple access interference (MAI) for transmitter k over channel n is denoted by $\alpha_{k,n}^{(i)}$, where $\alpha_{k,n}^{(1)} = \sigma^2$ and $\alpha_{k,n}^{(2)} = \sigma^2 + \sum_{j=1}^{k-1} p_{j,n} g_{j,n}$, where, for all $n \in \mathsf{N}$, $p_{0,n} = 0$ and $g_{0,n} = 0$. The SINR for transmitter k over channel n is denoted by $\gamma_{k,n}^{(i)}$ and $\forall k \in \mathsf{K} \text{and} \forall n \in \mathsf{N}$,

$$\gamma_{k,n}^{(i)} = \frac{p_{k,n} g_{k,n}}{\alpha_{k,n}^{(i)}}. \tag{2.82}$$

In both scenarios each transmitter $k \in \mathsf{K}$ aims to maximize its own data rate $R_k(\boldsymbol{\gamma}_k)^{(i)}$, i.e.,

$$R_k(\boldsymbol{\gamma}_k)^{(i)} = \sum_{n=1}^{N} \log_2\left(1+\gamma_{k,n}^{(i)}\right), \tag{2.83}$$

with $\boldsymbol{\gamma}_k^{(i)} = (\gamma_{k,1}^{(i)}, \ldots, \gamma_{k,N}^{(i)})$ subject to its power limitations and independently of the data rate of the other devices.

Assuming that each channel bandwidth is normalized to 1 Hz, a given transmitter k sets out its transmit power levels $p_{k,n}$, $\forall n \in \mathsf{N}$ by solving the optimization problem (OP)

$$\begin{aligned} \max_{p_{k,n}, \forall n \in \mathsf{Z}_k^{(i)}} \quad & \sum_{n \in \mathsf{Z}_k^{(i)}} \log_2\left(1+\gamma_{k,n}^{(i)}\right) \\ \text{s.t.} \quad & \frac{1}{N} \sum_{n \in \mathsf{Z}_k^{(i)}} p_{k,n} \leq p_{\max}, \end{aligned} \tag{2.84}$$

where, for all $k \in \mathsf{K}$, the set $\mathsf{Z}_k^{(1)} = \mathsf{N} \backslash \mathsf{L}_1 \cup \ldots \cup \mathsf{L}_{k-1}$, with $\mathsf{L}_0 = \varnothing$, and $\mathsf{Z}_k^{(2)} = \mathsf{N}$. Thus, $\mathsf{Z}_k^{(i)}$ is the set of channels available for user k in scenario i. The solution to the OP in (2.84) is given in [78] and thus, we only provide the solution hereafter; $\forall k \in \mathsf{K}$ and $\forall n \in \mathsf{Z}_k^{(i)}$,

$$p_{k,n} = \left[\beta - \frac{\alpha_{k,n}^{(i)}}{g_{k,n}} \right]^+, \tag{2.85}$$

and, $\forall k \in \mathsf{K}$ and $\forall n \in \mathsf{Z}_k^{(1)}$

$$p_{k,n} = 0. \tag{2.86}$$

Here, the operator $[.]^+$ is the same as $\max(0,.)$. Given the sets A, B and the complement of the latter, B', in a given universal set, the operation $\mathsf{A} \backslash \mathsf{B} = \mathsf{A} \cap \mathsf{B}'$. The term β is a Lagrangian multiplier, known as water-level, chosen to satisfy (2.80). The transmit power levels in (2.85) can be iteratively obtained by using the water-filling algorithm described in [68]. From expression (2.85), it can be implied that $\mathsf{L}_k^{(i)} \subseteq \mathsf{Z}_k^{(i)}$.

Once the OP in (2.84) has been solved, the data rate per channel of transmitter $k \in \mathsf{K}$, is

$$\overline{R}_k(\boldsymbol{\gamma}_k)^{(i)} = \frac{1}{|\mathsf{Z}_k^{(i)}|} \sum_{n \in \mathsf{Z}_k^{(i)}} \log_2\left(1 + \gamma_{k,n}^{(i)}\right), \tag{2.87}$$

and then, its spectral efficiency Φ_k is

$$\Phi_k^{(i)} = \underbrace{\frac{|\mathsf{Z}_k^{(i)}|}{N}}_{\Omega_k^{(i)}} \overline{R}_k(\boldsymbol{\gamma}_k)^{(i)}, \tag{2.88}$$

where, $\Omega_k^{(i)}$ represents the fraction of spectrum accessible for transmitter k. Note that due to the decentralized nature of the network, the individual spectral efficiency is maximized independently by each transmitter. As described in [77], it might lead to significant losses in the network spectral efficiency. We study this effect in the next section.

Let us define the network spectral efficiency (NSE) $\Phi^{(i)}$ as

$$\begin{aligned} \Phi^{(i)} &= \sum_{k=1}^{K} \Phi_k^{(i)} \\ \Phi^{(i)} &= \sum_{k=1}^{K} \Omega_k^{(i)} \overline{R}_k^{(i)}, \end{aligned} \tag{2.89}$$

for both scenarios, spectral resource partition (scenario 1) and spectral resource sharing (scenario 2). The analysis of the NSE in the asymptotic regime is presented in [79]. We assume that both the number of channels (N) and the number of transmitters (K) grow to infinity at a constant ratio $\frac{N}{K} = L < \infty$. Under these conditions, we determine the NSE using BL and provide closed form expressions. We have observed that the asymptotic model perfectly describes the system in the finite case i.e., when K and N are small numbers.

2.4.2.4 NSE With BL

Now, we limit the number of channels each transmitter can use. For the ease of calculations, we keep the conditions that both K and N grow to infinity at the same rate, i.e., $N \to \infty$, and $K \to \infty$, and $\frac{N}{K} = L < \infty$. To provide at least one channel to each user, we assume that $L \geq 1$.

Let us first consider Scenario 1: Spectral Resource Partition. When the number of accessible channels for transmitter $k \in \mathsf{K}$ is limited to $L \in \mathsf{N}$ channels, the fraction of accessible spectrum $\Omega_k^{(1,\mathrm{BL})}$ for each transmitter is

$$\Omega_{k,\infty}^{(1,\mathrm{BL})} = \min\left\{ \Pr\left(\beta^* < \frac{\sigma^2}{\lambda} \right), \frac{L}{N} \right\}. \tag{2.90}$$

Then, BL has an effect if and only if $\frac{L}{N} < \Pr\left(\beta^* \ \frac{\sigma^2}{\lambda} \right)$. This condition is equivalent to state that we should limit the transmitters to use a smaller number of channels of that used on the absence of BL. Hence, under the asymptotical assumptions, we have that

$$\Omega_{k,\infty}^{(1,\mathrm{BL})} = \frac{L}{N}, \tag{2.91}$$

and

$$\Phi_{\infty}^{(1,\mathrm{BL})} = \sum_{i=1}^{K} \Omega_{k,\infty}^{(1,\mathrm{BL})} \overline{R}_{\infty} = \frac{KL}{N} \overline{R}_{\infty}. \tag{2.92}$$

In Scenario 2: Spectral Resource Sharing, each transmitter can access all the channels and thus, $\Omega_{k,\infty}^{(2)} = 1$. When we limit the bandwidth for transmitter k we impose that $\Omega_{k,\infty}^{(2),\mathrm{BL}} \ \ \Omega_{k,\infty}^{(2)}$. Then, the NSE under BL is

$$\Phi_{\infty}^{(2),\mathrm{BL}} = \sum_{k=1}^{K} \Omega_{k,\infty}^{(2),\mathrm{BL}} \overline{R}_{k,\infty}^{(2),\mathrm{BL}}. \tag{2.93}$$

We have provided expressions for the NSE in both absence and presence of BL in the asymptotic regime. Now, it remains to determine the conditions over which BL brings benefits to the network in terms of spectral efficiency.

2.4.2.5 Optimal Bandwidth Limiting

In this section, we investigate the existence of an optimal BL point, i.e., optimal values of the fractions $\Omega_k^{(i,\mathrm{BL})}$, with $i \in \{1,2\}$ such that $\Phi_{\infty}^{(i),\mathrm{BL}} \ \ \Phi_{\infty}^{(i)}$.

In case of Scenario 1 (Spectral Resource Partition), to improve the NSE by introducing BL in the network, the following condition must be met,

$$\begin{array}{c} \Phi_{\infty}^{(1)} \quad \Phi_{\infty}^{(1),\mathrm{BL}} \\ \dfrac{1-\left(\Omega_{\infty}^{(1)}\right)^{K}}{1-\Omega_{\infty}^{(1)}}\overline{R}_{\infty} \quad \dfrac{KL^{*}}{N}\overline{R}_{\infty} \\ L^{*}\dfrac{N}{K}\dfrac{1-\left(\Omega_{\infty}^{(1)}\right)^{K}}{1-\Omega_{\infty}^{(1)}} \end{array} \tag{2.94}$$

In the expression above we show that the optimal BL parameter L^{*} depends mainly on the network load (transmitters per channel, $\frac{K}{N}$) and the SNR of the transmitters. Note that the factor $\Omega_{\infty}^{(1)}$ is a function of $p_{\max}$, σ^{2} and the probability distribution of the channels gains $f_{g}(\lambda)$ described in (2.79).

In case of Scenario 2 (Spectral Resource Sharing), we follow the same reasoning as in scenario 1, i.e. we improve the NSE by using BL, if

$$\Phi_{k,\infty}^{(2)} \quad \Phi_{k,\infty}^{(2),\mathrm{BL}}. \tag{2.95}$$

However, under BL we have that $\Omega_{k,\infty}^{(2),\mathrm{BL}} \quad \Omega_{k,\infty}^{(2)}$ and thus,

$$\sum_{k=1}^{K}\Omega_{k,\infty}^{(2)}\overline{R}_{k,\infty}^{(2)} \sum_{k=1}^{K}\Omega_{k,\infty}^{(2),\mathrm{BL}}\overline{R}_{k,\infty}^{(2),\mathrm{BL}}. \tag{2.96}$$

Then, we have shown that in the asymptotic regime, any kind of BL does not bring any improvement on the NSE. On the contrary, it might introduce significant losses of NSE.

2.4.2.6 Simulation Results

Below, we provide numerical results of our mathematical model. We present simulations of the NSE obtained in both scenarios as a function of the BL parameter L for different network loads. In Figure 2.23, we observe the existence of an optimum BL point for scenario 1. Conversely, in the second scenario, the existence of such optimal is not evident, as at a certain point, the NSE is invariant with respect of the BL parameter L.

We compare the optimal BL parameter L obtained from simulations with that obtained from expression (2.94). In Figure 2.24 we plot both results. Therein, we show that the asymptotical approximation (2.94) is a precise approximation of the optimal number of channels each transmitter must use to maximize the NSE.

Finally, we show in Figure 2.25 the NSE obtained with absence and presence of BL. In the first scenario, we observe a significant gain in NSE when BL is used. This gain is more important for non-overloaded networks, whereas for quasi full-loaded or overloaded networks ($K \quad N$), the gain obtained by BL approaches that of limiting the transmitters to use a unique channel. In the same figure, we observe that the NSE appears to be constant for certain intervals. This is due to the fact that inside those intervals the optimal BL parameter remains constant, as shown in Figure 2.24. Moreover, the gain in NSE is very significant at high SNR ($\mathrm{SNR} = \frac{p_{\max}}{\sigma^{2}}$) levels. On the contrary, for low SNR levels, small gains in NSE are obtained when the network is low loaded. In Figure 2.26 we plot the NSE for several values of SNR in the second scenario. In any case, we observe that there is not significant gain when all transmitters use the same BL parameter L.

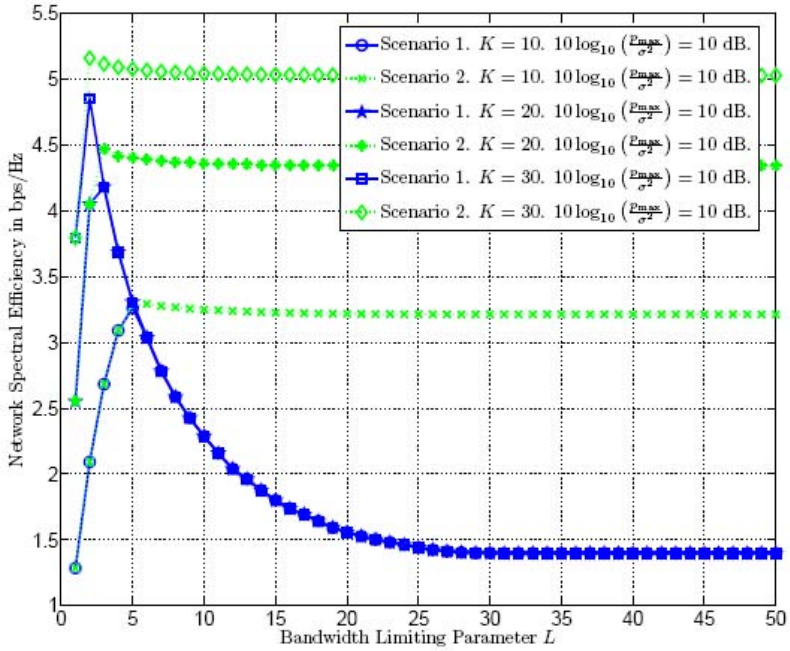

Figure 2.23 – Network Spectral Efficiency (2.89) in bps/Hz as a function of the maximum number of accessible channels L. Total number of available channels $N = 50$, and $10\log_{10}\left(\frac{p_{\max}}{\sigma^2}\right) = 10dB$.

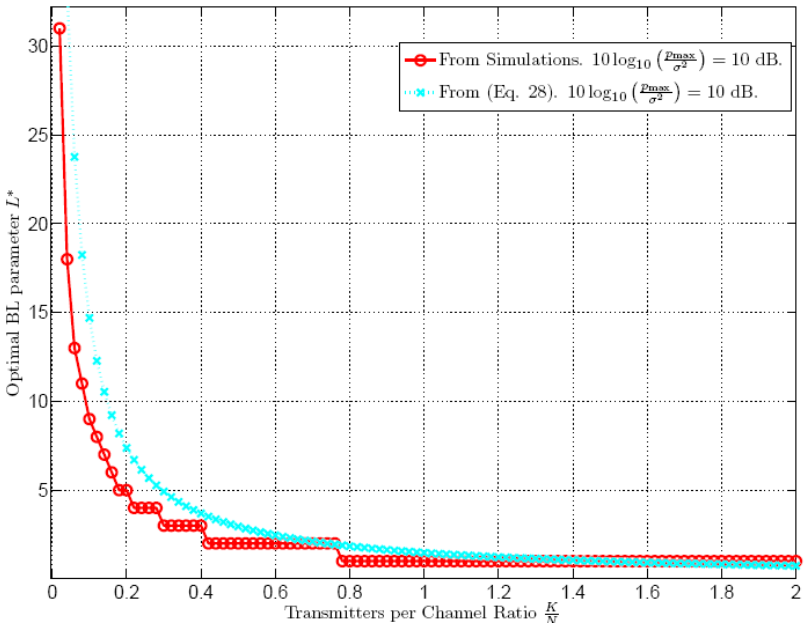

Figure 2.24 – Optimal BL parameter L (2.94) for scenario 1 as a function of the network load, $(\frac{K}{N})$. Total number of available channels $N = 50$, and $10\log_{10}\left(\frac{p_{\max}}{\sigma^2}\right) = 10dB$.

Reference DR9.2

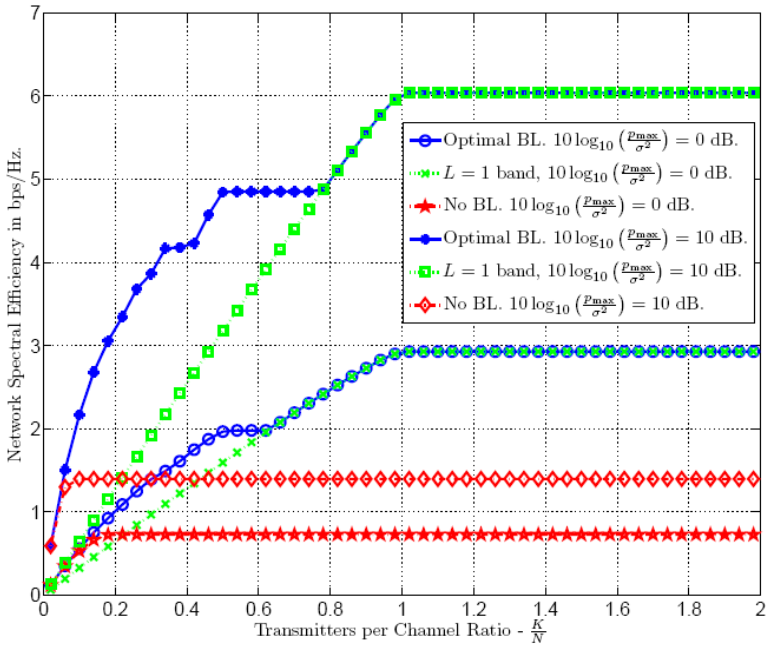

Figure 2.25 – Network Spectral Efficiency (2.89) in bps/Hz for scenario 1 as a function of the network load $(\frac{K}{N})$. Total number of available channels $N = 50$.

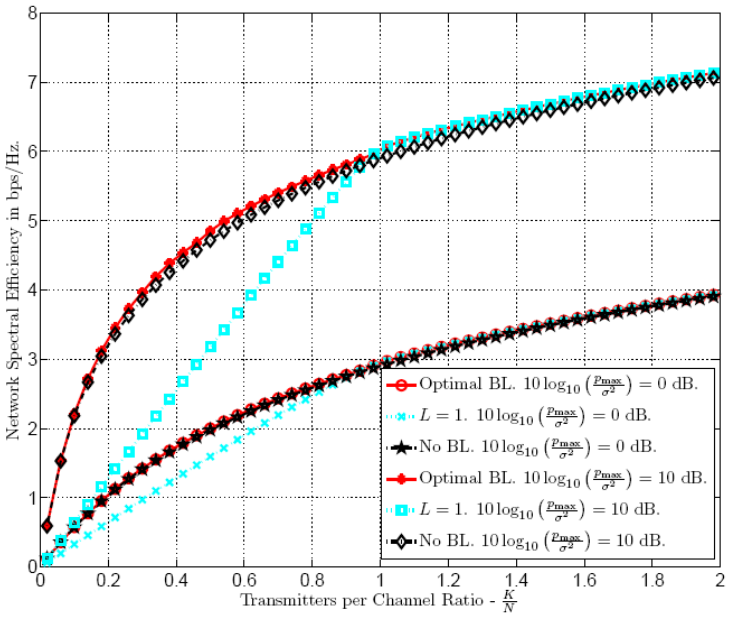

Figure 2.26 – Network Spectral Efficiency (2.89) in bps/Hz for scenario 2 as a function of the network load $(\frac{K}{N})$. Total number of available channels $N = 50$.

To summarize, in a decentralized vector MAC where each transmitter aims to maximize its own data rate by using water-filling based power allocation, the network sum-rate can be improved by limiting

the number of available channels for each transmitter (bandwidth limiting). We have provided a closed form expressions for the optimal maximum number of channels each transmitter must access in the case where transmitters use non-intersecting sets of channels. In this case, such an optimum operating point depends mainly on the network load (transmitters per channel) and the different signal to noise ratios. Contrary to the first scenario, in the case of spectrum resource sharing, we show that when all transmitters use the same BL policy, BL does not bring a significant improvement on the network spectral efficiency.

Further studies will focus to the case when transmitters have different channel statistics, since it might lead to the usage of different BL policies for each transmitter.

2.5 Conclusions

In this Section the scenarios and results considered and obtained within WG1, WG2 and WG3, have been presented. In particular, they are related to different RRM and JRRM strategies to be implemented over respectively homogeneous and heterogeneous networks. For this reason, different approaches have been considered like centralized vs. decentralized, and mathematical vs. simulative, which have been chosen from time to time according to the specific scenario under consideration.

In WG1, the focus of the analysis was on heterogeneous cellular networks: the scenario was composed by a train station where different systems (i.e., air interfaces) like UMTS, WiMAX and WLAN are deployed. The coverage areas offered by these systems are partially superimposed and uses can access to one/some/all of them. The problem was to design proper strategies to direct users over the best air interface according to considerations on users' conditions (e.g., channel, position, etc.) and traffic specifications. The scenario has been made even richer by the presence of a sensor network which conveys sensed data to the WiMAX air interface. Due to the complexity of the scenario where many realistic parameters are taken into account, in this case a simulative approach has been pursued. On another side, WG1 performed also investigations about VHO strategies to be applied to heterogeneous networks. In this case a mathematical framework was feasible, and hence it has been considered.

In WG2, the focus was on RRM in a cellular system, and in particular resource allocation. Also in this case, due to the complexity of the realistic scenario considered, a simulative approach has been pursued to obtain results. Several algorithms have been designed and evaluated with objectives on instantaneous parameters like, for example, rate maximization, with constraints on power. In this case, optimization tools have been used to properly design system parameters. As a benchmark, similar evaluations on system performance have been performed with resource allocation strategies based on utility functions. Several of them have been designed and evaluated. A significant amount of results have been already obtained by simulation for the single-cell scenario, whereas the multi-cell one will be considered in future investigations.

In WG3, the focus was on cognitive radio. It is clear that in this case the paradigm considered is completely different from the one considered in previously mentioned WGs, since CRs are distributed by nature. In such kind of systems, game theory is usually considered as a valuable tool, since it is based on the idea that each player takes decisions autonomously. In the scenario investigated, each node detects the spectrum available, with the goal of acquiring radio resources while maximizing the throughput at a minimum cost in terms of energy consumption. At this aim, two scenarios have been investigated: players are deliberately limited in their accessible resources through 1) the taxation of resources; and 2) the resource bandwidth limiting with successive interference cancellation of the players. Since game theory provides usually suboptimal solutions due to the lack of global information, an analysis of the benefits of bandwidth limiting has been performed, and a closed form expression for the optimal maximum number of channels each transmitter must access in the case where transmitters use non-intersecting sets of channels have been identified.

3 ASM ALGORITHMS AND STRATEGIES AND THEIR EVALUATION

3.1 Introduction

This chapter presents the activities that have been carried out inside WPR9 in the framework of Advanced Spectrum Management (ASM). They mainly contribute to one of the current research trends in the spectrum management which are the so-called Dynamic Spectrum Access Networks (DSANs), in which unlicensed radios, denoted as Secondary Users (SUs) are allowed to operate in licensed bands provided that no harmful interference is caused to the licensees, denoted as Primary Users (PU). One of the key enabling technologies for DSAN development is Cognitive Radio (CR), which has been claimed to be an adequate solution to the existing conflicts between spectrum demand growth and spectrum underutilization. This term Cognitive Radio, originally coined by J. Mitola III in [100], envisages a radio able to sense and be aware of its operational environment so that it can dynamically and autonomously adjust its radio operating parameters accordingly to adapt to the different situations.

Based on the above, this chapter is organised mainly in two main activities. The first one is devoted to perform a spectrum measurement campaign in order to identify primary user temporal and spatial usage patterns in specific environments for different ranges of frequencies. The outcome of this campaign can be an interesting input for the application and development of Dynamic Spectrum Access (DSA) to handle the access of secondary users to the available spectrum holes left by primary users. The main results of the measurement campaign are presented in section 3.2.

The second activity, presented in section 3.3, addresses the DSA problem by using machine learning strategies. Such strategies are executed at a cognitive agent of a secondary user to decide on the most appropriate channels to sense and access from a set of available channels. Learning is based on characterising the temporal occupancy of the set of channels by primary users, so that the cognitive agent will finally learn those channels in which it has more chances to succeed when trying to start a secondary transmission.

3.2 Measurements to Detect Spectrum Availability

3.2.1 Introduction

Measurements of the radio environment can provide valuable insights into current spectrum usage. A proper understanding of current spectrum usage patterns can be very useful to policy makers in order to define adequate dynamic spectrum policies and to the research community in general in order to identify appropriate frequency bands for the deployment of future Cognitive Radio (CR) networks, as well as the identification of usage patterns that can be exploited in the development of useful spectrum usage models and more efficient CR techniques. The measurement of real network activities therefore constitutes an important step towards a realistic understanding of dynamic spectrum utilisation and hence towards the deployment of future CR networks.

Several measurement campaigns covering both wide frequency ranges [80]–[85] as well as some specific licensed bands [86]–[90] have already been performed in diverse locations and scenarios in order to determine the degree to which allocated spectrum bands are occupied in real wireless communication systems. All these spectrum measurements provide a valuable source of information for a realistic understanding of dynamic spectrum utilisation and practical development of the CR technology. However, in order to enable a wide scale deployment, the CR technology cannot be developed based on the conclusions derived from the studies conducted in a few geographical areas or under a specific spectrum regulation. CR should take into account the possibility to operate under many different spectrum regulations and a wide variety of scenarios. Therefore, the number of measured locations can arguably be considered as insufficient. To enable a wide scale deployment, further spectrum measurements are consequently required.

The need for new spectrum measurements motivates the spectrum measurement campaign that is currently being carried out in Working Group 4 (WG4) of WPR9. After the initial results presented in

[2][91], this section reports spectrum occupancy measurements conducted in the frequency range from 75 MHz to 7075 MHz in urban Barcelona. The obtained results demonstrate the availability of a significant amount of white space that could potentially be used by CR networks.

3.2.2 Measurement Setup

The measurement setup and methodology employed in this work have been carefully designed based on the lessons learned from previous measurement campaigns and the findings of the study presented in [92], where some important methodological aspects to be accounted for when evaluating spectrum occupancy in the context of CR are analysed and discussed.

The employed measurement configuration relies on a spectrum analyser setup where various external devices have been added in order to improve the detection capabilities of the system and hence obtain more accurate and reliable results. The design is composed of two broadband antennas that cover the frequency range from 75 to 7075 MHz, a switch to select the desired antenna, several filters to remove undesired signals, a low-noise pre-amplifier to enhance the overall sensitivity and thus the ability to detect weak signals, and a high performance spectrum analyser to record the spectral activity. A simplified scheme with all the devices and their main technical characteristics is shown in Figure 3.27. Figure 3.28, Figure 3.29 and Figure 3.30 show the various parts of the measurement configuration.

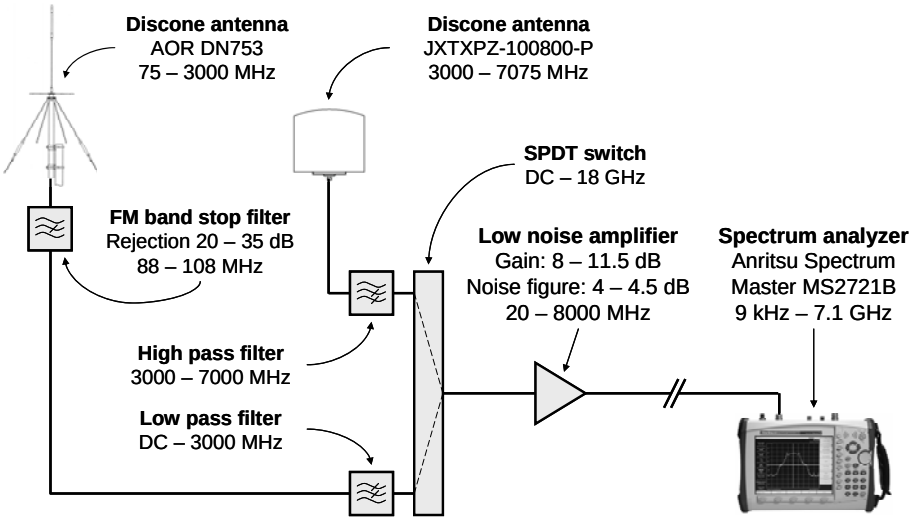

Figure 3.27 – Measurement setup employed in this study (complete scheme).

3.2.2.1 Antenna Subsystem

The antenna subsystem is shown in Figure 3.28. Two wideband discone-type antennas are used to cover the frequency range from 75 to 3000 MHz (AOR DN753) and 3000 to 7075 MHz (A-INFO JXTXPZ-100800/P). Discone antennas are wideband antennas with vertical polarisation and omni-directional receiving pattern in the horizontal plane. Even though some transmitters are horizontally polarized, they usually are high-power stations (e.g., TV stations) that can be detected even with vertically polarized antennas. The exceptionally wideband coverage (allowing a reduced number of antennas in broadband spectrum studies) and the omni-directional feature (allowing the detection of primary signals coming for any directions) make discone antennas attractive in radio scanning and monitoring applications, and have been a preferred option for many past spectrum studies.

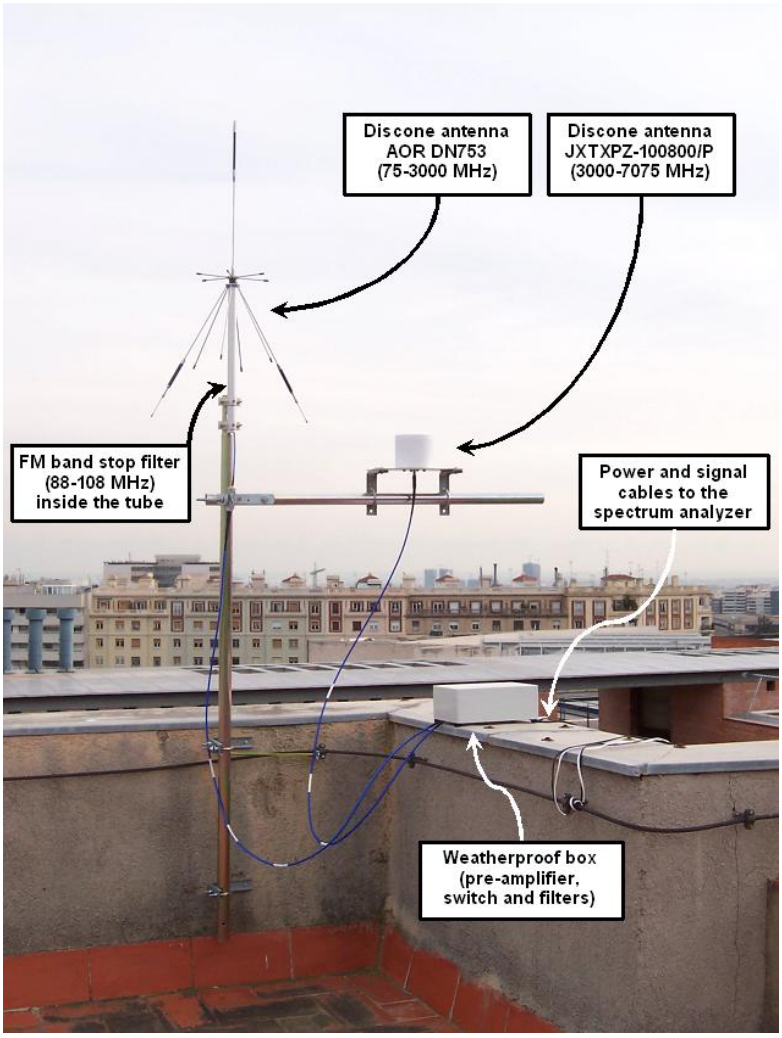

Figure 3.28 – Measurement setup employed in this study (antenna subsystem).

3.2.2.2 Radio Frequency Subsystem

The Radio Frequency (RF) subsystem is shown in Figure 3.29. This module performs antenna selection, filtering and amplification. The desired antenna is selected by means of a Single Pole Double Throw (SPDT) switch. An electromechanical switch has been selected because of its high isolation (90-100 dB) and low insertion loss (0.1-0.2 dB). In order to remove undesired signals, three filters are included. A band stop filter blocks signals in the frequency range of Frequency Modulation (FM) broadcast stations (87.5-108 MHz). Usually, such stations are high power transmitters that may induce overload in the receiver thus degrading the receiver performance by an increased noise floor or by the presence of spurious signals, which inhibits the receiver's ability to detect the presence of weak signals. Since the FM band is of presumably low interest for secondary use due to its usually high transmission power and expected high occupancy rate, a FM band stop filter has been employed in order to remove FM signals and avoid overload problems, improving the detection of weak signals at other frequencies. Low pass and high pass filters have been used to remove out-of-band signals and reduce the potential creation of inter-modulation products. To compensate for device and cable losses and increase the system sensitivity, a low noise pre-amplifier has been included. Higher amplification gains result in better sensitivities at the expense of reduced dynamic range and vice versa. The selected mid-gain amplifier provides significant sensitivity improvements while guaranteeing the Spurious-Free Dynamic Range (SFDR) required by the measured signals.

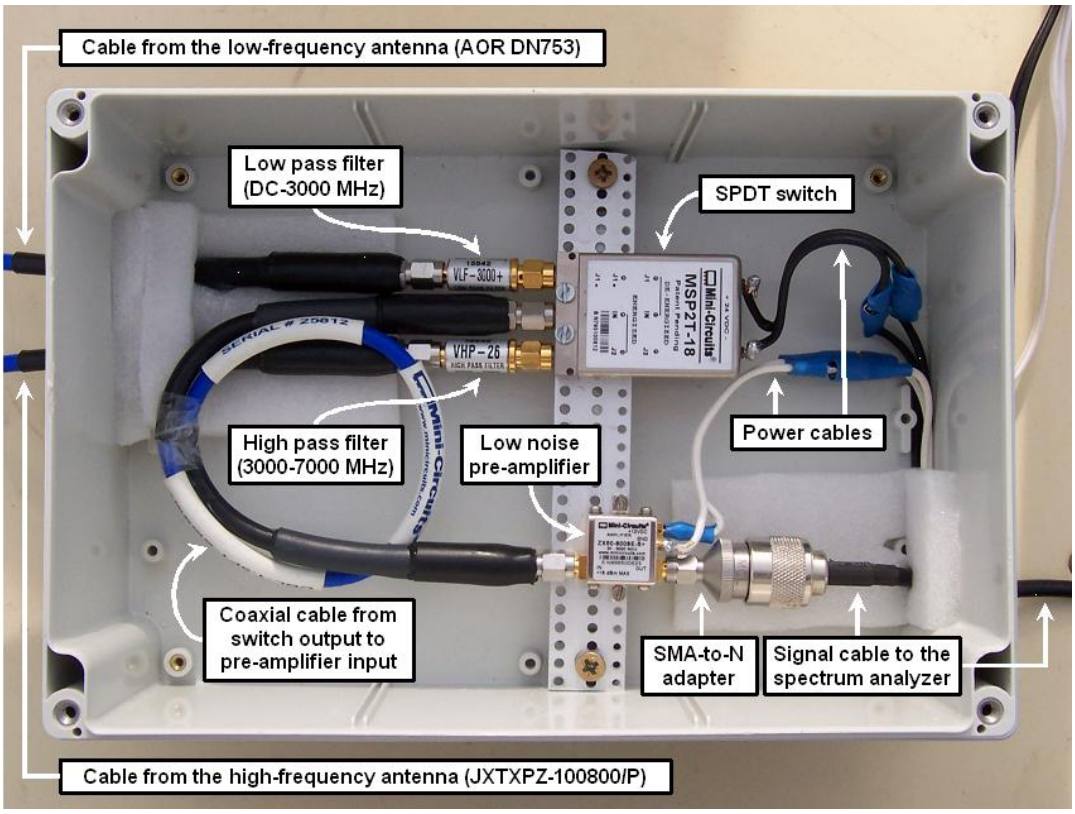

Figure 3.29 – Measurement setup employed in this study (radio frequency subsystem).

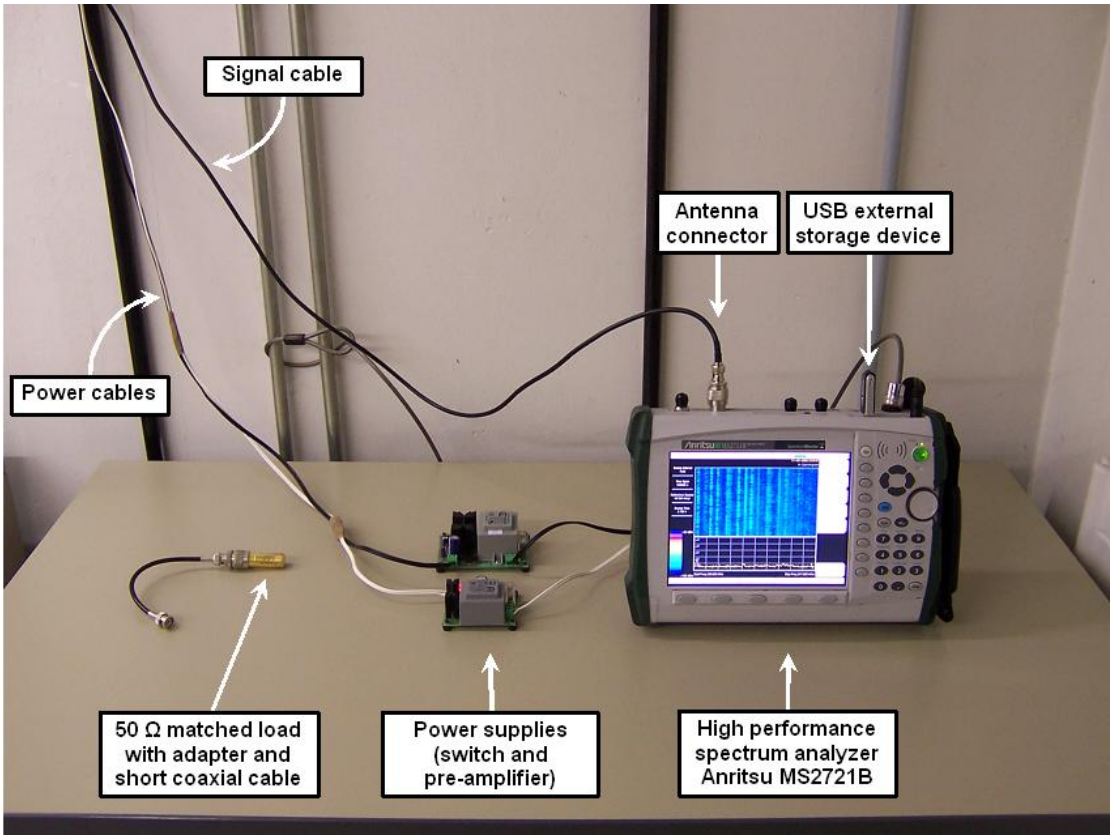

Figure 3.30 – Measurement setup employed in this study (spectrum analyser).

3.2.2.3 Spectrum Analyser

An Anritsu Spectrum Master MS2721B high performance handheld spectrum analyser has been used to provide power spectrum measurements and record the spectral activity over the complete frequency range. This spectrum analyser provides a measurement range from 9 kHz to 7.1 GHz, low noise level and a built-in pre-amplifier that facilitate the detection of weak signals, fast sweep speed automatically adjusted, and the possibility to connect an external USB storage device to save measurements for later data post-processing.

Since the different operating modes of spectrum analysers can significantly alter the results of a measurement, proper parameter selection is crucial to produce valid and meaningful results. The different parameters of the spectrum analyser have been set according to the basic principles of spectrum analysis [93][94] as well as some particular considerations specific to CR [92]. Table 3.17 shows the main spectrum analyser configuration parameters.

Table 3.17 – Spectrum analyser configuration.

	Parameter	**Value**	
Frequency	Frequency range	75-3000 MHz	3000-7075 MHz
	Frequency span	45-600 MHz	
	Frequency bin	81.8-1090.9 kHz	
	Resolution BW	10 kHz	
	Video BW	10 kHz	
Time	Measurement period	24 hours	
	Sweep time	Auto	
Amplitude	Built-in pre-amp	Deactivated	Activated
	Reference level	– 20 dBm	– 50 dBm
	Reference level offset	0 dB	– 20 dB
	Scale	10 dB/division	
	Input attenuation	0 dB	
	Detection type	Average (RMS) detector	

The measured frequency range (75-7075 MHz) has been divided into 25 blocks with variable sizes ranging from 45 MHz up to 600 MHz. The division has been performed following the local Spanish governmental spectrum allocations [95] (no spectrum band defined in [95] has been split off) and taking into account the transmitted signal bandwidth for each band (for example, frequency bins of 81.8 kHz were used to measure 200-kHz GSM channels while 745.5 kHz and 727.3 kHz bins were employed for 8-MHz TV and 5-MHz UMTS channels respectively).

The Resolution BandWidth (RBW) plays an important role in the obtained measurements. Narrowing the RBW increases the ability to resolve signals in frequency and reduces the noise floor (increasing the sensitivity) at the cost of an increased sweep time and hence a longer measurement period [93][94]. Based on the results presented in [92], a 10-kHz RBW has been selected as an adequate trade-off between detection capabilities and required measurement time. The Video BandWidth (VBW) is a smoothing function that dates to analogical spectrum analysers, but is now nearly obsolete. To eliminate this analogical form of averaging, the VBW has been set equal to the RBW.

Each one of the 25 sub-bands considered in this work has been measured during 24 hours. The number of recorded traces/sweeps during such measurement period is a function of the sampling rate (i.e., the

sweep time), which is automatically adjusted by the spectrum analyser according to various configuration parameters, including the frequency span.

For measurements below 3 GHz, where some overloading signals may be present, only the external amplifier has been used. For measurements above 3 GHz, where the received powers are lower, both the external and the spectrum analyser's internal amplifier have been employed resulting in a noise floor reduction of 20 dB. To simplify the data post-processing, the noise floor values in the 75-3000 MHz and 3000-7075 MHz bands have been equalized by adding a 20-dB offset to the power levels measured between 3000-7075 MHz (reference level offset). The reference level (the maximum power of a signal that enters the spectrum analyser and can be measured accurately) has then been adjusted according to the maximum power observed in each region, while the scale is adjusted according to the minimum signal level. No input attenuation has been employed. An average type detector has been used. This detector averages all the power levels sensed in one frequency bin in order to provide a representative power level for each measured frequency bin.

3.2.3 Measurement Scenarios

Most of previous spectrum occupancy studies are based on measurements performed in outdoor environments and more particularly in outdoor high points such as building roofs, balconies and towers. The main advantage of high points is that they provide direct line-of-sight to many kinds of important transmitters and therefore enable a more accurate measurement of their spectral activity. Nevertheless, this scenario may not be representative of the spectrum occupancy perceived by a secondary network in many other interesting practical situations where the secondary antenna is not placed in a static high point (e.g., a mobile secondary user communicating inside a building or while walking in the street between buildings). The measurement of real network activities in additional scenarios of practical significance are therefore required for an adequate and full understanding of the dynamic use of spectrum. In this context, this measurement campaign considers a rich diversity of measurement scenarios of interest in a densely populated urban environment in Barcelona, Spain. The variety of considered measurement scenarios provides a broader view and understanding of dynamic spectrum occupancy under different practical scenarios of interest.

The scenarios defined for this measurement campaign include not only outdoor but also indoor locations. Measurements in indoor locations provide information about the spectral activity that would be perceived by secondary users operating in indoor environments. Similarly, outdoor measurements give us some insights into the spectral activity that would be perceived by secondary users operating in outdoor environments, at various physical locations of practical interest. For the measurements in outdoor locations, three different kinds of scenarios have been considered, namely high points, narrow streets and open areas. Measurements in high points provide reliable information about the actual spectral occupancy patterns of several primary transmitters, while narrow streets and open areas give us an idea of the perception of secondary users moving within an urban environment with different levels of radio propagation blocking.

For indoor experiments, the measurement equipment was placed inside an urban building, in the middle floor of a three-floor building belonging to the Department of Signal Theory and Communications of the Universitat Politècnica de Catalunya (UPC). For outdoor high point measurements, the equipment was placed in the roof of the same building (latitude: 41º 23' 20" north; longitude: 2º 6' 43" east; altitude: 175 meters). The selected place is a strategic location with direct line-of-sight to several transmitting stations located a few tens or hundreds of meters away from the antenna and without buildings blocking the radio propagation. This strategic location enabled us to accurately measure the spectral activity of, among others, TV and FM broadcast stations, several nearby base stations for cellular mobile communications and a military head quarter as well as some maritime and aeronautical transmitters due to the relative proximity to the harbour and the airport. For measurements in narrow streets and open areas, the measurement equipment was moved within the UPC's Campus Nord. The different geographical locations considered in this measurement campaign are illustrated in Figure 3.31, where an aerial view of UPC's Campus Nord is shown. The description of measurement locations is provided in Table 3.18.

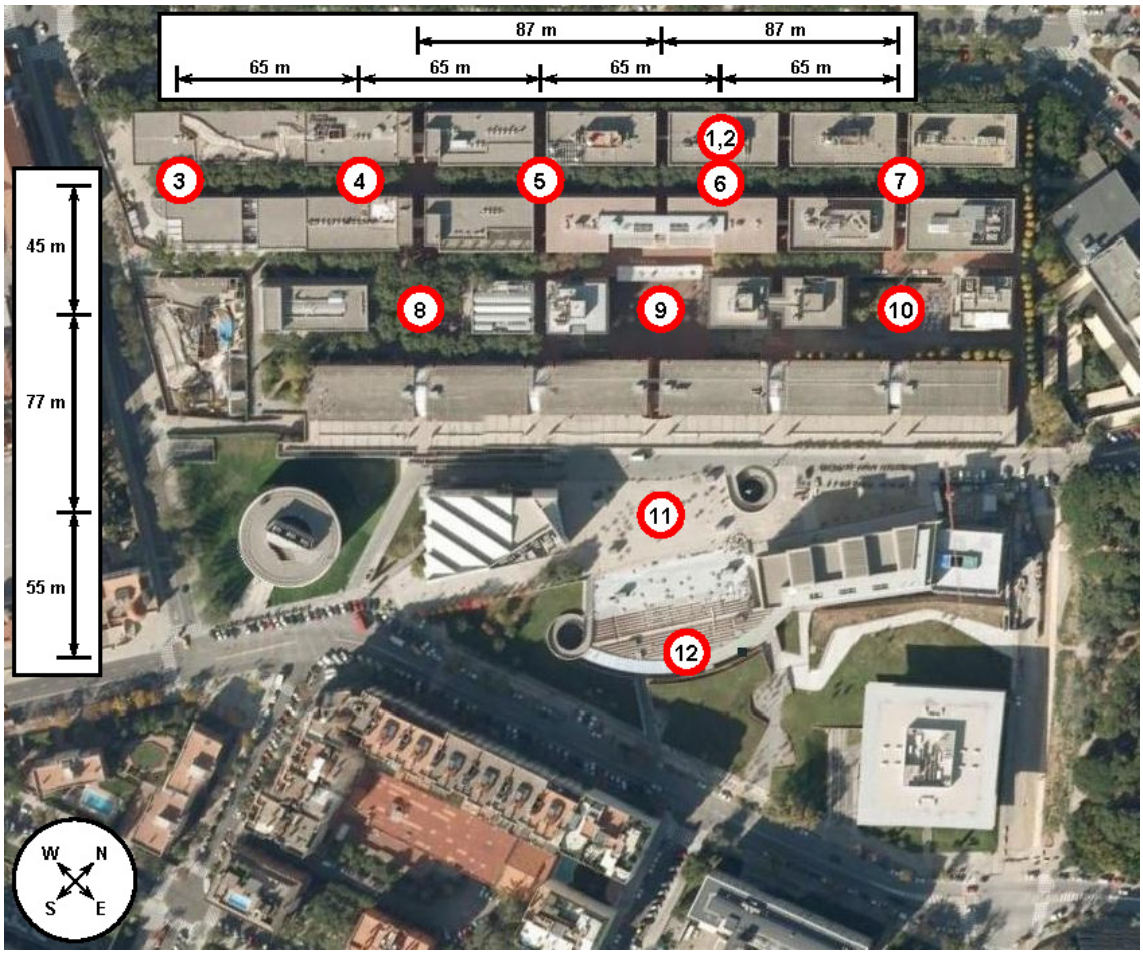

Figure 3.31 – Measurement locations at UPC's Campus Nord.

Table 3.18 – Description of measurement locations.

Measurement point	Environment
1	Outdoor high point (building roof)
2	Indoor (building room)
3 – 7	Outdoor at ground level in narrow streets
8 – 10	Outdoor at ground level between buildings
11 – 12	Outdoor at ground level in open areas

3.2.4 Measurement Results and Analysis

3.2.4.1 Occupancy Metrics

Three parameters have been considered to measure, evaluate and quantify the level of spectral occupancy. The results are here presented by means of figures composed of three graphs, each representing a specific occupancy metric.

The first occupancy metric is Power Spectral Density (PSD), which is the information provided by the spectrum analyser. The PSD is shown in the upper graph of each figure in minimum, maximum and

average values. When considered together, minimum, maximum and average PSD provide a simple characterization of the temporal behaviour of a channel. For example, if the three PSD values are quite similar, it suggests a single transmitter that is always on, experiences a low level of fading and is probably not moving. At the other extreme, a large difference among minimum, maximum and average suggests a more intermittent use of the spectrum [89].

The second occupancy metric, shown in the middle graph of each figure, represents the instantaneous evolution of the temporal spectrum occupancy during the whole measurement period. To determine whether a frequency band is used by a licensed user, different sensing methods have been proposed in the literature [96]. They provide different trade-offs among required sensing time, complexity and detection capabilities. Depending on how much information is available about the primary signal, different performances can be reached. However, in the most generic case no prior information is available. If only power measurements of the spectrum utilisation are available, the energy detection method is the only possibility left. Due to its simplicity and relevance to the processing of power measurements, energy detection has been a preferred approach for many past spectrum studies and is also employed in this study. Energy detection compares the received signal energy in a certain frequency band to a predefined threshold. If the signal lies above the threshold the band is declared to be occupied by the primary network. Otherwise the band is supposed to be idle and could be employed by a CR network. Following this principle, a spectral occupancy function $\Omega(t, f)$ has been defined as:

$$\Omega(t,f)=\begin{cases}0, & PSD(t,f)<\gamma \\ 1, & PSD(t,f)\geq\gamma\end{cases} \tag{3.1}$$

where $PSD(t, f)$ represents the PSD sample captured by the spectrum analyser at time index t and frequency index f, and γ is the decision threshold. This function has been employed to determine the instantaneous evolution of the temporal spectrum occupancy shown in the middle graph of each figure. PSD samples with $\Omega(t, f) = 0$ (corresponding to unused channels) are represented by white dots. Similarly, black dots represent PSD samples with $\Omega(t, f) = 1$ (corresponding to occupied channels).

The decision threshold is a critical parameter since its value severely impacts the obtained occupancy statistics. Several methods to determine the decision threshold have been employed in previous studies. Based on the results of the analysis conducted in [92], the decision threshold in this study has been selected according to the Probability of False Alarm (PFA) criterion. To compute the decision threshold, the system's noise has been measured by replacing the antennas with a 50 Ω matched load. At each frequency point f the decision threshold γ_f has then been fixed such that exactly 1% of the measured noise samples lie above the threshold, which implies a false alarm probability equal to 1%. It is worth noting that the decision threshold obtained with this method is not constant since the system's noise floor slightly increases with the frequency, and hence the sub-index f in γ_f. This criterion has been selected as a reasonable trade-off between ability to detect low-level signals and overestimation errors. For more details, the reader is referred to [92].

To more precisely quantify the detected spectral activity, a third occupancy metric referred to as duty cycle has been employed, which is shown in the lower graph of each figure. For each measured frequency point f, the duty cycle DC_f is computed as the proportion of PSD samples, out of all the PSD samples recorded at that frequency, that lie above the decision threshold γ_f and hence that are considered as samples of occupied channels. Assuming that N_t traces have been captured during a certain time span ($t = 1, 2, \ldots, N_t$), then:

$$DC_f=\frac{1}{N_t}\sum_{t=1}^{N_t}\Omega(t,f) \tag{3.2}$$

For a frequency point f, this metric represents the fraction of time that the frequency is considered to be occupied. For a certain frequency band/span (i.e., range of frequencies $f = 1, 2, \ldots, N_f$), the average

duty cycle DC of the band is computed by averaging the duty cycle DC_f of all the N_f frequency points measured within the band:

$$DC = \frac{1}{N_f}\sum_{f=1}^{N_f} DC_f = \frac{1}{N_t}\frac{1}{N_f}\sum_{t=1}^{N_t}\sum_{f=1}^{N_f}\Omega(t,f) \tag{3.3}$$

This metric represents the average degree of utilisation of spectrum within a certain bandwidth (f = 1, 2, …, N_f) and a specific time span (t = 1, 2, …, N_t). The duty cycle is usually given in percentage and this is the convention adopted in this study.

3.2.4.2 Location 1: Urban Outdoor High Point

The obtained measurement results are shown in Figure 3.32, Figure 3.33 and Figure 3.34. As it can be appreciated, spectrum experiences a relatively moderate use below 1 GHz and a low usage between 1 and 2 GHz, while remains mostly underutilised between 2 and 7 GHz (with some clear exceptions that will be discussed later on). In fact, while the average duty cycle between 75 and 2000 MHz is 31.02%, the value for this parameter between 2000 and 7075 MHz is only 2.75%, as shown in Table 3.19. The overall average duty cycle over the whole frequency range considered in this study is only 17.78%, which reveals the existence of significant amounts of unused spectrum that could potentially be exploited by future CR networks. Although these results clearly indicate low spectrum utilisation levels, they do not provide a clear picture of how spectrum is used in different frequency bands allocated to different specific services. Therefore, in the following we discuss in detail the spectrum usage in some allocated bands of interest.

Table 3.19 – Average duty cycle statistics.

<table>
<tr><th>Frequency range (MHz)</th><th colspan="3">Average duty cycle</th></tr>
<tr><td>75 – 1000</td><td>42.00 %</td><td rowspan="2">31.02 %</td><td rowspan="8">17.78 %</td></tr>
<tr><td>1000 – 2000</td><td>13.30 %</td></tr>
<tr><td>2000 – 3000</td><td>3.73 %</td><td rowspan="6">2.75 %</td></tr>
<tr><td>3000 – 4000</td><td>4.01 %</td></tr>
<tr><td>4000 – 5000</td><td>1.63 %</td></tr>
<tr><td>5000 – 6000</td><td>1.98 %</td></tr>
<tr><td>6000 – 7075</td><td>1.78 %</td></tr>
</table>

Although the highest spectral activity is observed below 1 GHz, some opportunities for CR networks can still be found in this frequency range, even in those bands with the highest observed average duty cycles. For example, the frequency band 470-862 MHz (depicted in Figure 3.35), which is allocated to analogical and digital terrestrial TV in Spain, shows an average duty cycle of 82.08%, one the highest values observed in this study. Although the sub-band 830-862 MHz (exclusively reserved for digital TV systems) exhibits an intensive usage of nearly 100% that precludes any CR applications, the rest of the band between 470 and 830 MHz (allocated to both analogical and digital TV systems) shows some spectrum white spaces. Notice that occupied TV channels show a duty cycle of about 100%, i.e. continuous broadcasting, which impedes temporary opportunistic usage of those channels. Only one channel out of all the TV channels received at our measurement location (channel 38, 606-614 MHz) was disconnected during a short period in the night, which might be due to maintenance operations since this behaviour was not observed in some previous experiments. In general, occupied TV channels show an average duty cycle of 100%. Spectrum opportunities in this band usually come from TV channels that are received with very weak signal levels. In our case, the measured average duty cycle between 470 and 830 MHz was 80.49%, meaning that one fifth of the TV band (approximately 80 MHz) is unoccupied due to the weak reception of the signals broadcasted from distant TV stations.

Therefore, although the TV band appears as considerably populated in our study, it provides some interesting opportunities for secondary usage.

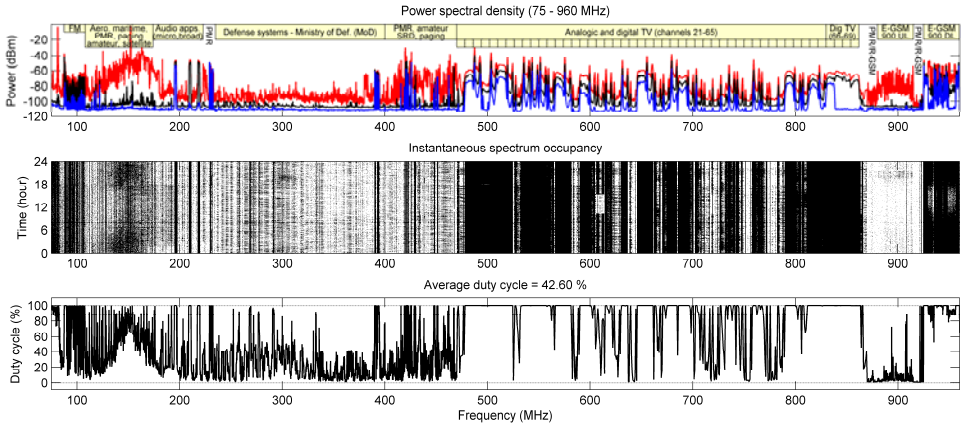

Figure 3.32 – Spectrum occupancy between 75 and 960 MHz.

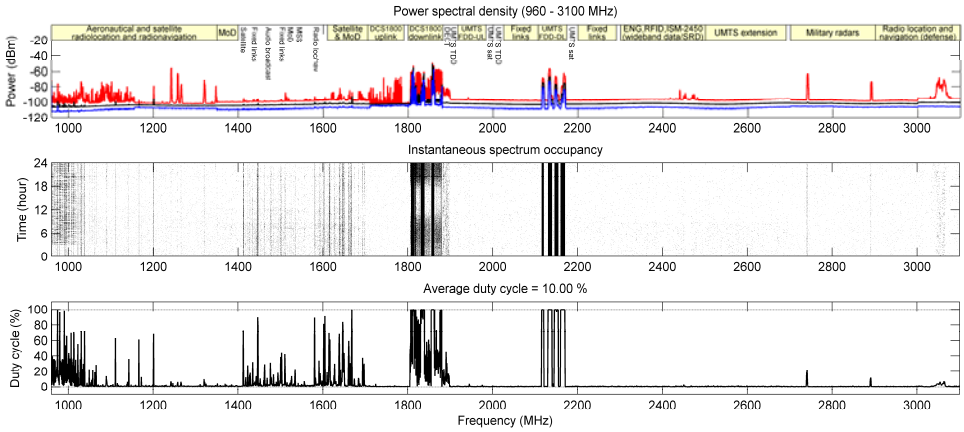

Figure 3.33 – Spectrum occupancy between 960 and 3100 MHz.

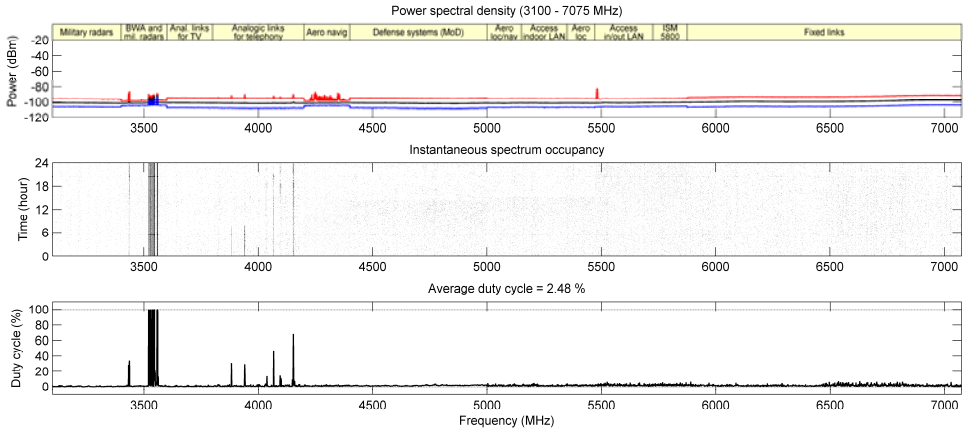

Figure 3.34 – Spectrum occupancy between 3100 and 7075 MHz.

Another interesting case below 1 GHz is observed in the frequency bands allocated to the Global System for Mobile communications (GSM). The Enhanced GSM (E-GSM) 900 system operates in the 880-915 MHz (uplink) and 925-960 MHz (downlink) bands as shown in Figure 3.36. The uplink band appears as a potential candidate for CR applications with an average duty cycle equal to 6.26%. However, in this case it is important to highlight that the low activity recorded in this band does not necessarily imply that it could be used by CR networks. As a matter of fact, the maximum PSD observed in Figure 3.36 reaches significant values, revealing the presence of primary signals in uplink. The considerably higher activity in downlink (96.33%) and the fact that GSM is based on Frequency-Division Duplex (FDD) suggest that the actual usage of the uplink band might be higher than the activity level recorded by our system at our measurement location. The unbalanced occupancy patterns observed between uplink and downlink in Figure 3.36 can be explained as follows. First, the transmission power of GSM base stations is considerably higher than that of cellular phones. Therefore, the presence of GSM downlink signals can be more easily detected. Moreover, the antenna employed in our study was placed on the roof of a building with direct line-of-sight to several nearby base stations, which enabled us to accurately measure the high spectral activity of the downlink. On the other hand, the low usage observed in the uplink may be due to the usually low transmission power of cellular phones and the resulting weak uplink signal received at the antenna. The detection of such signals might be hindered by the fact that cellular phones usually operate at the ground level or low altitudes and usually have no direct line-of-sight neither with the serving base station nor the antenna employed in our study, which makes more difficult to detect the uplink activity. In fact, the maximum PSD observed in uplink in Figure 3.36 may be due to phone calls from nearby locations, e.g. the upper floors of the building. Therefore, from the obtained results we cannot conclude low activity levels in the E-GSM 900 uplink. Similar trends were observed in previous studies, e.g. [85].

In the lower spectrum bands 75-235 MHz, 235-400 MHz and 400-470 MHz, low to moderate average duty cycles of 48.59%, 24.88% and 29.85% are observed respectively. These bands are populated by a wide variety of narrowband systems, including Professional Mobile Radio/Public Access Mobile Radio (PMR/PAMR) systems (75.2-87.5 MHz, 223-235 MHz, 406-430 MHz and 440-470 MHz), FM analogical audio broadcasting (87.5-108 MHz), aeronautical radio-navigation and communication systems, maritime systems (GMDSS), paging systems (ERMES) and fixed links (108-174 MHz), audio applications such as wireless microphones (174-195 MHz) and Digital Audio Broadcasting (DAB) systems (195-223 MHz), satellite systems (137-138 MHz and 400-406 MHz) and amateur systems (144-146 MHz and 430-440 MHz). Although these bands exhibit low to moderate average duty cycles, the free spectrum gaps found in this region of the spectrum are of considerably narrow bandwidths due to the narrowband nature of the systems operating within these bands. Moreover, the whole band from 235 to 400 MHz is exclusively reserved for security services and defence systems of the Spanish Ministry of Defence, which in principle precludes the use of such spectrum bands for CR applications. Other bands below 1 GHz with low or moderate levels of activity but narrower available free bandwidths are those assigned to wireless microphones and RFID (862-870 MHz), CT1 cordless phones (870-871 and 915-916 MHz), cellular access rural telephony (874-876 and 919-921 MHz) and R-GSM 900 (876-880 and 921-925 MHz).

Between 1 and 2 GHz, spectrum is subject to a low level of utilisation, while remains mostly unused between 2 and 7 GHz. Above 1 GHz the highest spectrum usage is observed for the bands allocated to the Digital Cellular System (DCS) 1800 operating at 1710-1785 MHz and 1805-1880 MHz (Figure 3.37), the Universal Mobile Telecommunication System (UMTS) operating at 1920-1980 MHz and 2110-2170 MHz (Figure 3.38), and Broadband Wireless Access (BWA) systems operating in the 3.4-3.6 GHz band between 3520 and 3560 MHz (Figure 3.39).

Notice that the differences between uplink and downlink usage patterns that were appreciated for E-GSM 900 are also observed for DCS 1800 and UMTS. In the case of DCS 1800 the differences are more accentuated due to the fact that mobile stations in DCS 1800 have lower transmission powers than in GSM 900, which results in a reduced occupancy in the uplink. In the case of UMTS the difference is higher due to the spread spectrum nature of the Wideband Code Division Multiple Access (WCDMA) radio technology employed by UMTS. WCDMA signals are modulated over large bandwidths, which results in very low transmission powers. Such signals are difficult to detect with

spectrum analysers. As a result, a very low activity was recorded in UMTS uplink. Although DCS 1800 and UMTS show higher levels of occupancy in downlink (58.82% and 56.93% respectively), these bands also provide some opportunities for secondary access. In the case of DCS 1800 some portions of the downlink band show a well defined periodic usage pattern, as it is illustrated in Figure 3.40 where the average duty cycle computed over 1-hour periods is shown. Such temporal patterns could be exploited by some secondary CR applications by accessing spectrum during low-occupancy periods. In the case of UMTS, spectrum opportunities are due to several 5-MHz channels that appear to be unoccupied. Moreover, the UMTS bands reserved for the Time Division Duplex (TDD) component (1900-1920 and 2010-2025 MHz), the satellite component (1980-2010 MHz and 2170-2200 MHz) and extension (2500-2690 MHz) are not used.

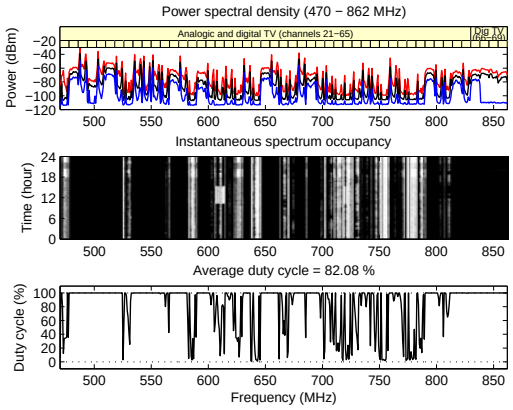

Figure 3.35 ─ Spectrum occupancy for TV bands (470-862 MHz).

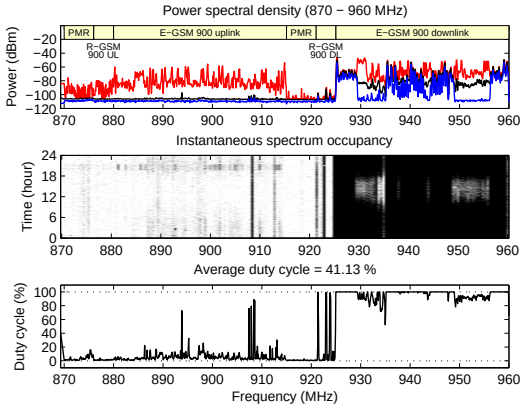

Figure 3.36 ─ Spectrum occupancy for E-GSM 900 (870-960 MHz).

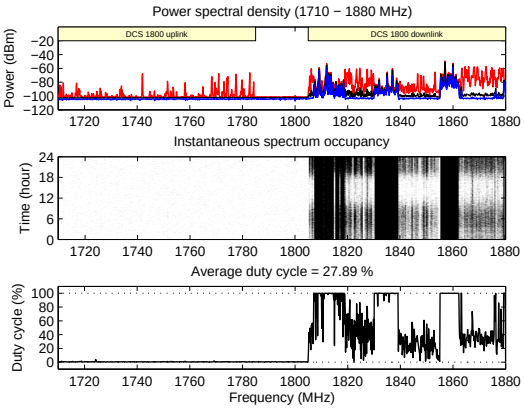

Figure 3.37 ─ Spectrum occupancy DCS 1800 (1710-1880 MHz).

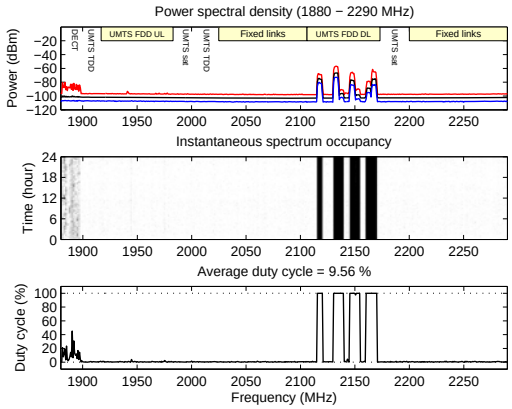

Figure 3.38 ─ Spectrum occupancy for UMTS (1880-2290 MHz).

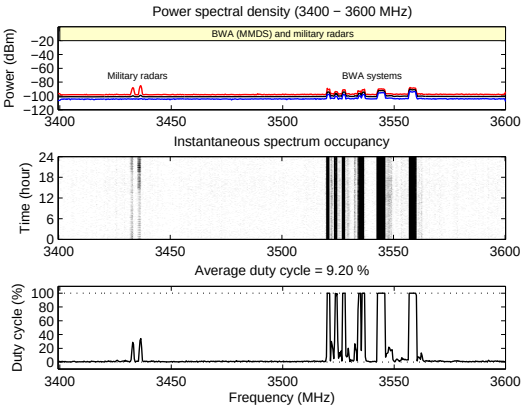

Figure 3.39 ─ Spectrum occupancy for BWA (3400-3600 MHz).

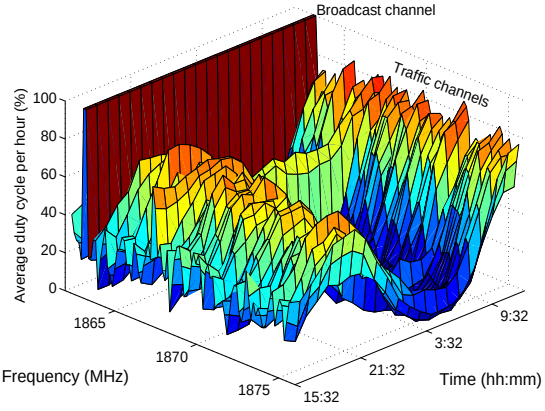

Figure 3.40 ─ Average duty cycle per hour for DCS 1800 (1862.5-1875.5 MHz).

Although the highest activity above 1 GHz is observed for DCS 1800, UMTS and BWA systems, some other bands are also clearly occupied but at lower occupancy rates, which in principle offer additional opportunities for CR applications. Some examples are the 1400-1710 MHz band, allocated to different wireless systems such as Satellite Personal Communication Systems (S-PCS) as well as aeronautical radio-navigation, audio broadcasting and defence systems, or the 3800-4200 MHz band, occupied by analogical links for telephony.

Finally, it is worth noting that some spectrum bands appear as unoccupied when judged by their average duty cycles. Nevertheless, the maximum PSD reveals that some primary users, although difficult to detect, are present in such bands. Some examples are the uplink bands for mobile communications, the 2400-2500 MHz band (ISM-2450), the 2900-3100 MHz band (radio navigation and location defence systems) and the 4200-4400 MHz band (allocated to aeronautical navigation).

To conclude this section, Figure 3.41 summarizes the band by band average spectrum occupancy statistics. The obtained results demonstrate that some spectrum bands are subject to intensive usage while some others show moderate utilisation levels, are sparsely used and, in some cases, are not used at all. In general, the average spectrum occupancy observed in frequency and time in this study was found to be significantly low, concretely 17.78% for the whole measured frequency range 75-7075 MHz.

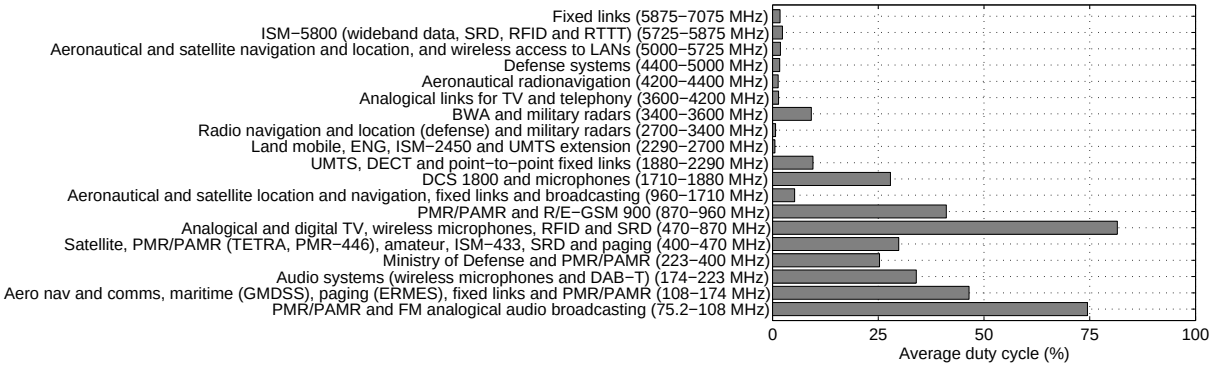

Figure 3.41 – Band by band average duty cycle statistics for the whole measurement range (75-7075 MHz).

The highest occupancy rates were observed for bands allocated to broadcast services (TV as well as analogical and digital audio), followed by digital cellular services as PMR/PAMR, paging, and mobile cellular communications (E-GSM 900, DCS 1800 and UMTS) among others. Other services and applications, e.g. aeronautical radio navigation and location or defence systems, show different occupancy rates depending on the considered allocated band. In general, spectrum experiences a relatively moderate use below 1 GHz, a low usage between 1–2 GHz, and remains mostly underutilised between 2–7 GHz.

Most of spectrum offers possibilities for secondary CR usage, even those bands with the highest observed activity levels in terms of average duty cycle. Nevertheless, it is worth high-lighting that the average duty cycle by itself is not a sufficient statistic to declare a spectrum band as unoccupied. Indeed, the maximum PSD of some portions of the spectrum reveals that some allocated frequency bands with null average duty cycles are actually being occupied by some operating primary systems. This issue should carefully be taken into account when selecting frequency bands for potential CR applications.

3.2.4.3 Location 2: Urban Indoor

Most of previous spectrum occupancy studies are based on measurements performed in outdoor high points such as building roofs, balconies and towers. As stated in section 3.2.3, this scenario may not be representative of the spectral activity perceived by secondary users in other interesting situations of practical significance, making necessary the analysis and characterization of spectrum occupancy in other scenarios. In this context, this section presents and analyzes the results obtained in location 2

(urban indoor environment) taking as a reference the results obtained in location 1 (urban outdoor high point). The aim of this section is to determine the impact of considering an indoor environment on the spectral activity perceived by a secondary user with respect to that observed in an outdoor high point. Although the measurement conditions considered in both cases were identical, the time instants were different (i.e., both locations were not measured simultaneously). This circumstance introduces some random component in the obtained results since different transmissions were present in each case. However, it is worth noting that the aim of this section is not to characterize the instantaneous spectrum occupancy in the time domain but the average occupancy rate from a statistical point of view. For sufficiently long measurement periods as those considered in this study, the impact of different instantaneous transmissions is averaged and the obtained average duty cycle value can be considered as a representative indication of the spectral activity in the bands under study.

From a qualitative point of view, the results obtained in location 2 follow the same trend as in location 1, with higher occupancy rates at lower frequencies. As it can be appreciated in Table 3.20, the average spectrum occupancy is moderate below 1 GHz and very low above 1 GHz. The significantly lower average occupancy rates observed in Table 3.20 for the indoor location can be explained by the fact that most of wireless transmitters are located outdoor and the propagation loss due to outdoor-indoor signal penetration leads to lower signal strengths in the indoor scenario, which in turn results in lower occupancy rates. In principle, the lower average duty cycles obtained for the indoor case suggest the existence of a higher amount of free spectrum. However, this result should be interpreted carefully, taking into account the specific circumstances of particular bands.

Table 3.20 – Average duty cycle statistics in locations 1 and 2.

<table>
<tr><th rowspan="2">Frequency (MHz)</th><th colspan="6">Average duty cycle</th></tr>
<tr><th>Outdoor</th><th>Indoor</th><th>Outdoor</th><th>Indoor</th><th>Outdoor</th><th>Indoor</th></tr>
<tr><td>75 – 1000</td><td>42.00 %</td><td>33.70 %</td><td rowspan="2">31.02 %</td><td rowspan="2">21.54 %</td><td rowspan="8">17.78 %</td><td rowspan="8">12.10 %</td></tr>
<tr><td>1000 – 2000</td><td>13.30 %</td><td>1.94 %</td></tr>
<tr><td>2000 – 3000</td><td>3.73 %</td><td>1.63 %</td><td rowspan="6">2.75 %</td><td rowspan="6">1.39 %</td></tr>
<tr><td>3000 – 4000</td><td>4.01 %</td><td>1.44 %</td></tr>
<tr><td>4000 – 5000</td><td>1.63 %</td><td>1.09 %</td></tr>
<tr><td>5000 – 6000</td><td>1.98 %</td><td>1.34 %</td></tr>
<tr><td>6000 – 7075</td><td>1.78 %</td><td>1.38 %</td></tr>
</table>

To analyze the impact of the indoor location on the occupancy rate for various specific bands, it is convenient to distinguish four different possible cases according to the location of transmitters and receivers, as shown in Table 3.21. Based on this classification, the results for various bands of interest are shown in Figure 3.42. Notice that for certain bands the classification is not straightforward. For example, in the downlink direction of cellular mobile communication systems the receivers are mobile users that may be located indoor and outdoor simultaneously. In practice, it is not possible to reliably determine the location of every transmitter and receiver operating in a certain band, which results in some uncertainty. In spite of that, some general trends can be inferred from the results in Figure 3.42.

For bands allocated to systems where the transmitters are always outdoor (cases I/II), the indoor duty cycles are in general notably lower, as expected, due to the outdoor-indoor signal penetration loss. In case I (systems with outdoor receivers) the lower indoor occupancy rates indicate the availability of more free spectrum, since an indoor secondary user transmitting in channels sensed as free would not cause harmful interference to primary outdoor receivers. However, in case II (systems with indoor receivers) the lower indoor duty cycles do not necessarily imply the existence of more white spaces, since in this case transmitting in a channel sensed as unoccupied could potentially result in interference to primary indoor receivers.

Reference DR9.2

Table 3.21 – Cases considered in Figure 3.42.

Case	Transmitter location	Receiver location
I	Outdoor	Outdoor
II	Outdoor	Indoor
III	Indoor	Outdoor
IV	Indoor	Indoor

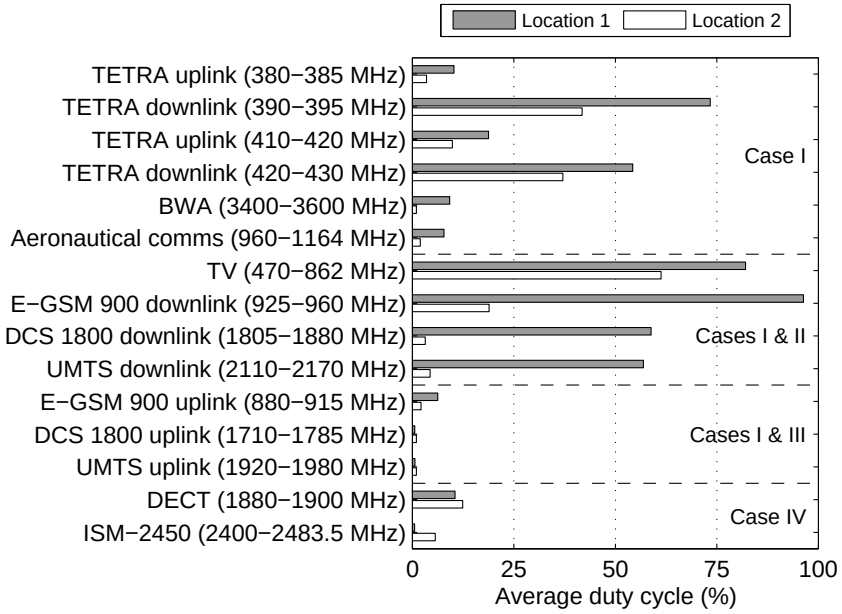

Figure 3.42 – Average duty cycle statistics in locations 1 and 2 for specific bands.

For bands allocated to systems with indoor transmitters (cases III/IV), in general the average duty cycles tend to be higher in the indoor location (with some exceptions as the E-GSM 900 uplink band, which might be due to the presence of outdoor transmitters in such band). Following a similar argument, in case IV (systems with indoor receivers) this indicates the availability of a lower amount of free spectrum, while it could not be necessarily the situation in case III (systems with outdoor receivers). In any case, the differences observed in this experiment between outdoor and indoor occupancy rates in cases III/IV are not as significant as in cases I/II.

In summary, although average duty cycles tend to be lower in indoor locations (with some unimportant particular exceptions), this does not necessarily indicate the existence of more free spectrum. The particular circumstances of the specific bands being sensed and the characteristics of the systems operating over them need to be carefully considered before declaring a band as truly available for a potential secondary usage; otherwise, harmful interference could be caused to the primary licensed system.

Based on the previous results, from a practical point of view it can be stated that the output of spectrum sensing procedures is not enough to declare a band as truly available for secondary access. Some additional techniques may be required such as, for example, sensing both the uplink and downlink directions of FDD-based systems in order to guarantee that the channel can be accessed opportunistically, or employing signal processing techniques as the one described in [97] in order to determine the signal standard present in a certain band before deciding whether a band may be accessed without inducing harmful interference.

3.2.4.4 Locations 3 to 12: Urban Narrow Streets and Open Areas

This section presents and analyzes the results obtained in locations 3 to 12 (urban narrow streets and open areas) taking as a reference the results obtained in location 1(outdoor high point). The aim of this section is to determine the impact of considering different outdoor locations at the ground level on the spectral activity perceived by a secondary user with respect to that observed in an outdoor high point. The locations under study in this section can be considered as a representative scenario for secondary mobile users communicating while walking on the street in an urban environment.

As in section 3.2.4.3, each location has been measured at a different time instant. The random component introduced by the presence of different transmissions at different times could be averaged by considering a sufficiently long measurement period. However, since the presence of an operative was required in the measurements, periods of 24 hours as in location 1 were infeasible and were therefore shortened to 1 hour in locations 3–12. To reduce the impact of random components and make the results of locations 1 and 3–12 comparable, the average duty cycle obtained in locations 3–12 has been normalized by the average duty cycle in location 1 obtained when considering the samples corresponding to the same time interval. Therefore, if an average duty cycle DC_i is obtained for location i (i = 3, 4, …, 12) based on the samples captured during a 1-hour interval between time instants t_{start} and t_{stop}, the samples captured at location 1 between t_{start} and t_{stop} are used to compute an average duty cycle DC_1. The normalized average duty cycle for location i is then obtained as:

$$\overline{DC_i} = \frac{DC_i}{DC_1} \tag{3.4}$$

This procedure reduces the randomness of the obtained results and enables a fairer comparison between the outdoor high point and the rest of outdoor positions.

For most of the bands and locations measured in this experiment the obtained normalized average duty cycle is lower than one, meaning that the average duty cycle measured in different locations at the ground level is in general lower than in high points. This is a consequence of the radio propagation blocking caused by buildings and other obstacles: under non-line-of-sight conditions, the direct ray (i.e., the strongest signal component) is lost; only multi path propagation components attenuated by reflection, refraction and diffraction are received, thus resulting in lower received signal levels and therefore in lower average duty cycles. From a practical point of view, this indicates that a secondary user at the ground level would perceive an amount of white space higher than that predicted by measurements performed in high points. Nevertheless, it is worth highlighting that this should be interpreted carefully, taking into account the specific circumstances of each band. In the following, some particular bands of interest are discussed. The obtained results are shown in Figure 3.43.

Figure 3.43(a), Figure 3.43(b), Figure 3.43(c) and Figure 3.43(d) show the spatial distribution of the normalized average duty cycle for the TV, UMTS downlink, E-GSM 900 downlink and DCS 1800 downlink bands, respectively. The common feature of these bands is that the transmitters are located outside the region under study. In the TV band, it can be clearly appreciated that the normalized average duty cycle is lower in closed regions. Thus, in locations 4 and 6, where radio propagation blocking caused by buildings is more intense, its value is lower than in other less closed regions such as locations 3, 5 and 7. A similar trend is observed for UMTS, E-GSM 900 and DCS 1800 downlink bands. In the two last cases, however, location 5 constitutes an exception, which could be explained by the different relative position of transmitters and by the fact that the same physical scenario may result in very dissimilar propagation scenarios at different frequencies. Comparing locations 8, 9 and 10, the deepest region (location 9) exhibits the lowest normalized average duty cycle in the case of TV, as expected, but the highest value in the case of the cellular mobile communication bands, which could be explained by the use of micro-cells and repeaters in shadowed regions as location 9. Regarding locations 11 and 12, it is interesting to note that a higher spectral activity level was recorded in location 11 despite the presence of some surrounding buildings with respect to the open region in location 12. The detection by the measurement equipment of some additional signal components reflected in such buildings could explain the recording of higher activity levels in a less open region.

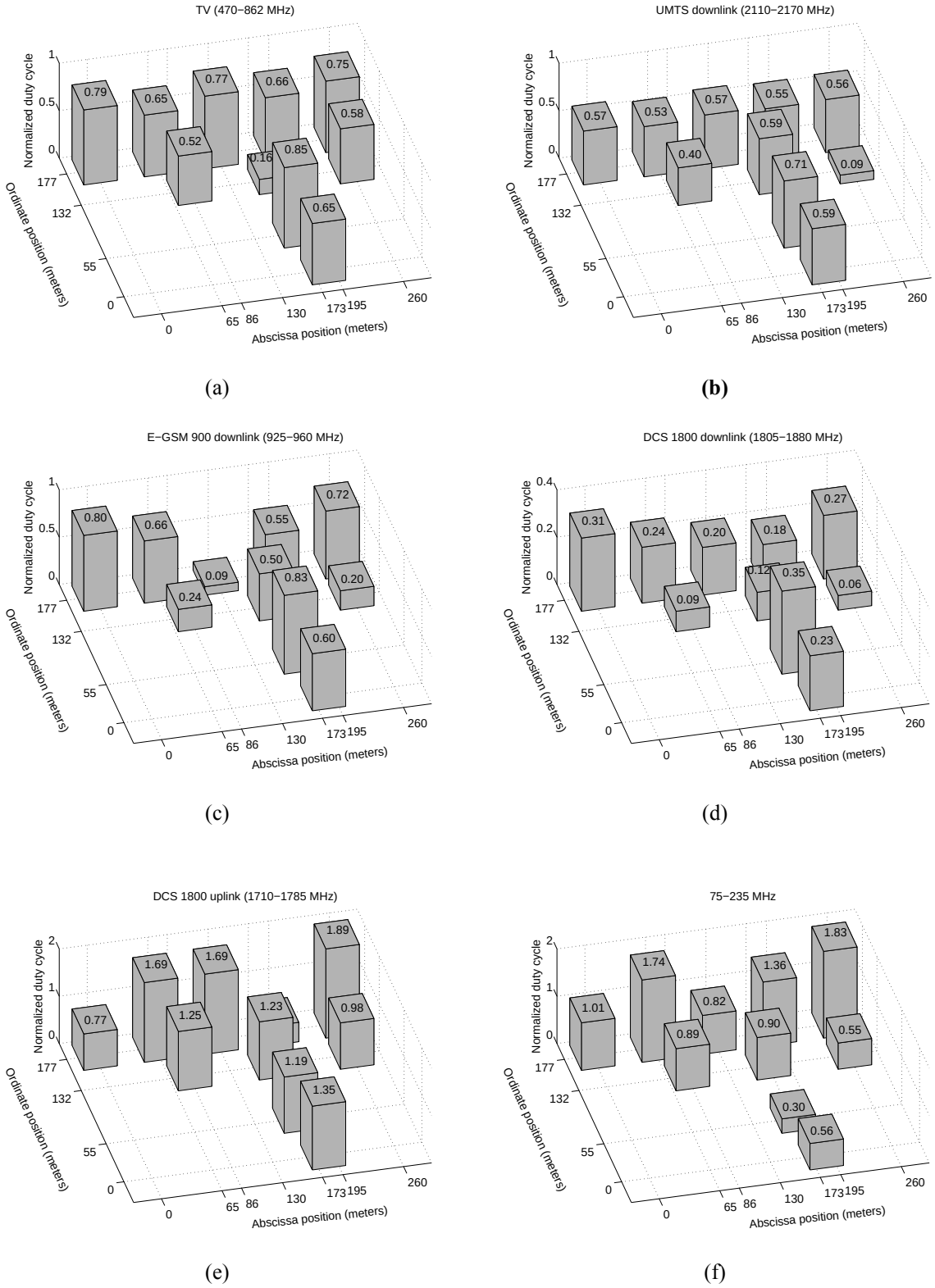

Figure 3.43 – Normalized average duty cycle statistics in locations 3 to 12 for specific bands: (a) TV (470-862 MHz), (b) UMTS downlink (2110-2170 MHz), (c) E-GSM 900 downlink (925-960 MHz), (d) DCS 1800 downlink (1805-1880 MHz), (e) DCS 1800 uplink (1710-1785 MHz), and (f) 75-235 MHz. The positions of the bars correspond to the physical locations of points 3-12 in Figure 3.31.

Although lower duty cycles have been observed at the ground level in the TV, UMTS, E-GSM and DCS 1800 downlink bands, it is worth noting that this does not necessarily imply the existence of more opportunities for secondary access. As a matter of fact, some faded primary signals might be undetected at the ground level due to blocking buildings and other obstacles, in which case an exceptionally harmful interference would be caused to the intended primary receivers, who in these bands would be operating in the proximity of the secondary users. These experimental results highlight the importance of detection sensitivity in secondary networks and suggest the need of some additional techniques. For example, simultaneous sensing of both the downlink and uplink bands could result in a more effective detection, as suggested by the higher spectral activity levels recorded in uplink bands, see Figure 3.43(e).

In the previous bands, where the transmitters were outside the region under study, the results have shown some general occupancy trends in Figure 3.43(a), Figure 3.43(b), Figure 3.43(c) and Figure 3.43(d). For other bands with transmitters operating inside the region under study, i.e. Figure 3.43(e) and Figure 3.43(f), no particular occupancy trends have been observed. In this case, the obtained results might depend not on the actual spectral usage of such bands but rather on the random and fluctuating geographical distribution of transmitters inside the considered region.

The main conclusion derived from the obtained results is that the spectral activity perceived by a secondary user for a certain band in realistic urban scenarios strongly depends on the user location, with significant variations even in physical areas as reduced as the one considered in this study (≈180×260 m). This indicates that the conclusions derived from measurement studies performed in high points may not be well suited to other realistic outdoor scenarios with users at the ground level.

3.2.5 Envisaged Future Spectrum Measurements and Studies

Measurements of the radio environment can find many practical applications, from the definition of new dynamic spectrum policies by the regulatory bodies and the identification of appropriate frequency bands for the future deployment of the CR technology, to the development of useful spectrum usage models and more efficient CR techniques. As a potential application of the measurements performed in this measurement campaign, the development of spectrum usage models is envisaged. The measurements performed to the date, however, are based on a spectrum analyzer setup, the time resolution of which is relatively limited and could not be appropriate for certain levels of modelling. For modelling approaches requiring measurements with higher time resolutions, the use of an additional measurement platform is envisaged. Such measurement platform is based on the Universal Software Radio Peripheral (USRP) [98] and GNU Radio [99] architecture. USRP is an openly designed inexpensive Software Designed Radio (SDR) hardware platform that provides radio front-end functionalities, Analogical to Digital and Digital to Analogical Conversion (ADC/DAC), decimation/interpolation with filtering and a Universal Serial Bus 2 (USB2) interface to connect to an off-the-shell Personal Computer (PC). The PC runs the GNU Radio software, a free and open source toolkit that provides a library of signal processing blocks for building SDRs. In addition, it also provides blocks for communicating with the USRP. The general scheme of the measurement platform is illustrated in Figure 3.44.

This measurement platform is able to perform spectrum measurements over narrower bandwidths than a spectrum analyser, but with much higher time resolutions, in the order of micro- and nano-seconds. Moreover, the new measurement platform provides not only power spectrum measurements, as it is the case of a spectrum analyser, but true signal samples, from which the signal phase information can be extracted. As discussed in section 3.2.4.1, if only power measurements of the spectrum utilisation are available, the energy detection method is the only possibility left. However, the availability of the signal phase information jointly with the higher sampling rate enables the application of more sophisticated spectrum sensing algorithms in order to determine whether a given channel is occupied or not. The possibility of employing more sophisticated spectrum sensing algorithms enables us to determine, with an improved accuracy, the exact durations of the ON/OFF periods of spectrum occupancy, thus resulting in more accurate spectrum occupancy models. However, the possibility of employing different spectrum sensing algorithms also claims for a previous study on the performance

of spectrum sensing for various primary signals. In this sense, some research activities have started to analyse this issue. As an illustrative example, Figure 3.45 shows some preliminary results about the experimental performance of energy detection-based spectrum sensing for various primary technologies. Results show the probability of detection for different values of the SNR and with analogue and digital TV signals as well as TETRA and DVB-T technologies. As it can be appreciated, the resulting detection performance shows a notable dependence with the primary technology being detected. Since the development of accurate spectrum usage models require the ability to reliably and accurately determine the duration of the ON/OFF periods for various primary technologies, a previous and more detailed study on the performance of spectrum sensing for various primary signals is first required.

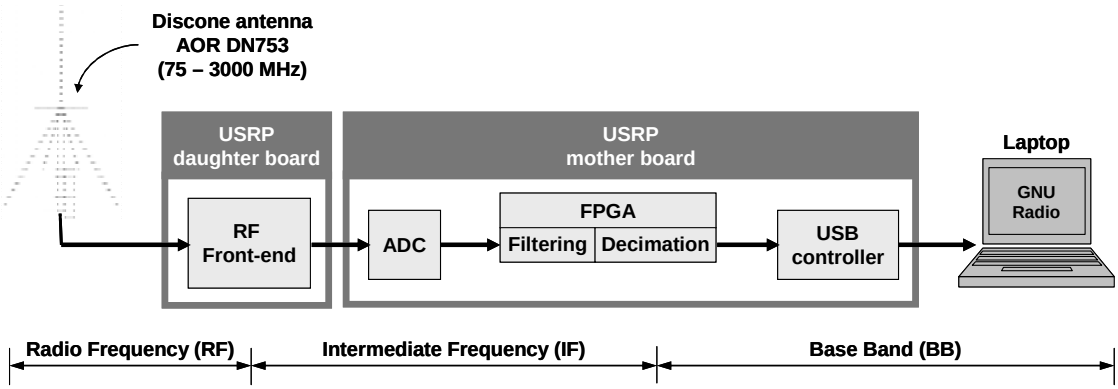

Figure 3.44 – Additional measurement platform envisaged for future spectrum measurements.

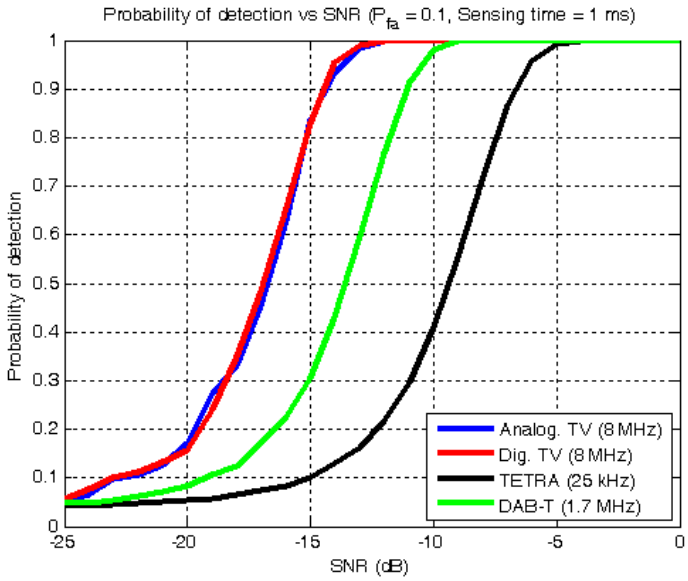

Figure 3.45 – Experimental performance of energy detection for various primary technologies.

3.3 Multi-armed bandit based policies for dynamic spectrum access

In this section, tools brorrowed from the machine learning community are used to tackle dynamic spectrum acces related issues within an unknown environment. For that purpose, we model the cognitive radio equipment's decision making engine as a cognitive agent. Then we show that the challenges faced by the cognitive agent can be seen as a particular case of the multi-armed bandit paradigm. Finally we suggest to use upper confidence bound algorithms to select the best channel, offering a good compromise between computational complexity and optimality.

Reference DR9.2

3.3.1 Decision making engine of a cognitive radio equipment

A Cognitive Radio (CR) device is a communication system aware of its environment as well as of its operational abilities and capable of using them intelligently. Thus it is a device that has the ability to collect information through it sensors and that can use the past observations on its surrounding environment to improve its behavior consequently. A simplified cognitive radio behavior in DSA is illustrated in Figure 3.46: the CR equipment observes its surrounding environment looking for opportunities. As illustrated by the magnifying glass, usually, a CR cannot see (or sense) the entire environment altogether. The results of these observations are taken into account by the decision making engine that decides on the next action to take (e.g. which part of the environment to sense? transmit or not transmit?). In some cases a numerical signal (reward or acknowledgment) is computed and help the CR equipment to evaluate its performance at that specific time.

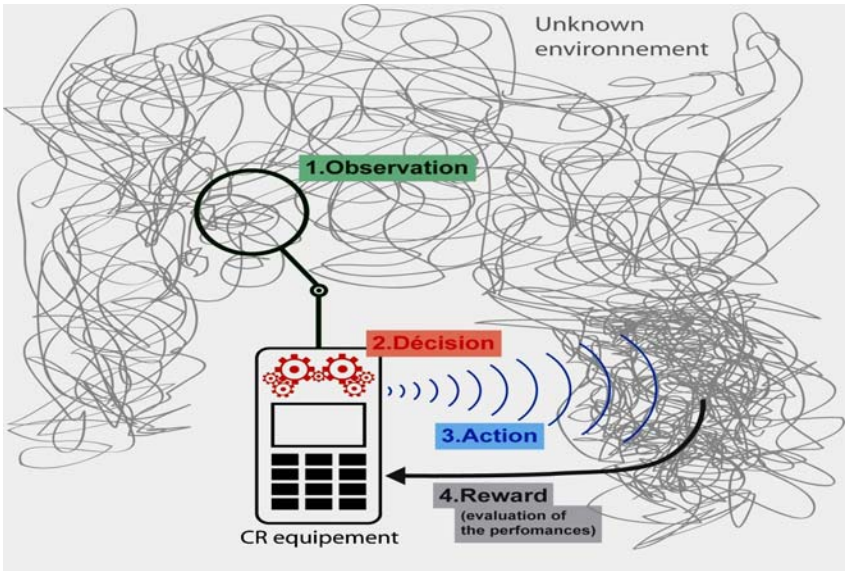

Figure 3.46 – Cognitive Radio context.

The design of such CR equipments to tackle OSA issues has been, recently, the center of a lot of attention (e.g. [100][101][102]). We refer to as Cognitive Agent (CA, Figure 3.46) the decision making engine of the CR equipment that can be seen as the brain of the CR device. At the level of the CA, the challenges are twofold: on the one hand, the SU must not compromise the efficiency of the primary network. Thus, a proper sensing of the environment must be done to avoid interfering with PUs. On the other hand, the SU has to find an allocation policy to select, and if possible, access the available resources. A simple representation of the different interactions between the environment and the cognitive agent is described in Figure 3.47.

In this section, we assume that the CA can only take actions, (e.g. select and access a channel if possible) at discrete time instants $t = 0,1,2,\ldots$. At every instant t, the CA observes its radio frequency environment and can collect different kind of information (e.g., available frequency bands, noise level, position, throughput, etc.). All the information collected by the CA up to instant t is supposed to be gathered in a vector i_t. We assume that the CA has to select at every instant t an action a_t in a discrete set A. Without loss of generality, the behavior of the CA can be seen as a policy (decision strategy) π that maps the information vector i_t into the action $a_t \in \mathsf{A}$, that is:

$$a_t = \pi(i_t) \tag{3.5}$$

The purpose of this section is to study the performance of a particular policy on an academic DSA problem. The academic DSA problem is described in section 3.3.2. The policy which is based on the computation of upper confidence bound indexes is described in section 3.3.3. Section 3.3.4 reports the simulation results.

Reference DR9.2

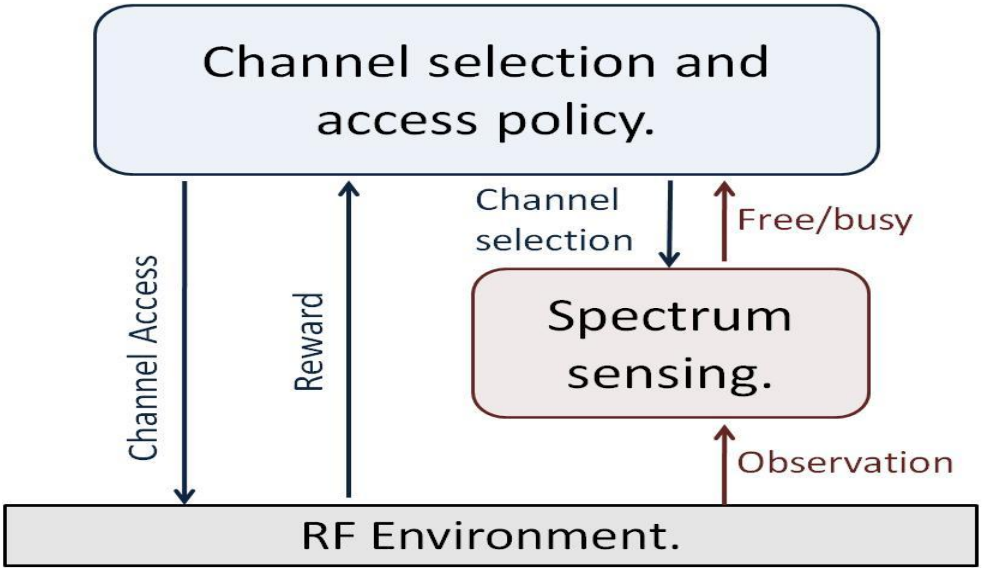

Figure 3.47 – Cognitive radio resource selection and access.

3.3.2 Dynamic spectrum access: network model

We consider a single secondary user (SU) operating in a primary network composed of K channels referenced by the integers $\{1,2,\ldots,K\}$. The CR equipment of the SU can only sense (then access if possible) one channel at a time. As illustrated in Figure 3.48, we address the particular case where the time is divided into slots $t = 0,1,2,\ldots,$ and that PUs are synchronous.

The temporal occupancy pattern of every channel k is supposed to follow an unknown Bernoulli distribution θ_k. Moreover, the distributions $\theta_1,\theta_2,\ldots,\theta_K$ are assumed to be stationary. When the SU senses a channel k at the slot number t, the cognitive agent computes a binary signal X_t that provides information on the availability of the sensed slot at that particular instant t. X_t is an independent realization of the distribution θ_k, at the slot t.

Let us define μ_k as follows: $\forall k$,

$$\mu_k = E[\theta_k] = P(\text{channel k is free})$$

Without loss of generality, we assume that $\mu_1 \leq \mu_2 \leq \ldots \leq \mu_{K-1} < \mu_K$. Moreover, we assume in this document that the outcome of the sensing process is error free. However the distribution probabilities $\theta_1,\theta_2,\ldots,\theta_K$ are assumed to be unknown to the CA.

At every instant t, and for every channel k the state of the channel observed by the SU can be either free or busy. If the channel is free, the CR equipment can transmit a certain number of bits B_t. Otherwise, the CR equipment waits until the next slot and selects a new channel to sense. A slot is divided into 4 periods (cf. Figure 3.49). During the first period, the CA chooses the next channel to access. During the second period the CA senses the selected channel before communicating if it is possible (channel free during the slot). At the end of every slot t, the CA computes a numerical signal referred to as reward r_t that depends on the occupancy state of the selected channel and evaluates the CA's performance (e.g., throughput in this document) during the communication process. The added information at the end of every slot is used to improve the decision making behavior of the CA which

is characterized by the policy π. As mentioned earlier, this policy takes an information vector i_t as input and outputs the action to be selected at time t. The action is here the channel to select, $\mathsf{A} = \{1,2,\ldots,K\}$, and the information vector is $i_t = [a_0, r_0, a_1, r_1, \ldots, a_{t-1}, r_{t-1}]$.

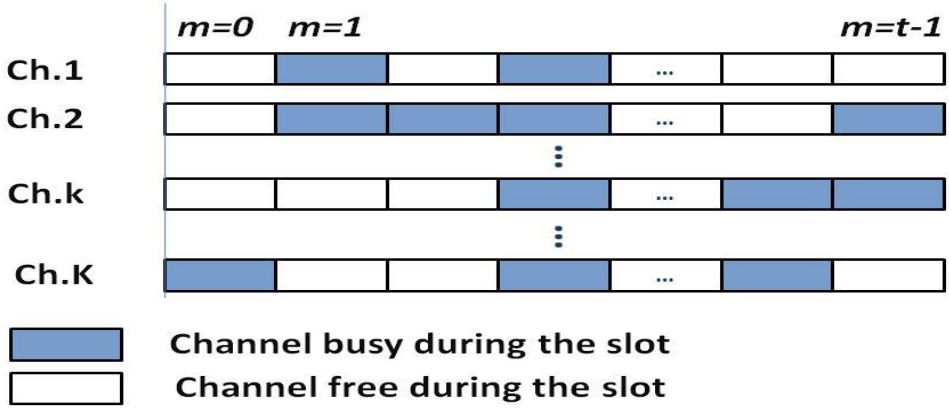

Figure 3.48 – Occupancy of the different channels considered by the SU.

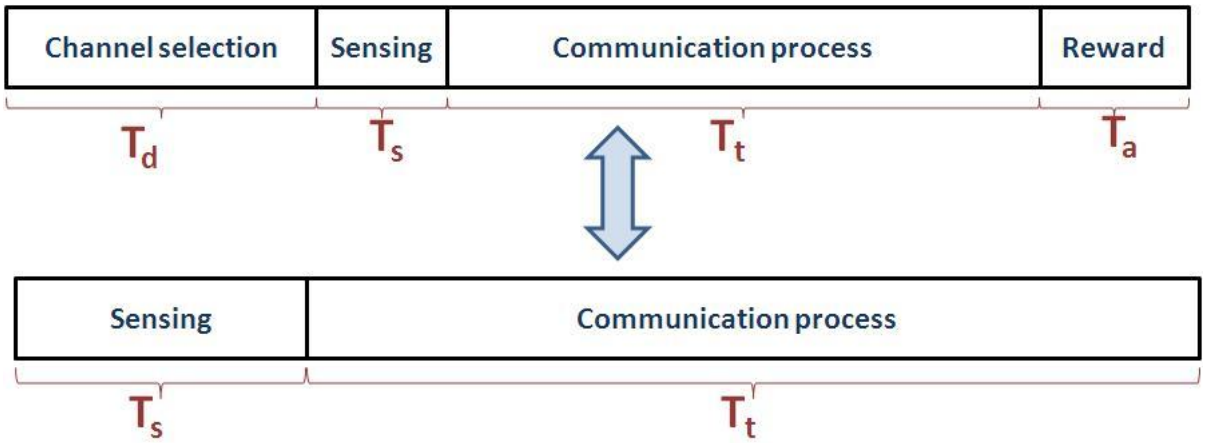

Figure 3.49 – Slot representation for a radio equipment controlled by a CA. It is assumed here that $T_d + T_a$ are small with respect to T_s and T_t.

The throughput achieved by the CR equipment at the slot number t can be defined as:

$$r_t \Delta = B_t \cdot X \tag{3.6}$$

which is the reward considered in this particular framework. For the sake of simplicity we assume here that if the channel is free the CR can always transmit $B_t = B$ bits. Thus, the cumulated throughput after t slots can be written:

$$W_t^{\pi} = \sum_{m=0}^{t-1} r_m = B \sum_{m=0}^{t-1} X_m$$

where the suffix π is used to emphasize that the CR equipment uses the policy π to select the channels.

The purpose of the CA is to maximize the expected cumulated throughput of the CR equipment:

$$E[W_t^\pi] = B\sum_{m=0}^{t-1} E[X_m] \tag{3.7}$$

Let R_t^π denote the regret of the CA at the slot number t, using a policy π. The regret R_t^π is defined as:

$$R_t^\pi = B.\mu_K.t - W_t^\pi \tag{3.8}$$

The general idea behind the notion of ``regret'' can be explained as follows: if the CA knew *a priori* the values of $\{\mu_k\}_{k\in\mathsf{A}}$, the best choice would be to always select the channel with the highest expected availability, i.e., μ_K. Unfortunately, the CA usually lacks that information and has to learn it. For that purpose, the CA has to explore the channels in order to have better estimations of their temporal occupancy pattern. While exploring it should also exploit the already collected information to minimize the regret during the learning process. This leads to an exploration-exploitation tradeoff. The ``regret'' represents the loss due to suboptimal channel selections during the learning process.

Maximizing the expected throughput is equivalent to minimizing the cumulated expected regret. The expected cumulated regret can be written as follows:

$$E[R_t^\pi] = B.\sum_{k=1}^{K} \Delta_k.E[T_k(t)] = B.E[\widetilde{R}_t^\pi] \tag{3.9}$$

where $\widetilde{R}_t^\pi = \frac{R_t^\pi}{B}$, $\Delta_k = \mu_K - \mu_k$ and $T_k(t)$ refers to the number of times the channel k has been selected from instant 0 to instant $t-1$.

We propose in the next section policies π that upper bound the expected cumulated regret of the CR equipment by a logarithmic function of the slot number.

3.3.3 Upper Confidence Bound index

3.3.3.1 UCB index

Building a cognitive agent to tackle the DSA issue requires to find a policy π for this agent that offers a good solution to the exploration-exploitation tradeoff behind the notion of regret's minimization. The general approach suggested in this section aims at selecting actions based on indexes that provide upper confidence bounds (UCB) on the rewards associated to the channels the secondary user can potentially exploit. Policies based on the computation of UCB indexes were initially introduced in the machine learning community to solve the so-called multi-armed bandit problem (see [103] and [107]).

A usual approach to evaluate the average reward provided by a resource k is to consider a confidence bound for its sample mean. Let $\overline{X}_{k,T_k(t)}$ be the sample mean of the resource $k \in \mathsf{A}$ after being selected $T_k(t)$ times at the step t:

$$\overline{X}_{k,T_k(t)} = \frac{\sum_{m=0}^{t-1} r_m.1_{\{a_m=k\}}}{t}$$

For every $k \in \mathsf{A}$ and at every step $t = 0,1,2,\ldots$, an upper bound confidence index (UCB index), $B_{k,t,T_k(t)}$, is a numerical value computed from i_t. For all k, $B_{k,t,T_k(t)}$ gives an optimistic estimation of the expected reward obtained when the CA selects the resource k at a time t after being tested $T_k(t)$.

The UCB indexes we use in this document have the following general expression:

$$B_{k,t,T_k(t)} = \overline{X}_{k,T_k(t)} + A_{k,t,T_k(t)} \tag{3.10}$$

where $A_{k,t,T_k(t)}$ is an upper confidence bias added to the sample mean.

An upper confidence bound (UCB) based cognitive agent uses a policy π to compute from i_t these indexes from which it selects a resource a_t as follows:

$$a_t = \pi(i_t) = \underset{k}{\operatorname{argmax}}(B_{k,t,T_k(t)}) \tag{3.11}$$

3.3.3.2 UCB$_1$ (cf. [104], [105])

When using the following upper confidence bias:

$$A_{k,t,T_k(t)} = \sqrt{\frac{\alpha.\ln(t)}{T_k(t)}} \tag{3.12}$$

with $\alpha > 1$, we obtain an upper confidence bound index referred to as UCB_1 in the literature. A fully detailed version of the policy using UCB_1 indexes is given in Figure 3.50.

Parameters: K, *exploration coefficient* α

Input: $i_t = [a_0, r_0, a_1, r_1, \ldots, a_{t-1}, r_{t-1}]$

Output: a_t

Algorithm:

If: $t \leq K$ *return* $a_t = t + 1$

Else:

- $T_k(t) \leftarrow \sum_{m=0}^{t-1} 1_{\{a_m = k\}}$, $\forall k$
- $A_{k,t,T_k(t)} \leftarrow \sqrt{\frac{\alpha.\ln(t)}{T_k(t)}}$, $\forall k$
- $B_{k,t,T_k(t)} \leftarrow \overline{X}_{k,T_k(t)} + A_{k,t,T_k(t)}$, $\forall k$
- return $a_t = \underset{k}{\operatorname{argmax}}(B_{k,t,T_k(t)})$

Figure 3.50 – A tabular version of a policy $\pi(i_t)$ using a UCB_1 algorithm for computing actions a_t.

3.3.3.3 UCB$_V$ [105]

The UCB_1 index uses only first order statistic information (empirical mean). It was suggested in [104] that adding the second order statistic information (empirical variance) to the UCB indexes could lead to better performances. The UCB_V index exploits the empirical variance of the estimated rewards. More specifically it uses the following upper confidence bias:

$$A_{k,t,T_k(t)} = \sqrt{\frac{2\xi.V_k(t).\ln(t)}{T_k(t)}} + \frac{3.c.\xi.\ln(t)}{T_k(t)} \tag{3.13}$$

with $c \geq 1$ and $3.\xi.c > 1$ and where $V_k(t)$ refers to the empirical variance of the channel k.

In section 3.3.4 we will compare the performances of UCB_1 and UCB_V policies on the dynamic spectrum access problem introduced in section 3.3.2.

3.3.3.4 Performance evaluation

When using a policy π, an interesting way to analyze its behavior is to consider the notion of consistency. This notion gives information on the growth rate of the regret. A policy π is said to be β*-consistent*, $0 < \beta \leq 1$, if it satisfies:

$$\lim_{t\to\infty} \frac{E[R_t^{\pi}]}{t^{\beta}} = 0 \tag{3.14}$$

We expect a good policy to be at least *1-consistent*. As a matter of fact, this property ensures that asymptotically the mean expected reward is optimal, i.e.:

$$\lim_{t\to\infty} \frac{\sum_{m=0}^{t-1} r_m}{t} = B.\mu_K \tag{3.15}$$

Theorem 1 *(cf. [104] and [105] for proofs) For all $K \geq 2$, if policy $UCB_1(\alpha > 1)$ is run on K channels having arbitrary reward distributions $\theta_1,...,\theta_K$ with support in [0,1], then:*

$$E[\widetilde{R}_t^{\pi=UCB_1}] \leq \sum_{k:\Delta_k>0} \frac{4.\alpha}{\Delta_k}.\ln(t) \tag{3.16}$$

Notice that a similar theorem could be written if the reward distributions had a bounded support rather than a support in [0,1].

An equivalent theorem also exists for the index UCB_V:

Theorem 2 *(cf. [105] for proofs) For all $K \geq 2$, if policy $UCB_V(\xi \geq 1, c = 1)$ is run on K channels having arbitrary reward distributions $\theta_1,...,\theta_K$ with support in [0,1], then $\exists C_\xi > 0$ s.t.*

$$E[\widetilde{R}_t^{\pi=UCB_V}] \leq C_\xi \sum_{k:\Delta_k>0} \left(\frac{\sigma_k^2}{\Delta_k} + 2\right).\ln(t) \tag{3.17}$$

Actually a similar result would still hold if $c \geq 1$ but satisfies nonetheless $3.\xi.c > 1$.

These results are of a particular interest for many reasons:

- They bound the expected regret of the UCB policies by a logarithmic functions for all t. This guarantees that the suggested policies are β consistent for all $0 < \beta \leq 1$. Thus these policies converge quickly to the optimal channel K.
- Moreover, the indexes these policies rely on to select actions can be computed incrementally [106]. Thus, their complexity, in terms of memory usage and computational needs, are low.
- Last but not least, it has been proven in [107] that when having no *a priori* information on the temporal occupancy pattern of the different channels $\theta_1, \theta_2, \ldots, \theta_K$, a logarithmic upper bound is the best we can expect.

3.3.4 Simulations

In our simulations, we consider that the CA agent can choose between 10 channels. The parameters of the Bernouilli distributions which characterize the temporal occupancy of these channels are: $[\mu_1, \mu_2, \ldots, \mu_{10}] = [0.1, 0.2, 0.3, 0.4, 0.5, 0.6, 0.7, 0.8, 0.85, 0.9]$. We consider that the number of bits a SU can transmit on a free channel is $B = 1$ bit.

Every numerical result reported hereafter is the average of the values obtained over 100 experiments.

In this section, the parameter α of the UCB_1 algorithm is chosen equal to 1.2. The parameters ξ and c of the UCB_V algorithm are equal to 1 and 0.4, respectively. With such values for c and ξ, the condition $3.\xi.c > 1$ is satisfied and the bound on the expected cumulated regret given in eq. (3.17) in section 3.3.3.4 still holds. The simulation results depend on the paramaters values, however we chose these values to be close to the critical ones ($\alpha = 1$, $\xi = 1$ and $c = 1/3$) without being too conservative.

Figure 3.51-top shows the evolution of the average cumulated regret for the different UCB policies. For both policies, the cumulated regret first increases rather rapidly with the slot number and then more and more slowly. This shows that UCB policies are able to process the past information in an appropriate way such that most available resources are favored with time. This is further illustrated by the 3 graphics on the bottom of Figure 3.51. These graphics show the average throughput achieved by the UCB policies. As we observe, the throughput increases with time. Actually, one has the theoretical guarantee that it will converge to 0.9, which is the largest probability of availability of a channel. Figure 3.52 shows the percentage p of times a UCB policy selects the optimal channel until the slot number t ($p = 100.\frac{\sum_{m=0}^{t-1} 1_{\{a_m = K\}}}{t}$). As one can observe, this percentage tends to get closer and closer to 100 as the slot number increases.

In our simulations results, we have always found out that UCB_1 seems to outperform UCB_V at the beginning of the learning process and that, afterwards, UCB_V outperforms UCB_1. This may be explained by the fact that at the beginning of the learning UCB_V spends more time collecting information on the different channels than UCB_1 since it also depends on the variances of the different channels and not only on their empirical mean. During this phase, it mainly has a pure exploration strategy while UCB_1 starts already exploiting the information that has been gathered. However, once it starts having good estimates of these variances, it can address the exploration-exploitation tradeoff in a more efficient way than UCB_1.

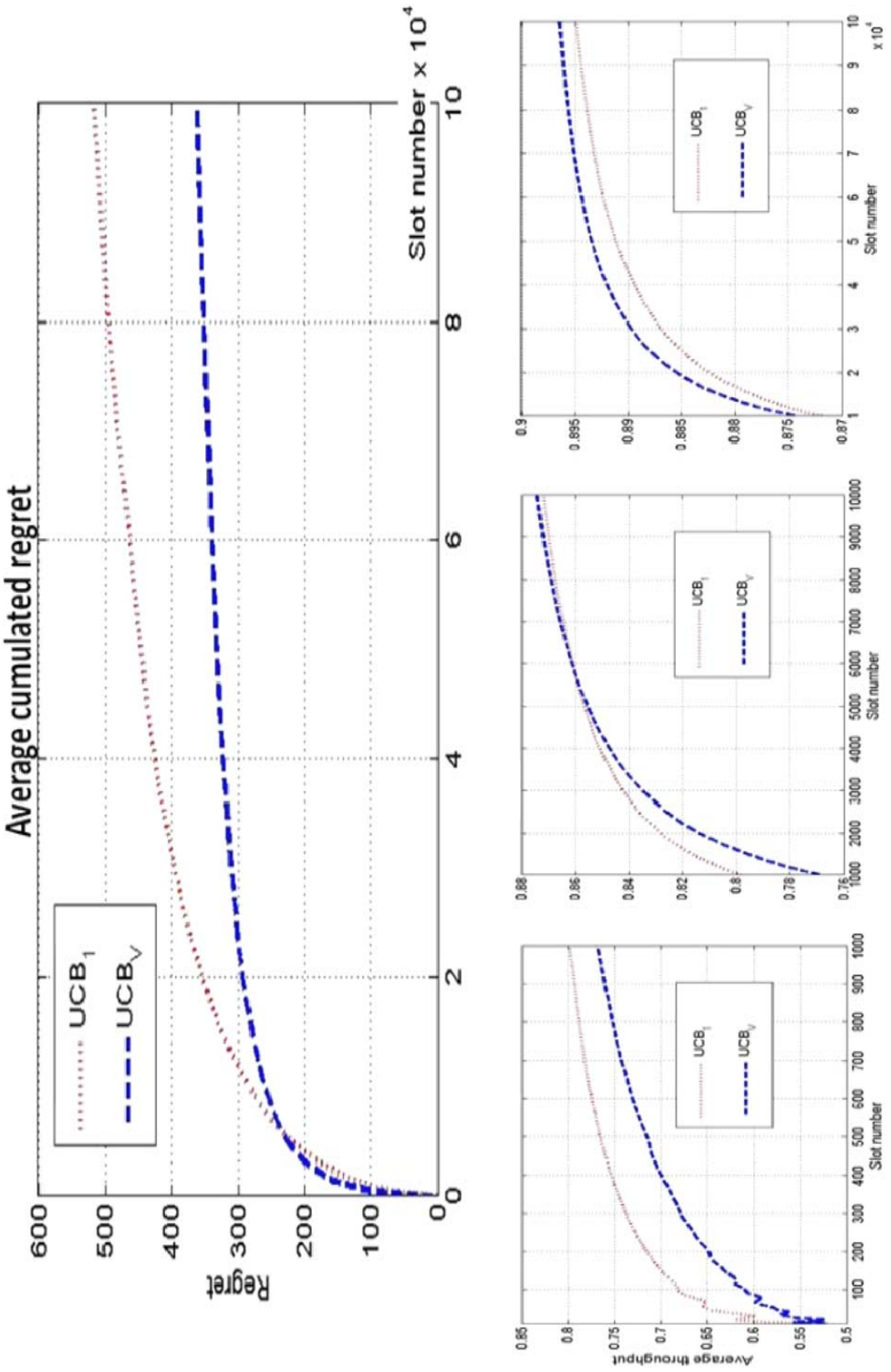

Figure 3.51 – UCB based policies and dynamic spectrum access problem: simulation results. Figure on top plots the average cumulated reward as a function of the number of slots for the different UCB based policies. The figures on the bottom represent the evolution of the normalized average throughput achieved by these policies.

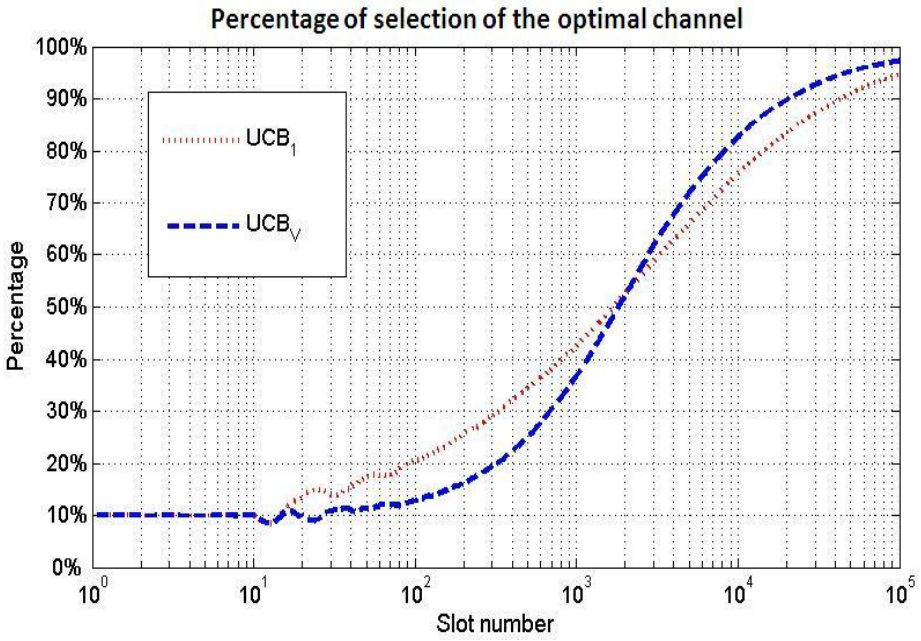

Figure 3.52 – Percentage of time a UCB-based policy selects the optimal channel.

3.4 Conclusions

This chapter has presented the main developments in the field of ASM inside WPR9, as summarised in the following:

- A measurement campaign to detect spectrum availability is being carried out at different locations of a in a densely populated urban environment and for a frequency range from 75 MHz to 7075 MHz. The purpose is to establish spatial and temporal usage patterns from primary users in different licensed bands. Measurement locations have included both outdoor and indoor measurements and have identified different metrics such as the power spectral density, the temporal spectrum occupancy and the duty cycle.
- In general, the average spectrum occupancy observed in frequency and time in the outdoor study in a high point was found to be significantly low, concretely 17.78% for the whole measured frequency range 75-7075 MHz, although important differences can be observed when analysing the different frequency ranges individually. In the case of indoor measurements, lower occupancy rates down to 12.10 % have been observed. Finally, by considering measurements at different spatial locations, the main conclusion derived from the obtained results is that the spectral activity perceived by a secondary user for a certain band in realistic urban scenarios strongly depends on the user location, with significant variations even in physical areas as reduced as the one considered in this study (≈180×260 m). This indicates that the conclusions derived from measurement studies performed in high points may not be well suited to other scenarios with users at the ground level.
- A machine learning based DSA strategy has been developed and analysed. It is executed at a cognitive agent of a secondary user to decide on the most appropriate channels to sense and access from a set of available channels. The general approach aims at selecting actions based on indexes that provide upper confidence bounds (UCB) on the rewards associated to the channels the secondary user can potentially exploit. Results show that UCB policies are able to process the past information in an appropriate way such that most available resources are favored with time, meaning that the cognitive agent will finally learn those channels having the highest availability for secondary users' access.

From an integration perspective, the outcome of these activities has led to the publication of two joint papers by UPC and CNRS in NEWCOM++ Acorn workshop 2009 and Crowncom 2009 conference, respectively. Also a joint presentation between UPC and CNRS was given at the workshop on Dynamic Spectrum Management in Cognitive Radio Networks in the ICT Mobile Summit in Santander, June 2009. The equipment used for the measurement campaign has been shown in two demonstrations at NEWCOM++ Acorn Workshop and ICT Mobile Summit. In turn, some lectures were given at the NEWCOM++ Winter School on Flexible Radio and related technologies, hold in Aachen during the days 3rd to 6th of February, covering topics related with this activities, in particular the talk “Dynamic Spectrum Access: Advanced Topics and Case studies” given by J. Pérez-Romero from UPC. Finally, two students from CNIT have collaborated with UPC in the measurement campaign at different outdoor locations and in the setting up of the USRP measurement platform. Finally, it is also worth mentioning that three NEWCOM++ special sessions on cognitive radio related topics are being organised at European Wireless 2010, at the 6th Kalsruhe Workshop on Software Radios (WSR-2010) and the Cognitive Information Processing (CIP 2010) conference.

4 CONCLUSIONS

4.1 Overview

This deliverable aims to propose and evaluate selected RRM, JRRM and ASM algorithms. In Section 2 several RRM techniques have been described, covering the areas of JRRM, spectrum allocation for OFDMA networks, and game-theoretic optimization of RRM for CR. Section 3 comprises the main developments in the field of ASM, presenting the details of measurement campaign to detect spectrum availability and a machine learning based DSA strategy for CR.

Selected aspects of JRRM have been addressed in Section 2.2, such as the multicell multicarrier power optimization, and vertical hand-over (VHO) in heterogeneous networks, where different systems like UMTS, WiMAX and WLAN are deployed. The proposed techniques have been evaluated by means of computer simulations in the train station scenario, described in [2], defining challenging users' conditions (e.g., channel, position, etc.) and traffic specifications. On the other hand, a theoretical approach to the investigations about VHO strategies has been considered, where a mathematical framework has been applied.

Section 2.3 focuses on RRM in a cellular system, particularly on the resource allocation problem. Several algorithms have been proposed with objectives on parameters like rate or fairness maximization, with constraints on power. A detailed investigation of the proposed techniques has been performed for the single-cell scenario by simulation. On the other hand, for the multi-cell scenario state-of-the-art analysis is presented, with few selected solutions described in more details, which are considered for future investigations.

The main scope of Section 2.4 is on cognitive radio and the related RRM optimisation using game theory. A scenario has been investigated, where each node detects the available spectrum, with the aim of acquiring radio resources to maximize the throughput. Two different techniques of limiting the usage of resources have been considered: the taxation of resources and the resource bandwidth limiting with successive interference cancellation.

A measurement campaign to detect spectrum availability has been described in Section 3.2. Different locations in a densely populated urban environment have been considered for a frequency range of analysis up to over 7 GHz. The purpose of the analysis is to establish spatial and temporal usage patterns from primary users in different licensed bands, and consequently, find the possibilities of spectrum usage by secondary users.

Finally, in Section 3.3 a machine learning based strategy has been proposed for dynamic spectrum assignment (DSA). A scenario with a cognitive agent of a secondary user deciding on the channel sensing and access procedures is considered. The results show that the proposed policies are able to process the past information in an appropriate way to optimize the cognitive agent actions.

4.2 Future work

The activities for the third year inside WPR9 will continue with further analysis to consolidate the studies in the identified topics within the different working groups.

In particular, focusing on RRM and JRRM strategies, it is expected to further develop the resource allocation in multi-cell OFDMA for both centralized and distributed scenarios. Special emphasis will be given to the femtocell scenario, which is one of the most relevant for future applications. Moreover, the impact of multi-sector and/or multi-site cooperation will be investigated in MIMO-aware scheduling OFDMA systems with the aim of increasing the spectral efficiency of cell edge users.

Similarly, from the perspective of the application of game theory to cognitive radio, further studies are envisaged for instance analysing the bandwidth limiting (BL) algorithm when transmitters have

different channel statistics, since it might lead to the usage of different BL policies for each transmitter.

In turn, focusing on spectrum management mechanisms, it is envisaged that studies will continue on the one hand with the applicability of the results of the measurement campaign to the development of spectrum usage models and more efficient CR techniques. On the other hand, and given that the measurements performed to the date are based on a spectrum analyzer setup, whose time resolution is relatively limited and could not be appropriate for certain levels of modelling, further measurements are envisaged with the use of an additional platform based on USRP and GNU radio, which allows much higher time resolutions than the spectrum analyser but over narrower bandwidths. In this context, it allows the possibility to develop new spectrum sensing mechanisms to determine whether a given channel is occupied or not.

4.3 Integration activities

One of the main aims of the NEWCOM++ project is the integration of the researchers and dissemination of the investigation results. Thus, several joint papers summarizing the outcomes of different WGs have been submitted to selected international conferences and workshops. These include:

- E. B. Rodrigues, Marco Moretti, Pawel Sroka, Giulio Dainelli, Fernando Casadevall, “Sub-carrier Allocation and Packet Scheduling in OFDMA-based Cellular Networks”, NEWCOM++ Acorn Workshop, Barcelona, 30th March – 1st April 2009.
- Emanuel B. Rodrigues, Fernando Casadevall, Pawel Sroka, Marco Moretti, Giulio Dainelli, “Resource Allocation and Packet Scheduling in OFDMA-Based Cellular Networks”, Crowncom 2009, Hannover, 22nd – 24th June 2009.
- Emanuel B. Rodrigues, Michael L. Walker, and Fernando Casadevall "On the Influence of Packet Scheduling on the Trade-Off Between System Spectral Efficiency and User Fairness in OFDMA-Based Networks", EUNICE Conference 2009, Barcelona, September, 2009.
- S. Medina, M. Debbah, S. Lasaulce, H. Bogucka, "On the Benefits of Bandwidth Limiting in Decentralized Vector Multiple Access Channels", Crowncom 2009, Hannover, 22nd – 24th June 2009.
- Miguel López-Benítez, Fernando Casadevall, Anna Umbert, Rachid Hachemani, Jacques Palicot, Christophe Moy “Spectral Occupancy Measurements in Urban Areas and their Applicability to the Blind Standard Recognition Sensor Concept”, NEWCOM++ Acorn Workshop, Barcelona, 30th March – 1st April 2009.
- M. López-Benítez, F. Casadevall, A. Umbert, J. Perez-Romero, R. Hachemani, J. Palicot, C. Moy, "Spectral Occupation Measurements and Blind Standard Recognition Sensor for Cognitive Radio Networks", Crowncom 2009, Hannover, 22nd – 24th June 2009
- Miguel López-Benítez, Fernando Casadevall, Anna Umbert , Rachid Hachemani, Christophe Moy, Jacques Palicot “Blind Standard Recognition Sensor Validation with Data from Measurement Campaign”, presentation at the workshop on Dynamic Spectrum Management in Cognitive Radio Networks hold the day before the ICT Mobile Summit in Santander, 9th June 2009.

Moreover, two demonstrations were given at different fora:

- “Spectral Occupancy Measurements in Urban Areas” ICT Mobile Summit in Santander, Spain, 10-12 June, 2009,
- “Spectral Occupancy Measurements in Urban Areas” NEWCOM++ Dissemination day, Barcelona, Spain, April 2009.

The partners involved in research within WPR.9 were also active tutors. Three lectures were given at the NEWCOM++ Winter School on Flexible Radio and related technologies, held in Aachen during the days 3rd to 6th of February 2009:

- H. Bogucka (PUT), “Game Theory Approach to Flexible RRM and Spectrum Sharing”,
- R. Agustí (UPC), “Adaptive Radio Resource Management Techniques”,
- J. Pérez-Romero (UPC), “Dynamic Spectrum Access: Advanced Topics and Case studies”.

Another aspect of integration of researchers working in WPR.9 were the face-to face meetings, where aspects of collaboration between partners and common research topics were identified. In addition to four WPR9 plenary meetings, different on-line interactions through phone calls and some exchanges of students, also the following short visits of researchers took place:

- A visit of Mérouane Debbah from CNRS to PUT was carried out on 15th and 16th of June. He gave a talk on Mobile Flexible Networks and the use of game theoretic techniques to design the deployment of dense networks. Also different research issues were discussed.
- A visit of António Serrador from IST-TUL to CNIT-Pisa was carried out on June 22-24 in order to coordinate activities on distributed radio resource allocation.

Finally, several special sessions have been or are being organised with the participation of WPR9 members:

- “Flexible and Opportunistic Wireless Access - the Newcom ++ vision”, Crowncom Conference, June 24th 2009.
- "Newcom++ Special Session on Cognitive Radio" in European Wireless 2010 conference, Lucca Italy, 12-15 April 2010.
- “Advances in Signal Processing for Cognitive Radios - Newcom++ Results” in 6th Kalsruhe Workshop on Software Radios (WSR), 3-4 March 2010.
- “Cognitive Radio: the NEWCOM++ vision” in Cognitive Information Processing (CIP 2010) conference, 14-16 June 2010, Elba Island, Italy.

Summarizing, a lot of effort has been made to integrate and increase the cooperation of WPR.9 members. Several papers disseminating the results of research in different WGs were published and the demonstrations and lectures on selected areas of investigation in WPR.9 were given. Finally, the cooperation between partners has been tightened by two scientific visits.

REFERENCES

[1] Emanuel B. Rodrigues, Marco Moretti, Pawel Sroka, Giulio Dainelli, and Fernando Casadevall, "Sub-carrier Allocation and Packet Scheduling in OFDMA-Base Cellular Networks", In *Proc. of NEWCOM++ - ACORN Joint Workshop*, Barcelona, Spain, March-April, 2009.

[2] NEWCOM++ DR9.1 v.1 "Identification of relevant scenarios, use cases and initial studies on JRRM and ASM strategies", December 2008.

[3] ETSI, "Universal Mobile Telecommuincations System (UMTS); Selection procedures for the choice of radio transmission technologies of the UMTS", TR 101 112 v3.2.0, Sophia Antipolis, France, April, 1998.

[4] Liu,M., Li,Z.C., Guo,X.B. Dutkiewicz,E. and Zhang,D.K., "Performance Evaluation of Vertical Handoff Decision Algorithms in Heterogeneous Wireless Networks," In *Proc. of GLOBECOM '06 - IEEE Global Telecommunications Conference*, San Francisco, CA, USA, Nov. 2006.

[5] Zahran, A.H. and Liang,B., "Performance Evaluation Framework for Vertical Handoff Algorithms in Heterogeneous Networks", In *Proc. of ICC'05 - IEEE International Conference on Communications*, Seoul, Korea, May 2005.

[6] Hou,J. and O'Brien,D.C., "Vertical Handover-Decision-Making Algorithm Using Fuzzy Logic for the Integrated Radio-and-OW System", IEEE Transactions Wireless Communications, Vol. 5, No. 1, pp. 176-185, Jan. 2006.

[7] Liu,M., Li,Z., Guo,X. and Dutkiewicz,E., "Performance Analysis and Optimization of Handoff Algorithms in Heterogeneous Wireless Networks", IEEE Transactions on Mobile Computing, Vol. 7, No. 7, pp. 846-857, July 2008.

[8] Li,B., ChengKe,W and Fukuda,A. "Performance analysis of flexible hierarchical cellular systems with a bandwidth-efficient handoff scheme" IEEE Transactions on Vehicular Technology, Vol. 50, No. 4, July 2001. pp. 971-980.

[9] Ljung,R. (ed.) et al., *Target Scenarios specification: vision at project stage 1*, IST-AROMA Project, Deliverable D05, EC-IST Office, Brussels, Belgium, Mar. 2006.

[10] C.Y. Wong, R.S. Cheng, K.B. Letaief and R.D. Murch, "Multiuser OFDM with Adaptive Subcarrier, Bit and Power Allocation," IEEE J. Select. Areas Commun., vol. 17, no. 10, pp. 1747-1758, Oct. 1999.

[11] M. Moretti and M. Morelli, "A novel dynamic sub-carrier assignment scheme for multiuser OFDMA systems," Proc. VTC 2006-Spring, May 2006.

[12] J. Jang and K. B. Lee, "Transmit power adaptation for multiuser OFDM systems," IEEE Journal on Selected Areas in Communications, vol. 21, no. 2, pp. 171–178, 2003.

[13] W. Rhee and J. M. Cioffi, "Increase in capacity of multiuser OFDM system using dynamic subchannel allocation," in Proc. IEEE 51st Vehicular Technology Conference - VTC Spring, 2000, pp. 1085–1089.

[14] G. Song and Y. G. Li, "Cross-layer optimization for OFDM wireless networks - part I: Theoretical framework and part II: Algorithm development," IEEE Transactions on Wireless Communications, vol. 4, no. 2, pp. 614–634, Mar. 2005.

[15] 3GPP, "Technical Specification Group Radio Access Networks; Deployment aspects," TR 25.943 v5.1.0, June, 2002.

[16] Z. Shen and J. G. Andrews and B. L. Evans, "Adaptive resource allocation in multiuser OFDM systems with proportional rate constraints," IEEE Transactions on Wireless Communications, vol. 4, no. 6, pp. 2726– 2737, 2005.

[17] J. Tang and X. Zhang, “Cross-Layer Design of Dynamic Resource Allocation with Diverse QoS Guarantees for MIMO-OFDM Wireless Networks,” in Proc. Sixth IEEE International Symposium on a World of Wireless Mobile and Multimedia Networks - WoWMoM, 2005, pp. 205–212.

[18] S. Shakkottai and R. Srikant, “Network Optimization and Control,” Foundations and Trends in Networking, vol. 2, no. 3, pp. 271–379, 2007.

[19] P. J. G. Ameigeiras, Packet Scheduling and Quality of Service in HSDPA, Ph.D. dissertation, Aalgorg University, Aalborg, Denmark, 2003.

[20] F. Kelly, “Charging and Rate Control for Elastic Traffic,” European Transactions on Communications, vol. 8, pp. 33–37, 1997.

[21] E. B. Rodrigues and F. Casadevall, “Adaptive Radio Resource Allocation Framework for Multi-User OFDM,” IEEE 69th Vehicular Technology Conference - VTC Spring, Barcelona, Spain, April, 2009.

[22] H. Lei, L. Zhang, X. Zhang and D. Yang, “A Packet Scheduling Algorithm Using Utility Function for Mixed Services in the Downlink of OFDMA Systems,” in Proc. IEEE 66th Vehicular Technology Conference VTC 2007-Fall, pp. 1664-1668, September 2007.

[23] S. Shakkottai and A. L. Stolyar, “Scheduling Algorithms for a Mixture of Real-Time and Non-Real-Time Data in HDR”, in Proc. 17th International Teletraffic Congress (ITC), pp. 793-804.

[24] M. Andrews, K. Kumaran, K. Ramanan, A. Stolyar, P. Whiting and R. Vijayakumar, “Providing Quality of Service over a Shared Wireless Link”, in IEEE Communications Magazine, vol. 32, no. 2, pp. 150-154, 2001.

[25] S. Ryu, B. Ryu, H. Seo, M. Shi, “Urgency and efficiency based wireless downlink packet scheduling algorithm in OFDMA system”, in Proc. IEEE 61st Vehicular Technology Conference VTC 2005-Spring, June 2005

[26] Y. Zhang and S.C. Liew, "Link-adaptive largest-weighted-throughput packet scheduling for real-time traffics in wireless OFDM networks," Proc. IEEE GLOBECOM'05, vol.5, pp.2490–2494, Nov. 2005.

[27] J. Bingham, “Multicarrier modulation for data transmission: an idea whose time has come,” , *IEEE Comm. Mag.*, vol. 28, no. 5, pp. 5–14, May 1990.

[28] T. Keller and L. Hanzo, “Adaptive modulation techniques for duplex OFDM transmissions,” *IEEE Trans. Veh. Techn.*, vol. 49, no. 9, pp. 1893–1906, September 2000.

[29] 3GPP, “Evolved Universal Terrestrial Radio Access (E-UTRA) and Evolved Universal Terrestrial Radio Access (E-UTRAN); Overall description; Stage 2,” TS 36.300 v.8.4.0, Tech. Rep., March 2008.

[30] Chuang and Sollenberg, “Beyond 3G: Wideband Wireless Data Access Based on OFDM and Dynamic Packet Assignment” IEEE Comm. Magazine 2000

[31] M. Bohge, J. Gross, A. Wolisz, and M. Meyer, "Dynamic resource allocation in OFDM systems: an overview of cross-layer optimization principles and techniques," *IEEE Network*, vol. 21, no. 1, pp. 53-59, 2007.

[32] Hamouda et al., “Enhanced capacity for multi-cell OFDMA systems with efficicent power control and reuse partitioning”, IEEE Int. Conf. Oct. 06

[33] Y.-J. Choi, C.S. Kim and S. Bahk, “Flexible design of frequency reuse factor in OFDMA cellular networks,” *Proc. IEEE ICC 2006*.

[34] T. Kwon, H. Song, Y. Kim, J. Lee and D. Hong, “A power division reuse partitioning scheme with half frequency reuse factor for OFDMA downlink systems,” *Proc. IEEE ICC 2008*.

[35] M. C. Necker, “Interference Coordination in Cellular OFDMA Networks”, *IEEE Network*, vol. 22, pp. 12-19, Nov-Dec 2008

[36] H.W. Seok, J. P. Hyeong, J.O. Neel, J.H. Reed, “Inter-Cell Interference Coordination/Avoidance for Frequency Reuse by Resource Scheduling in an OFDM-Based Cellular System”, IEEE VTC-2007

[37] Elayoubi et al., “Performance Evaluation of Frequency Planning Schemes in OFDMA-based Networks”, IEEE TWC, May 08

[38] G. Li and H. Liu, “Downlink radio resource allocation for multi-cell OFDMA system,” *IEEE Trans. Wireless Comm*, vol. 5, no. 12, pp. 3451–3459, December 2006.

[39] A. Abrardo, A. Alessio, P. Detti, and M. Moretti, “Centralized radio resource allocation for OFDMA cellular systems,” in *Proc. IEEE ICC 2007*, 2007.

[40] Abrardo et al., “Radio resource allocation problems for OFDMA cellular systems”, Comp. Science, March 2008.

[41] M. Rahman, H. Yanikomeroglu, “Interference Avoidance through Dynamic Downlink OFDMA Subchannel Allocation using Intercell Coordination”, IEEE VTC Spring 2008

[42] F. Boccardi, H. Huang, “Limited Downlink Network Coordination in Cellular Networks”, IEEE PIMRC 2007, pp. 1-5, 2007

[43] K. Xu, X. Tao, Y. Wang, P. Zhang, “Inter-Cell Packet Scheduling In OFDMA Wireless Network”. IEEE 66th Vehicular Technology Conference VTC-2007, pp. 3115-3119, Spring 2007;

[44] L. Venturino N. Prasad, and X. Wang, “Coordinated scheduling and power allocation in downlink multicell OFDMA networks”, *IEEE Trans. On Vehicular Technology*, vol. 58, no. 6, pp. 2835-2848

[45] Tanabalasingham et al., “Joint Allocation of Subcarriers and Transmit Powers in a Multiuser OFDM Cellular Network”, Proc. ICC 06

[46] S. Gault, W. Hachem, and P. Ciblat, “Performance analysis of an OFDMA transmission system in a multicell environment,” *IEEE Trans. Comm.* vol. 55, no. 4, pp. 740–751, April 2007.

[47] C. Koutsimanis and G. Fodor, “A dynamic resource allocation scheme for guaranteed bit rate services in OFDMA networks, *Proc. IEEE ICC 2008*.

[48] Pischella, Belfiore, “Distributed Allocation for rate constrained users in multi-cell OFDMA networks” IEEE comm. Letters Apr. 08.

[49] C. Zhong, C. Li, L. Yang, and Z. He, “Dynamic resource allocation for the downlink of multi-cell systems with full spectral reuse”, *IEEE Int. Conference Neural Networks & Signal Processing*, June 2008.

[50] T. Hasegawa, R. Zhou, and I. Sasase, “Resource allocation for multi-cell OFDMA considering the interference to cell-edge users”, *Proc. APCC 2008*, Oct. 2008.

[51] Moretti, Todini, “A Resource Allocator for the Uplink of Multi-Cell OFDMA Systems”, IEEE TWC, Aug. 07

[52] T. Liu, A. Mader, and D. Staehle, “A novel linear-programming based approach for near-optimal rate allocation in the UMTS enhanced uplink”

[53] Abaii, Liu, Tafazolli, “An Efficient Resource Allocation Strategy for Future Wireless Cellular Systems” IEE TWC Aug 08

[54] A. Forenza et al, “Adaptive MIMO Transmission for Exploiting the Capacity of Spatially Correlated Channels,” IEEE Trans. Vehic. Tech., vol. 56, no. 2, Mar. 2007, pp. 619–30.

[55] W. Ahn and Y. Kim, "An Efficient Resource-Allocation Scheme Using Subcarrier Sharing in MIMO/OFDM Multi-cell Environment", *Proc. APCC 2008*, Oct. 2008.

[56] A. Benjebbour, M. Shirakabe, Y. Ohwatari, J. Hagiwara, T. Ohya, "Evaluation of user throughput for MU-MIMO coordinated wireless networks", IEEE PIMRC 2008, pp. 1-5, 2008;

[57] L. Giordano, L. Reggiani, L. Dossi, "Interference evaluation in multi-cell environment with resource allocation algorithms" IEEE VTC Spring 08

[58] M. Vemula, D. Avidor, J. Ling, C. Papadias, "Inter-Cell Coordination, Opportunistic Beamforming and Scheduling", IEEE ICC '06, pp. 5319-5324, June 2006

[59] Y.J. Chang, Z. Tao, J. Zhang, and C.-C. J. Kuo, "A graph-based approach to multi-cell OFDMA downlink resource allocation", *IEEE Globecom 2008*, Dec. 2008.

[60] H. Dahrouj, W. Yu, "Coordinated Beamforming for the Multi-Cell Multi-Antenna Wireless System", CISS 2008, March 19-21, 2008;

[61] R. Veronesi, V. Tralli, J. Zander, M. Zorzi, "Distributed Dynamic Resource Allocation for Multicell SDMA Packet Access Networks", IEEE Transactions on Wireless Communications, vol. 5, no. 10, pp. 2772-2783, October 2006;

[62] V. Chandrasekhar, J. G. Andrews and A. Gatherer, "Femtocell Networks: A Survey," IEEE Communications Magazine, September 2008, pp. 59-67.

[63] V. Chandrasekhar and J. Andrews, "Uplink Capacity and Interference Avoidance in Two-Tier Femtocell Networks," IEEE Trans. Wireless Commun.

[64] Ericsson, "Home NodeB Output Power," 3GPP TSG Working Group 4 meeting; http://www.3gpp.org/ftp/tsg_ran/WG4_Radio/TSGR4_43bis/Docs/

[65] D. López-Pérez, G. de la Roche, A. Valcarce, A. Jüttner and J. Zhang, "Interferente Avoidance and Dynamic Frequency Planning for WiMAX Femtocells Networks," ICCS 2008, pp. 1579-1584.

[66] S.-p. Yeh, S. Talwar, S.-C. Lee and H. Kim, "WiMAX Femtocells: A Perspective on Network Architecture, Capacity, and Coverage," IEEE Communications Magazine, October 2008, pp. 58-65.

[67] H. Claussen, L. T. W. Ho and L. G. Samuel, "An Overview of the Femtocell Concept," Bell Labs Techncal Journal, vol. 13, no. 1, pp. 221-246, 2008.

[68] G. Owen, *Game Theory*, Academic Press, 1995.

[69] P. D. Straffin, *Game Theory and Strategy*, The Mathematical Association of America, Washington DC, USA, 2002, Chapter 10.

[70] Ed. A. Serrador, "Identification of relevant scenarios, use cases and initial studies on JRRM and ASM strategies", Newcom++ Public Deliverable DR9.1

[71] W. Yu, W. Rhee, S. Boyd, and J. Cioffi, "Iterative water-filling for Gaussian vector multiple-access channels," IEEE Transactions on Information Theory, vol. 50, no. 1, pp. 145–152, Jan. 2004

[72] P. Viswanath, D. Tse, and V. Anantharam, "Asymptotically optimal water-filling in vector multiple-access channels," IEEE Transactions on Information Theory, vol. 47, no. 1, pp. 241–267, Jan 2001

[73] A. Ghasemi and E. Sousa, "Capacity of fading channels under spectrumsharing constraints," IEEE International Conference on Communications, vol. 10, pp. 4373–4378, June 2006.

[74] S. M. Perlaza, S. Lasaulce, and M. Debbah, "Game theory for dynamic spectrum sharing," Cognitive Radio Networks: Architectures, Protocols and Standards, 2008.

[75] S. Haykin, "Cognitive Radio: Brain-Empowered Wireless Communications", *IEEE Journal Select. Areas In Commun*., Vol. 23, No. 2, Feb. 2005, pp. 201-220

[76] A. Goldsmith, *Wireless Communication,* Cambridge Univ. Press, 2005

[77] G. Hardin, "The Tragedy of the Commons", Science, 162(1968), pp. 1243-1248.

[78] T. M. Cover and J. A. Thomas, *Elements of information theory,* 1991.

[79] M. Haddad, A. Hayar, and M. Debbah, "Spectral efficiency of spectrumpooling systems," IET Communications, vol. 2, no. 6, pp. 733–741, July, 2008.

[80] F. H. Sanders, "Broadband spectrum surveys in Denver, CO, San Diego, CA, and Los Angeles, CA: methodology, analysis, and comparative results," in Proc. 1998 IEEE International Symposium on Electromagnetic Compatibility, Aug 1998, vol. 2, pp. 988–993.

[81] M. A. McHenry et al., "Spectrum occupancy measurements," Shared Spectrum Company, technical reports (Jan 2004 – Aug 2005). URL: http://www.sharedspectrum.com/measurements.

[82] A. Petrin, P. G. Steffes, "Analysis and comparison of spectrum measurements performed in urban and rural areas to determine the total amount of spectrum usage," in Proc. International Symposium on Advanced Radio Technologies (ISART 2005), Mar 2005, pp. 9–12.

[83] R. I. C. Chiang, G. B. Rowe, K. W. Sowerby, "A quantitative analysis of spectral occupancy measurements for cognitive radio," in Proc. IEEE 65th Vehicular Technology Conference (VTC 2007-Spring), Apr 2007, pp. 3016–3020.

[84] M. Wellens, J. Wu, P. Mähönen, "Evaluation of spectrum occupancy in indoor and outdoor scenario in the context of cognitive radio," in Proc. Second International Conference on Cognitive Radio Oriented Wireless Networks and Communications (CrowCom 2007), Aug 2007, pp. 1-8.

[85] M. H. Islam et al., "Spectrum Survey in Singapore: Occupancy Measurements and Analyses," in Proc. 3rd International Conference on Cognitive Radio Oriented Wireless Networks and Communications (CrownCom 2008), May 2008, pp. 1–7.

[86] P. G. Steffes, A. J. Petrin, "Study of spectrum usage and potential interference to passive remote sensing activities in the 4.5 cm and 21 cm bands," in Proc. IEEE International Geoscience and Remote Sensing Symposium (IGARSS 2004), Sep 2004, vol. 3, pp. 1679–1682.

[87] J. Do, D. M. Akos, P. K. Enge, "L and S bands spectrum survey in the San Francisco bay area," in Proc. Position Location and Navigation Symposium (PLANS 2004), Apr 2004, pp. 566–572.

[88] M. Biggs, A. Henley, T. Clarkson, "Occupancy analysis of the 2.4 GHz ISM band," IEE Proc. on Comms, Oct 2004, vol. 151, nº 5, pp. 481–488.

[89] S. W. Ellingson, "Spectral occupancy at VHF: implications for frequency-agile cognitive radios," in Proc. IEEE 62nd Vehicular Technology Conference (VTC 2005-Fall), Sep 2008, vol. 2, pp. 1379–1382.

[90] S. D. Jones, E. Jung, X. Liu, N. Merheb, I.-J. Wang, "Characterization of spectrum activities in the U.S. public safety band for opportunistic spectrum access," in Proc. 2nd IEEE International Symposium on New Frontiers in Dynamic Spectrum Access Networks (DySPAN 2007), Apr 2007, pp. 137–146.

[91] M. López-Benítez, A. Umbert, F. Casadevall, "Evaluation of spectrum occupancy in Spain for cognitive radio applications", in Proc. IEEE 69th Vehicular Technology Conference (VTC 2009 Spring), Apr 2009, pp. 1–5.

[92] M. López-Benítez, F. Casadevall, "Methodological aspects of spectrum occupancy evaluation in the context of cognitive radio", in Proc. 15th European Wireless Conference (EW 2009), May 2009, pp. 199–204.

[93] Agilent, Application note 150: Spectrum analysis basics (www.agilent.com).

[94] Agilent, Application note 1286-1: 8 Hints for Better Spectrum Analysis (www.agilent.com).

[95] *Secretaría de Estado de Telecomunicaciones y para la Sociedad de la Información* (State Agency for Telecommunications and Information Society), "*Cuadro Nacional de Atribución de Frecuencias* (Table of National Frequency Allocations)," Spanish Ministry of Industry, Tourism and Commerce, Tech. Rep., Nov. 2007.

[96] A. Sahai, N. Hoven, R. Tandra, "Some fundamental limits on cognitive radio," in Proc. Forty-second Allerton Conference on Communications, Control, and Computing (Allerton Conference 2004), Sep 2004, pp. 1–10.

[97] M. López-Benítez, F. Casadevall, A. Umbert, J. Pérez-Romero, R. Hachemani, J. Palicot, and C. Moy, "Spectral occupation measurements and blind standard recognition sensor for cognitive radio networks," in Proc. 4th International Conference on Cognitive Radio Oriented Wireless Networks and Communications (CrownCom 2009), Jun 2009, pp. 1–9.

[98] Ettus Research LLC, "Universal Software Radio Peripheral (USRP)," Available at: http://www.ettus.com.

[99] E. Blossom, "Exploring GNU Radio," Nov. 2004, Available at: http://www.gnu.org/software/gnuradio/doc/exploringgnuradio.html.

[100] Mitola, J. and Maguire, G.Q. Cognitive radio: making software radios more personal. *Personal Communications, IEEE*, 6:13-18, 1999.

[101] Haykin, S. Cognitive radio: brain-empowered wireless communications. *IEEE Journal on Selected Areas in Communications*, 23, no. 2:201-220, 2005.

[102] Yucek, T. and Arslan, H. A Survey of Spectrum Sensing Algorithms for Cognitive Radio Applications. *In IEEE Communications Surveys and Tutorials*, 11, no.1, 2009.

[103] Agrawal, R. Sample mean based index policies with O(log(n)) regret for the multi-armed bandit problem. *Advances in Applied Probability*, 27:1054-1078, 1995.

[104] Auer, P. and Cesa-Bianchi, N. and Fischer, P. Finite time analysis of multi-armed bandit problems. *Machine learning*, 47(2/3):235-256, 2002.

[105] Audibert, J.-Y. and Munos, R. and Szepesvári, C. Tuning bandit algorithms in stochastic environments. *Proceedings of the 18th international conference on Algorithmic Learning Theory*, 2007.

[106] Jouini, W. and Ernst, D. and Moy, C. and Palicot, J. Multi-armed bandit based policies for cognitive radio's decision making issues. *In Proceedings of the 3rd international conference on Signals, Circuits and Systems (SCS)*, 2009.

[107] Lai, T.L. and Robbins, H. Asymptotically efficient adaptive allocation rules. *Advances in Applied Mathematics*, 6:4-22, 1985.